Lithogeochemistry of the Goldenville-Halifax
Transition (GHT) of the Meguma Group in
the Manganiferous Zinc-Lead Deposit at
Eastville, Nova Scotia

Submitted by

Ian Neil MacInnis

March, 1986

In partial fulfillment of a
Bachelor of Science Combined Honours Degree,
Departments of Chemistry and Geology,
Dalhousie University, Halifax, Nova Scotia

Distribution License

DalSpace requires agreement to this non-exclusive distribution license before your item can appear on DalSpace.

NON-EXCLUSIVE DISTRIBUTION LICENSE

You (the author(s) or copyright owner) grant to Dalhousie University the non-exclusive right to reproduce and distribute your submission worldwide in any medium.

You agree that Dalhousie University may, without changing the content, reformat the submission for the purpose of preservation.

You also agree that Dalhousie University may keep more than one copy of this submission for purposes of security, back-up and preservation.

You agree that the submission is your original work, and that you have the right to grant the rights contained in this license. You also agree that your submission does not, to the best of your knowledge, infringe upon anyone's copyright.

If the submission contains material for which you do not hold copyright, you agree that you have obtained the unrestricted permission of the copyright owner to grant Dalhousie University the rights required by this license, and that such third-party owned material is clearly identified and acknowledged within the text or content of the submission.

If the submission is based upon work that has been sponsored or supported by an agency or organization other than Dalhousie University, you assert that you have fulfilled any right of review or other obligations required by such contract or agreement.

Dalhousie University will clearly identify your name(s) as the author(s) or owner(s) of the submission, and will not make any alteration to the content of the files that you have submitted.

If you have questions regarding this license please contact the repository manager at dalspace@dal.ca.

Grant the distribution license by signing and dating below.

_____   _____

Name of signatory   Date

DR. MARCOS ZENTILLI
DEPT. EARTH SCIENCES
DALHOUSIE UNIVERSITY
HALIFAX, N.S., B3H 3J5
CANADA

Abstract

Zentilli *et al.* (1984) have pointed out that most metalliferous deposits within the Cambro-Ordovician Meguma Group have a spatial relation to the Goldenville – Halifax Formation transition (GHT). The GHT is generally more finely bedded than regular Meguma rocks, and is locally calcareous, manganiferous, and rich in carbonaceous material. The Eastville deposit also exhibits these characteristics and is of special interest as the only significant zinc-lead deposit in the Meguma Group.

The deposit is anomalous compared to the Goldenville Formation in manganese (up to 11 Wt% MnO), and zinc and lead (1-3 Wt% Zn+PB for up to 10 m sections). The stratigraphy is marked by a finely laminated, locally calcareous, manganiferous unit at the top of the Goldenville which is overlain by black, pyrrhotitic slate comprising the base of the Halifax Formation.

The manganese predominantly is contained in spessartine garnets, which appear to have derived the Mn from carbonates and sulphides during metamorphic growth. The carbonates appear to have formed diagenetically due to the oxidation of the resident carbonaceous material. Stratiform zinc and lead are present in the rocks, but appear to have been largely remobilized by low oxygen fugacity fluids into structurally controlled concentrations.

The concentration of some metals can be ascribed to the abundance of minerals such as smectites and jarosite in the original sediments. The features of the deposit are consistent with at least <u>some</u> of the manganese and zinc being concentrated from the available sea water by diagenetic processes. Lead could have been fixed in the original sediments by adsorption to the abundant organic material. However, it is possible that an outside source, such as hydrothermal sedimentary exhalative fluids, has been involved in the concentration of Mn, Zn, and Pb in the original sediments at Eastville.

A better sedimentological understanding of the GHT at Eastville and possibly analyses of rare earth elements would give hints on the sea water chemistry at the time of deposition. Similarly, the discovery of synsedimentary feeder zones would strengthen arguments for a sedimentary exhalative contribution to the deposit.

DR. MARCOS ZENTILLI
DEPT. EARTH SCIENCES
DALHOUSIE UNIVERSITY
HALIFAX, N.S., B3H 3J5

Acknowledgements

Table of Contents

Table of Figures

Table of Tables

Chapter 1

Introduction

1.1 General Statement

An examination of the metallogenic map of southern Nova Scotia reveals the close proximity of most iron, gold, tungsten, antimony, and arsenic showings to the manganiferous Goldenville-Halifax Formation Transition (*GHT*) of the Cambro-Ordovician Meguma Group. The idea that this horizon is a fundamental control on the metallogeny of the Meguma Group has raised the need to know more about its sedimentological, physical and chemical properties (Zentilli and MacInnis, 1983).

The Eastville deposit provides an excellent opportunity to study the GHT for two reasons. It is the only significant zinc lead deposit in the Meguma Group. Secondly, the Eastville drill core and chemical analyses probably comprise the most complete data set for any section of the GHT.

1.2 Location

Eastville is located about 40 km southeast of Truro, Colchester County, Nova Scotia (Fig. 1.1). The deposit covers the area 45°15'30"W latitude, 62°52'30" longitude to 45°17'45"W latitude, 62°44'30" longitude. From Halifax,
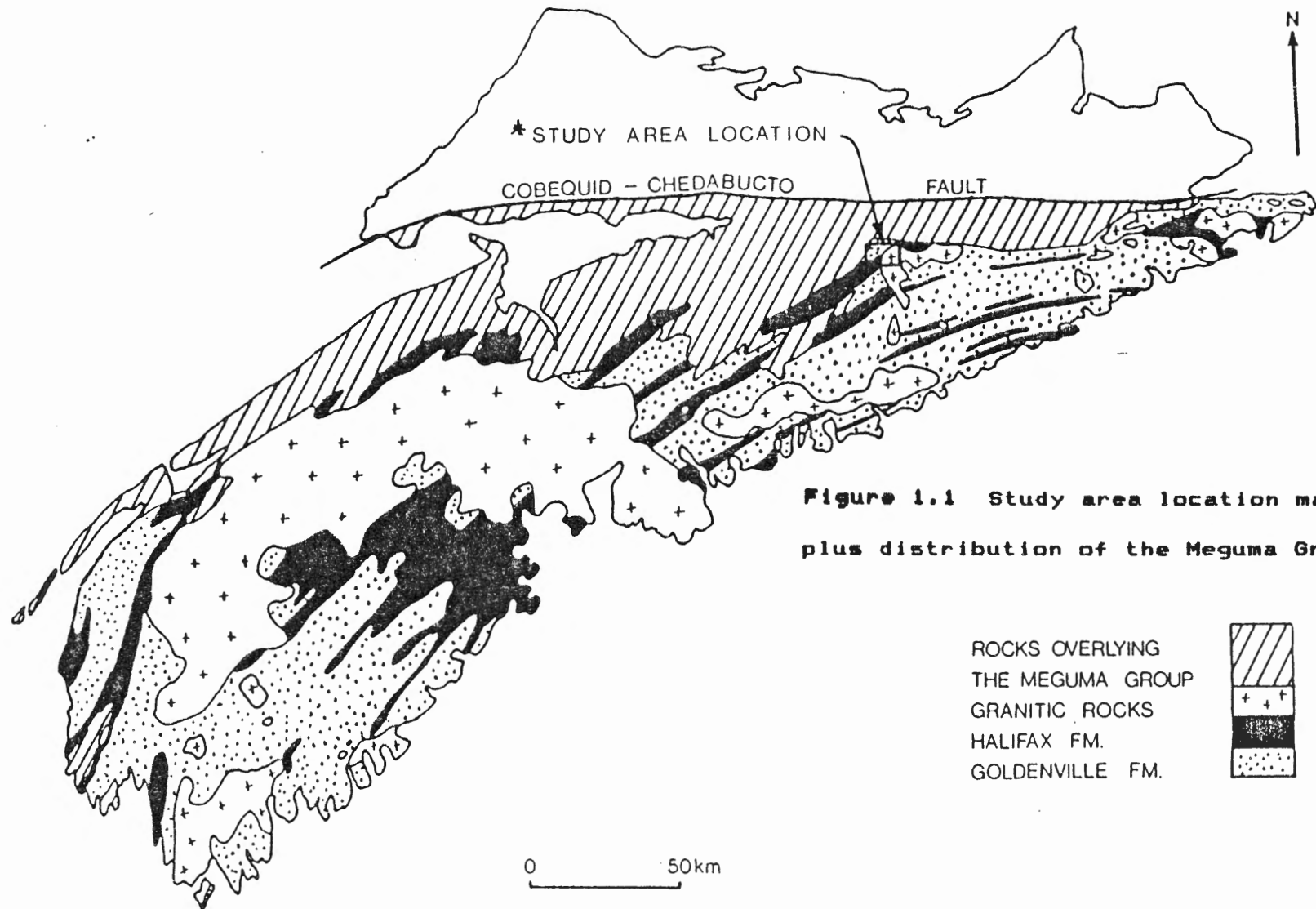
Figure 1.1 Study area location map plus distribution of the Meguma Group

STUDY AREA LOCATION

COBEQUID – CHEDABUCTO   FAULT

N

ROCKS OVERLYING
THE MEGUMA GROUP
GRANITIC ROCKS
HALIFAX FM.
GOLDENVILLE FM.

0   50km
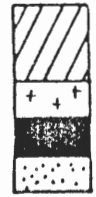
follow Route 102 to the Brookfield EXIT 12, followed by
Route 289 east to Springside Cross Rd., Cross Rd., and
finally the community of Eastville. From Eastville the
Harrison and Fisher Roads lead to the Eastville Road which
passes over the deposit.

The topography of the densely wooded area is irregular
and hummocky to the west and gently rolling to the east.
Outcrop is rare, except in brooks, owing to the heavy
glacial overburden.

1.3 Previous Work

The Eastville area was first mapped at a 1:63360 scale
by Fletcher and Faribault (1902). Sulpetro Minerals
(formerly St. Joseph Explorations Ltd.) placed 28 diamond
drill holes based on geophysical and till geochemical
anomalies which roughly delineated a northeast striking
section of the GHT. Up to 10m sections of drill core exhibit
1-3 Wt% combined zinc+lead. A 9.33m section of faulted GHT
in Hole 28 bearing 4.09 Wt% Zn+Pb appears especially
promising, but no move towards development of the prospect
has been made.

Jenner (1982) described the styles of sulphide
mineralization and general aspects of the stratigraphy for
drill hole 15. Burke (1985) modelled the geophysical
properties of the GHT in the deposit. Cameron (1985) carried
out a detailed study of the metmorphism of the deposit,
including the affect of a granitic pluton on the deposit, as

-3-

well as a study of the pluton itself.

1.4 Purpose and Scope

The first purpose of this thesis is to characterise the
chemistry of the Goldenville-Halifax Transition at
Eastville. Second, this thesis endeavours to deduce
information on the chemical conditions from the time of
sediment deposition through diagenesis and low grade
metamorphism, in the hope of determining which chemical
factors were prominent. The genesis of the Zn and Pb is also
examined, in order to determine how early in the history of
the deposit the Zn and Pb sulphides were introduced. A
comparison with various models for the development of
metalliferous sediments is made in an attempt to classify
the deposit and identify the metal source. However, the true
test of such models must be made at the regional scale and
is thus beyond the scope of this thesis.

1.5 Methods and Approach

Only limited field work was carried out due to poor
exposure of the most critical portions of the stratigraphic
section. Statistical treatment of bulk analyses for 50 drill
core samples, logging of a portion of the drill core for
diamind drill hole 27 and some petrography were carried out
in the summer of 1983.

Sampling and logging of all 28 drill holes was carried

-4-

out with Mahmood Hasan in the summer of 1984. An attempt to
analyse small samples by Inductively Coupled Plasma Atomic
Emission Spectroscopy (ICP-AES) was made, but the technique
proved to be inaccurate. A set of carbonate samples were
prepared for stable carbon and oxygen isotope analysis, and
the data were interpreted in September, 1984. A small set of
mineral analyses were obtained using the electron beam
microprobe in February, 1985. Some transmitted and reflected
light microscopy was also carried out at that time. Samples
were prepared for rare earth element analysis in October,
1985, however, instrumentation problems at St. Mary's
University prevented completion of the experiment.

1.6 Organization

A brief review of the regional geology of the Meguma
Terrane is provided in Chapter 2. The local geology, and
stratigraphy of the Eastville deposit are presented in
Chapter 3. Bulk rock, mineral, and isotope geochemistry are
described and discussed in Chapter 4. A general discussion
and comparison with models is given in Chapter 5.
Conclusions are found in Chapter 6 and Recommendations in
Chapter 7.

Chapter 2

Regional Geology

The Eastville deposit is situated near the northern limit of the Meguma Terrane, as defined by the Glooscap Fault system (Figure 1.1). This Terrane has a unique pre-Carboniferous geological history compared to the adjacent Avalon Terrane (Zentilli and Graves, 1977; Schenk, 1983).

2.1 Geological History of the Meguma Terrane

Clarke and Halliday (1985) have effectively summarized the events in the geological history of the Meguma Terrane in the following table:

Table 2.1
Tectono-thermal events in the history of the Meguma Terrane.
(from Clarke and Halliday, 1985)

Event	Age (Ma)	Reference
(1) Carboniferous and post-Carboniferous		
(I) Mafic igneous activity	202	Poole *et al*. (1970)
(II) Minas Geofracture	Dev. – Carb. – Perm.	Keppie (1982)
(III) Maritime disturbance	Late Carboniferous	Poole (1967)
(IV) Dunbrack Pb–Zn–Ag deposit	304	MacMichael (1975)
(V) Southern satellite plutons	350 – 258	Reynolds *et al*. (1981, 1984)
(2) Granite intrusion age	372 – 361	Clarke and Halliday (1980)
(3) Thermal aureole reset age	400 – 370	Reynolds *et al*. (1973)
(4) Acadian deformational age	415 – 400	Reynolds and Muecke (1978)
(5) Meguma Group depositional age	Cambro-Ordovician	Schenk (1983)
(6) Meguma Group detrital mica age	496 – 476	Poole (1971)

The Meguma Group metasedimentary rocks are the oldest rocks in the Terrane. They are thought to be Cambro-Ordovician in age, resulting from a network of submarine fans and channels on a prograding continental rise and

-6-

abyssal plain (Schenk, 1983). Provenance studies have suggested a deeply eroded craton of granodioritic composition situated to the southeast as the sediment source (Schenk, 1983).

The Meguma Group was then subjected to regional metamorphism over the range of the greenschist facies through to the sillimanite zone in response to the deformation of the Acadian Orogeny, dated by $^{40}Ar/^{39}Ar$ techniques to be at least 400-415 Ma (Reynolds and Muecke, 1978). A second metamorphic event involved the intrusion of peraluminous granites with resulting contact aureoles in the Meguma country rocks at ~367 Ma (Reynolds *et al.*, 1981; Clarke and Halliday, 1980).

Movement during the Devonian through Permian along the Glooscap and associated faults brought the Meguma Terrane into its present position (Keppie, 1982). In the Carboniferous, block faulting of the uplifted Meguma with associated erosion resulted in the deposition of the Horton Group, followed by the evaporites of the Windsor Group due to localized shallow sea transgressions. The North Mountain basalts reflect the early stages of the opening of the Atlantic Ocean at ~200Ma. Pleistocene glaciation further eroded the region and produced thick till deposits.

2.2 The Meguma Group

2.2.1 Stratigraphy of the Meguma Group

The Meguma group, comprised of the Goldenville and Halifax Formations (up to 10-14 km combined thickness; Fig. 1.1) makes up the bulk of the stratigraphic section of the Meguma Terrane, which includes the younger (pre-Carboniferous) White Rock, Kentville, and Torbrook Formations (Schenk, 1981).

The older basal Goldenville Formation consists primarily of metagreywacke and feldspathic quartzite, while the conformably overlying Halifax Formation is comprised of thin-bedded grey to black slate, metasiltstone, and minor quartzite (Taylor and Schiller, 1966). The Cambro-Ordovician age for the Meguma Group has been derived from the rare occurrences of the graptolite _Dictyonema flabelliforme_ (Eichwald) in the Halifax Formation (Schenk, 1983).

The boundary between the Goldenville and Halifax is transitional in nature, notably with increasingly frequent occurrences of argillaceous beds toward the top of the Goldenville. A value of ~1 for the ratio of sandy to shaley beds has been taken by some workers as the boundary between the two Formations (Schenk, 1970). In addition, this transitional portion of the section is manganiferous and/or carbonaceous at many localities, and hosts a remarkably high proportion of the mineral deposits (Au, W, Sn, Zn-Pb) in the Meguma Group compared to its limited stratigraphic thickness (Zentilli _et al._, 1984). Hence, while it cannot be

-8-

classified as a separate Formation, due to poorly defined limits (simply a transitional section at the top of the Goldenville and the base of the Halifax), and often not comprising a regionally mapable thickness, Zentilli *et al.* (1984) have suggested that this transition be studied as a distinct unit, the Goldenville-Halifax Transition (GHT).

2.2.2 Structure

The most obvious artifacts of the Acadian deformation are the northeast-striking folds (F_I) of the Meguma Group (Fyson, 1966). These tight, isoclinal, slightly plunging folds result in repeated sections of the GHT (at the surface) lying parallel to strike (Fig. 1.1). On the hand sample scale, the associated axial planar cleavage (S_I) is most noticeable in more argillaceous layers.

Smaller folds (F_2) and kink bands (F_3) have been identified as younger than F_I by Fyson (1966). In addition, the F_I folds are locally offset by up to kilometers by northwest striking left lateral strike-slip faults.

Chapter 3

Local Geology

The Eastville deposit incorporates a 10 km, northeast-striking section of the GHT (Fig. 3.1). The Meguma rocks are terminated by the Liscomb granitoid pluton to the south, east, and possibly north (Cameron, 1985). The western extremity of the map area is unconformably overlain by Carboniferous Windsor Group evaporites and sandstones of the Shubenacadie Basin.

3.1 Metamorphism and Structure

The metamorphism of the deposit has been studied in detail by Cameron (1985). The Meguma rocks contain coexisting metamorphic chlorite, biotite, and spessartine garnet, indicating a regional metamorphic grade in the biotite zone of the chlorite facies. The contact metamorphic assemblage:

almandine garnet + biotite + quartz

± staurolite ± andalusite

is found in the Meguma slates and metawackes adjacent to the pluton.

Comprising the northwest limb of a large syncline, the Goldenville metawackes and Halifax slates dip ~45°S in the southeast section compared to dipping steeply or being slightly overturned in the northeastern section (Fig. 3.1).

-10-
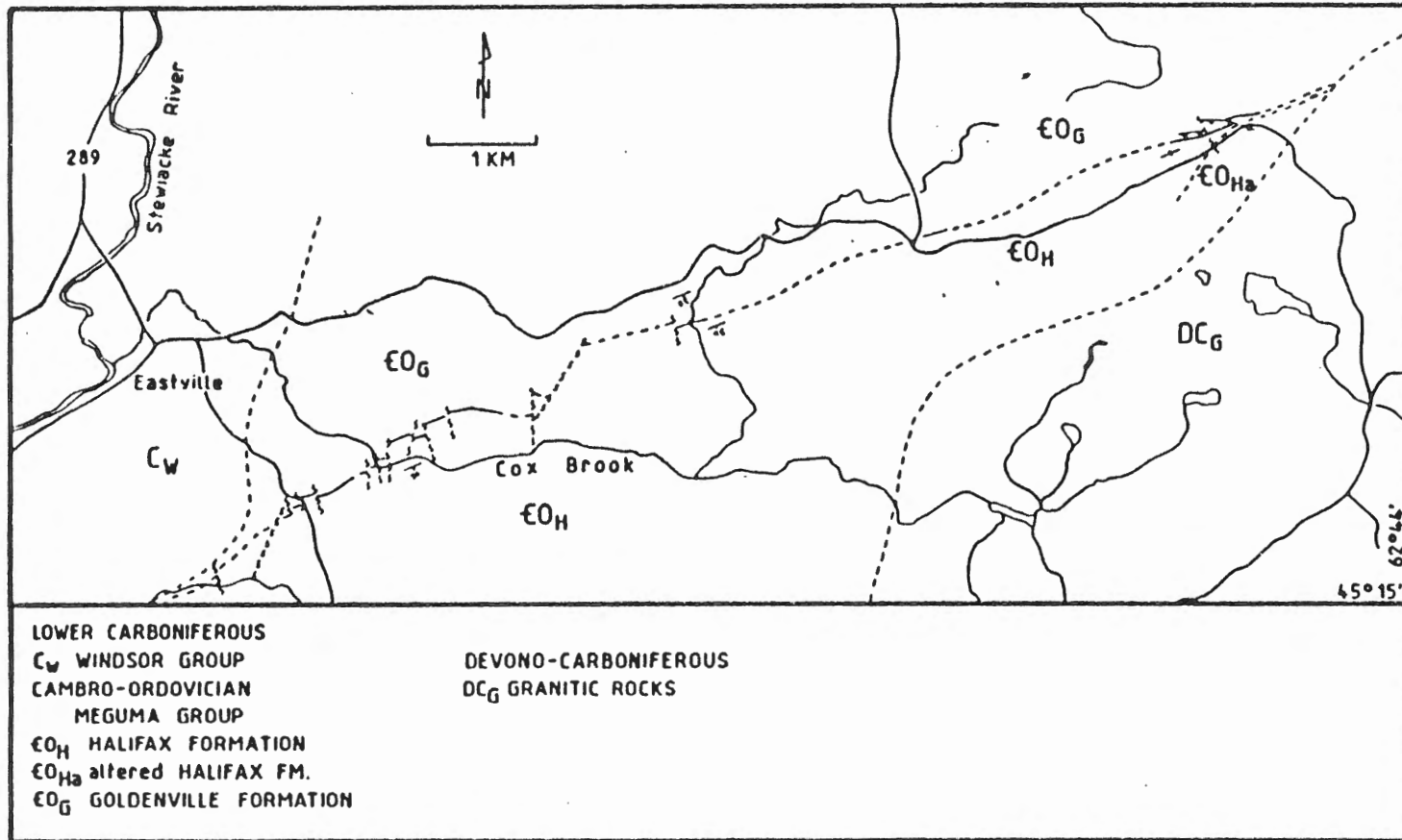
Figure 3.1 Geological map of the Eastville prospect.

Hence, the prominent axial planar slaty cleavage (S_1) is generally oriented sub-parallel to the bedding. A second, weaker foliation (S_2) oriented at a high angle to the bedding and S_1 is suggested by a lineation in drill core samples.

The western portion of the GHT is transected by several northwest trending strike-slip faults with up to hundreds of meters of left-lateral offset. A large low-angle reverse fault cutting the eastern section of the GHT is evidenced in magnetic profiles, and directly as lithified fault gouge and competent blocks of up to tens of cm in size in diamond drill hole 28. Deformed andalusites within these blocks might suggest that this fault postdates the apparently Devonian contact metamorphism due to granite emplacement, but deserves closer study for confirmation. Repeated sections of the stratigraphy in some eastern drill holes suggest the presence of other thrust faults.

In the contact aureole, the shaly beds are commonly present as schists. These are pervasively crenulated, possibly as a result of the emplacement of the pluton. Cameron (1985) also pointed out that the pluton itself is deformed.

3.2 Stratigraphy

The Sulpetro diamond drill holes penetrated a maximum of about 150 m for each of the upper Goldenville and the base of the Halifax. Logging of this section revealed the

-12-

presence of five conformable lithological stratigraphic units - three sandy and silty units of the Goldenville Formation, and two shaly units of the Halifax Formation (Fig. 3.2, and Fig. 3.3). The units are described below in order of decreasing geological age (compiled from this work, Jenner (1982), and Binney (1979)).

3.2.1 Goldenville Formation

3.2.1.a Unit 1 - Massive Quartz Metawacke (*MQM*)

This unit is comprised of a monotonous sequence of massive, grey-green fine-grained (~0.05 mm), recrystallized quartz metagreywacke. Abundant metamorphic chlorite and minor muscovite define the foliation and wrap around pre-tectonic idiomorphic to subidiomorphic *spessartine* (Mn-rich) garnet (~0.1 mm) and biotite. The unit contains mm-sized ("slatey") layers rich in chlorite and garnet revealing bedding and cross-bedding on a cm scale, contrasting with the thickly bedded sequences in "typical" Goldenville sections from Taylor Head described by Liew (1979). Folding of these layers in thin section testifies to the scale at which the regional deformation can be seen. About 1 percent (by volume) opaques are present, consisting primarily of pyrite and minor low grade graphite.

The thickness of the argillaceous silty layers increases up section.

3.2.1.b Unit 2 - Interbedded Zone (*IZ*)

The overlying Interbedded Zone is similar to Unit 1

-13-

			THICKNESS (metres)
	HALIFAX FORMATION	BLACK SLATE AND FINE-LAMINATED TO CROSS-BEDDED QUARTZ WACKE.	+150
		Black, pyrrhotitic slate	0-10
	GOLDENVILLE FORMATION	Mn Zone — Thin, contorted interbeds of calcareous, manganiferous quartz wacke, and black slate.	7-10
MEGUMA GROUP		INTERBEDDED ZONE - MASSIVE QUARTZ WACKE AND INTERBEDDED BLACK SLATE.	30-35
		MASSIVE QUARTZ WACKE	+30

Figure 3.2 Schematic stratigraphic section of the GHT at Eastville
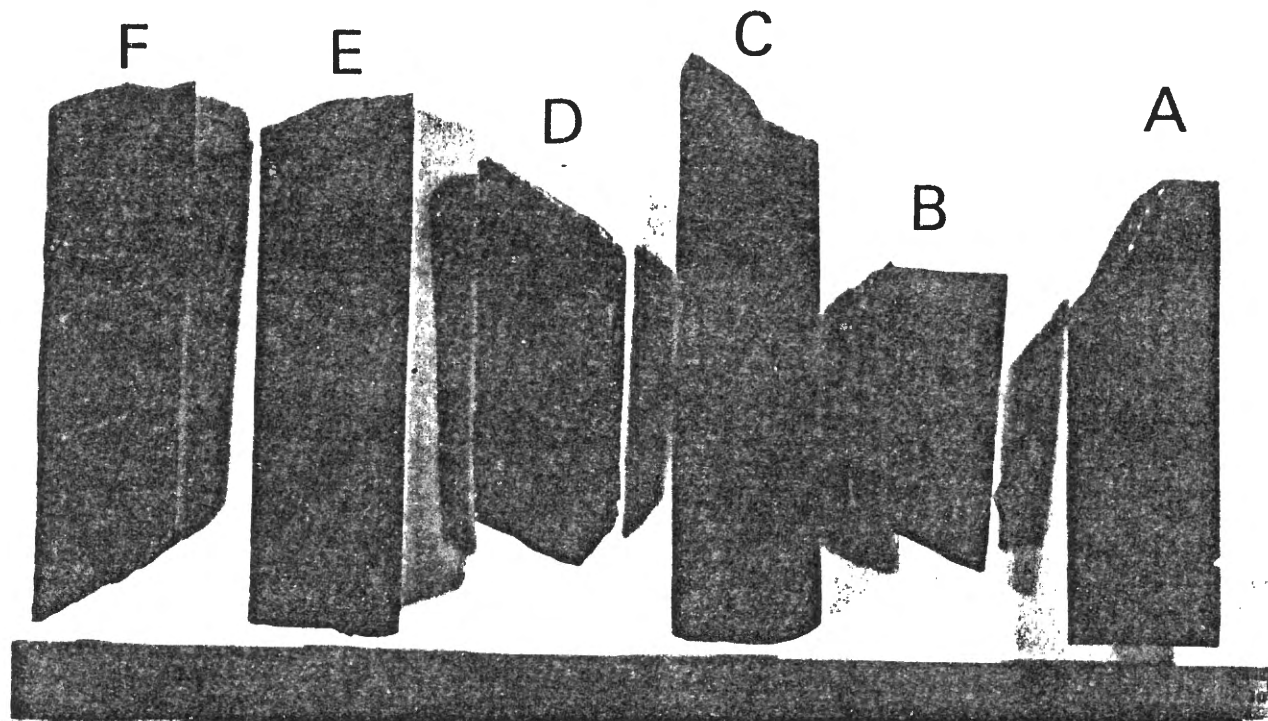
Figure 3.3 Samples from the GHT at Eastville (cm scale is provided). (A) Massive Quartz Metawacke displays very fine cross bedding. (B) Example from the Interbedded Zone contains a dark bleb. (C) Highly contorted, finely laminated Manganese Zone. (D) Sample of MZ from very close to the Black Slate unit (ie. at the Goldenville-Halifax contact). (E) Black pyrrhotitic slate from the BS. (F) Slate and metawacke beds from the Halifax Slate.

except that the shaly and quartzitic layers are found in similar proportions. The finely laminated grey to black argillite interbeds range from 2 to 30 cm in thickness.

The mineralogy of this unit is similar to that of *MQM* with the exception that spessartine garnet is rare, and pyrrhotite, both disseminated and in mm sized blebs, constitutes up to several percent (by volume) of the rock. The abundance of carbonaceous material in many of the argillaceous layers (increasing up section) contributes strongly to the banded appearance of the rock.

3.2.1.c Unit 3 - Manganese Zone (*MZ*)

The Manganese Zone is the most striking , and variable unit at Eastville. It is locally calcareous, and is more regularly banded than the underlying *IZ*, with layers generally being less than ~2 cm thick. The bands range from white quartzite to grey slate and finely interlaminated black slate and pyrrhotite. The most outstanding feature of the *MZ* is that many of the bands are ptygmatically folded, leaving nearby layers apparently undisturbed (Fig. 3.4, 3.5).

The whitest quartzite bands are composed almost exclusively of recrystallized quartz and idiomorphic spessartine garnet (up to 50%). At the edges of these bands the garnets are commonly found in linear clumps leading away from the interface with more argillaceous layers (ie. perpendicular to the bedding). The shaly layers are composed

-16-

DR. MARCOS ZENTILLI
DEPT. EARTH SCIENCES
DALHOUSIE UNIVERSITY
HALIFAX, N.S., B3H 3J5
CANADA
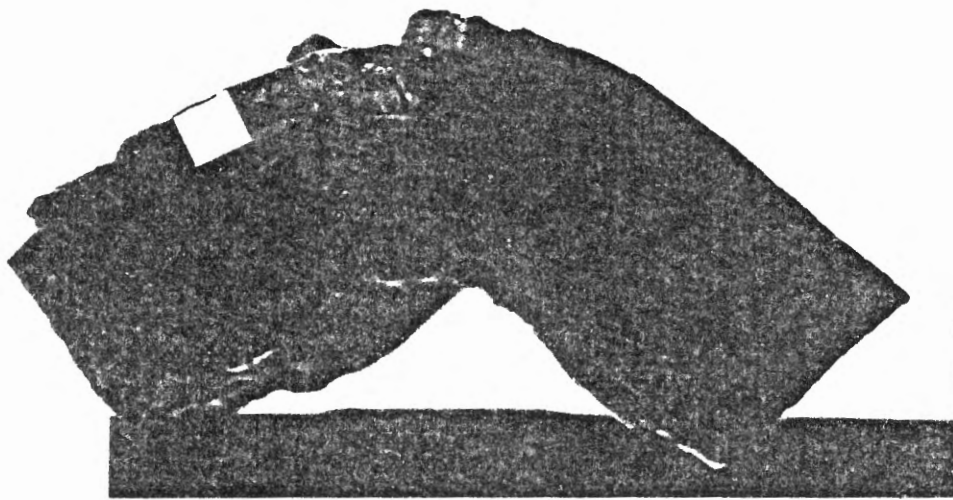
Figure 3.4 Ptygmatic folding is superimposed upon a larger fold. The ptygmatic folding of the finer layers does not affect the surrounding thicker layers. Square is 1cm on each side.

Figure 3.5 Thin-section of a ptygmatically folded layer
(not the same sample as Fig. 3.4). Note the fine
layering and the presence of alternating dark and light
coloured "blocks" or boudins in the folded layer. White
square is 1cm on each side. Arrows point up section.

of white mica, biotite, quartz, and poorly crystallized carbonaceous material in the groundmass. The fine foliation is deflected by spessartine garnets (up to 50 % by volume) which are slightly smaller than those in more quartz-rich layers. These garnets often have pyrrhotite cores or tend to be clustered around pyrrhotite blebs. The garnets are commonly more densely distributed near the edges of the slate layers, being associated with a chlorite matrix.

Study of the *MZ* unit is complicated by the presence of a diverse assemblage of opaque minerals (see Section *4.2* for compositional details). Pyrrhotite and minor pyrite form up to 5% of some bands, often concentrated as elongate blebs at the interface between layers. Carbonaceous material obscures the mineralogy in thin section, but is not observed in reflected light. Small amounts of sphalerite, galena, ilmenite, and rutile are also present. Galena occurs as tiny isolated cubes or within sphalerite blebs. The sphalerite (up to 5% by volume) is identified by its amber to yellow-green colour in transmitted light, but is often obscured by carbonaceous matter. Sphalerite occurs as disseminated blebs and is even found in the cores of some garnets. Elongate blebs of sphalerite appear almost identical to prisms or laths of ilmenite under reflected light. Xenoblastic rutile appears blood-red in transmitted light.

Another unique characteristic of this unit are beds comprised of alternating dark and light coloured

equidimensional segments or "blocks" (Fig. 3.4, 3.5). These beds are generally contorted. The light coloured blocks consist almost entirely of quartz, either as small recrystallized grains or as strained, elongated grains which are oriented either parallel to or perpendicular to the bedding (Fig. 3.5). The dark blocks cover a continuum in composition. At one extreme are segments consisting of carbonate, quartz, micas, opaques (carbonaceous matter, ilmenite, and pyrrhotite blebs), and minor spessartine garnet. These sometimes contain laminations like the regular slaty layers. The blocks at the other extreme are similar to the former but contain densely packed garnets instead of the carbonate, quartz, and micas.

The existence of carbonaceous and carbonate nodules is another remarkable feature of the MZ. Rare black blebs of up to 3 cm are comprised of mainly carbonaceous material and very fine quartz grains (actually found at the top of IZ and the base of MZ). The carbonaceous material in one such bleb appears to have "flowed" along the crenulation in the surrounding metawacke. One black bleb was found to be surrounded by a 2 mm rim of very fine crystals of carbonate and minor quartz. This rim might be an intermediate to the more common carbonate nodules or concretions of similar composition. The carbonate nodules range from 2 mm to 1 cm in size. It appears that beds containing carbonate nodules have higher sphalerite and galena contents.

3.2.2 Halifax Formation

3.2.2.a Unit 4a - Black Slate (*BS*)

Compared to the boundaries between units 1, 2, and 3, the boundary between the Manganese Zone and the Black Slate (ie. between the Goldenville and Halifax Formations) is very sharp. Over as little as 1 meter, the core changes from contorted, locally calcareous interbedded argillite and metawacke to pyrrhotitic black slate.

The very fine grained quartz, and muscovite in the matrix of the unit are completely obscured by carbonaceous material (up to 10-15 volume %). Unlaminated beds of up to 5 cm in thickness consisting of chlorite "spots" and disseminated sphalerite and pyrrhotite blebs within this black matrix are common. Examples of these beds finely interlaminated (on the mm scale) with more silicious layers, and sulphide blebs, or continuous beds are also prominent. The sulphide layers are contorted at the base of the unit.

Sulphide minerals are prominent in this unit. Pyrrhotite makes up to 10 % of the rock. Larger blebs (> 0.5mm) and sulphide beds are composed of pyrrhotite, pyrite cubes, sphalerite (up to 50 %), and minor galena.

Spessartine garnets are rare in the *BS*, being found predominantly in association with pyrrhotite, either as clusters around blebs or having pyrrhotite cores. The garnets have inclusions of carbonaceous matter.

3.2.2.b Unit 4b - Halifax Slate (*HS*)

A reduction in the amount of graphitic material and the

-21-

presence of more prominent metawacke beds signal the beginning of the more typical slates of the Halifax Formation. The unit consists of fine grained grey to black slate, interbedded with coarser grained quartz metawacke.

The massive to finely laminated slates have a muscovite-rich groundmass which is darkened by carbonaceous material, and overprinted by chlorite and spessartine garnet (<5%). Garnets and sulphide blebs have pressure shadows of recrystallized quartz. The garnets commonly have graphitic material, pyrrhotite, sphalerite, or galena as cores or spectacularly aligned along crystallographic directions.

The metawackes have pyrite and pyrrhotite mineralization concentrated along both laminated and cross bedding structures. These beds are dominated by quartz with lesser amounts of muscovite. Garnets are smaller and less abundant than in the argillaceous layers.

The *HS* also contains rare beds are up to 5 cm thick, consisting of contorted layers of recrystallized quartz interbedded with fine layers of carbonaceous material. These are probably quartz veins similar to those described by Graves and Zentilli (1982).

3.2.3.b Lateral Variation in Stratigraphy

Figure 3.6 displays the variation in the thickness of each unit across the strike of the entire deposit. The drill log depths have been corrected for drill-bedding angles other than 90°. The base of the Black Slate unit was used as a datum in the plotting.
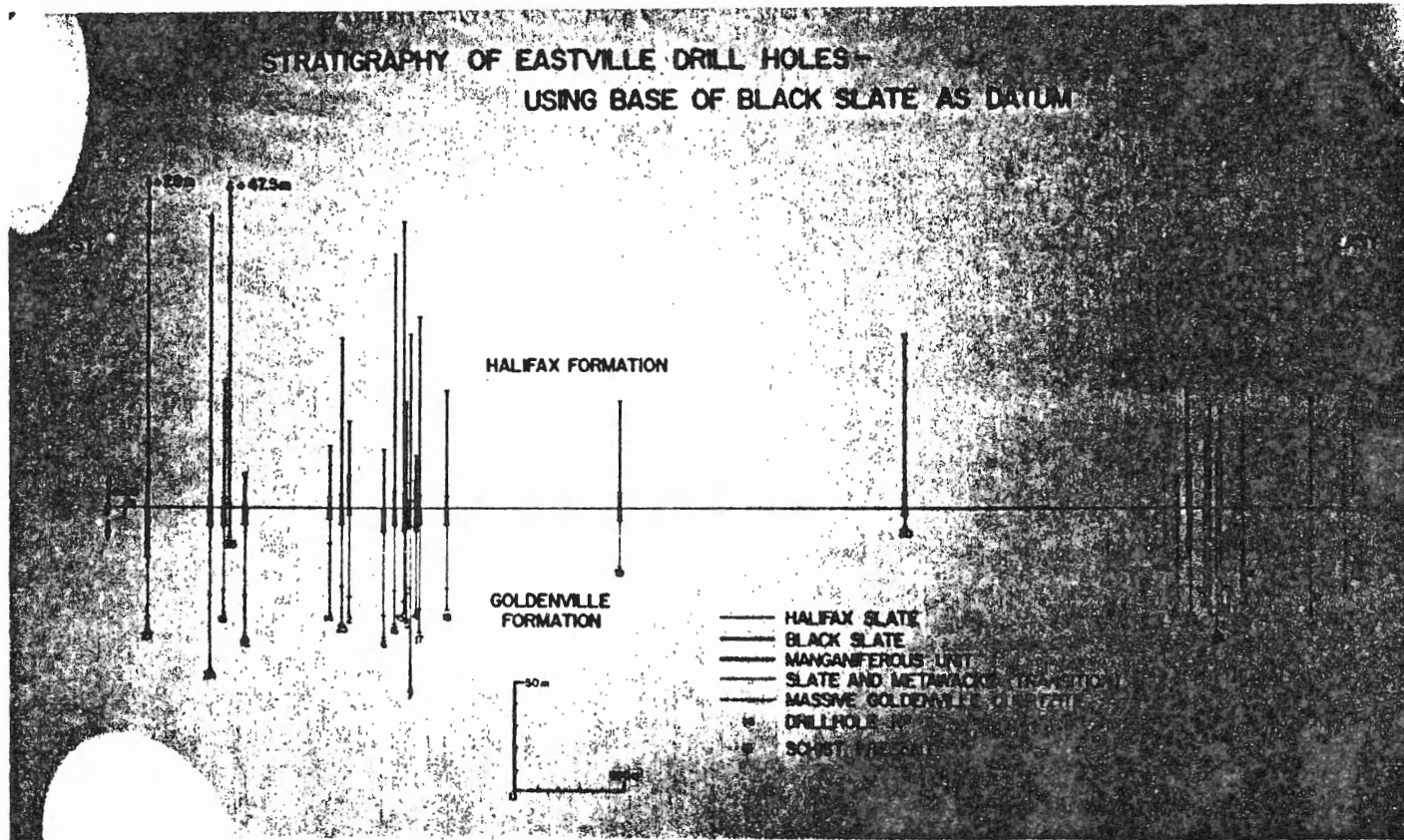
Figure 3.6 Lateral variation in stratigraphy over the
length of the deposit. Drill core distances have been
corrected for drilling angles, and the base of the
black slate has been given a value of 0.0m

While there is some variation in the thickness of the units, no consistent trends can be found to give evidence for large scale sedimentary structures, such as channels or sub-basins. In fact, the units are relatively uniform in thickness considering the length of the deposit.

It should be noted that the absence of units from some drill holes (eg. 23 and some of the eastern holes) can be explained by faulting. The contact metamorpism of the eastern sections also makes it difficult to distinguish the Goldenville units. In addition, the Manganese Zone in the eastern drill holes does not contain any carbonate cement, but does display the characteristic contorted, fine bedding.

3.3 Styles of Sulphide Mineralization

Sulphide mineralization at Eastville consists primarily of pyrrhotite, pyrite, sphalerite, galena, and minor chalcopyrite and arsenopyrite. The main styles of mineralization are: stratiform, disseminated, foliation controlled, and fracture or vein filling (Jenner, 1982) (See Fig.3.7).

Pyrrhotite and associated pyrite are the predominant stratiform sulphides, forming lenses and continuous laminae conforming with the bedding. Jenner (1982) indicated that the nature of intergrowths of the iron sulphides suggests the metamorphic growth of pyrrhotite from pyrite.

Stratiform sphalerite and galena are not as common as the Fe sulphides. Sphalerite occurs as independent lenses or

-24-
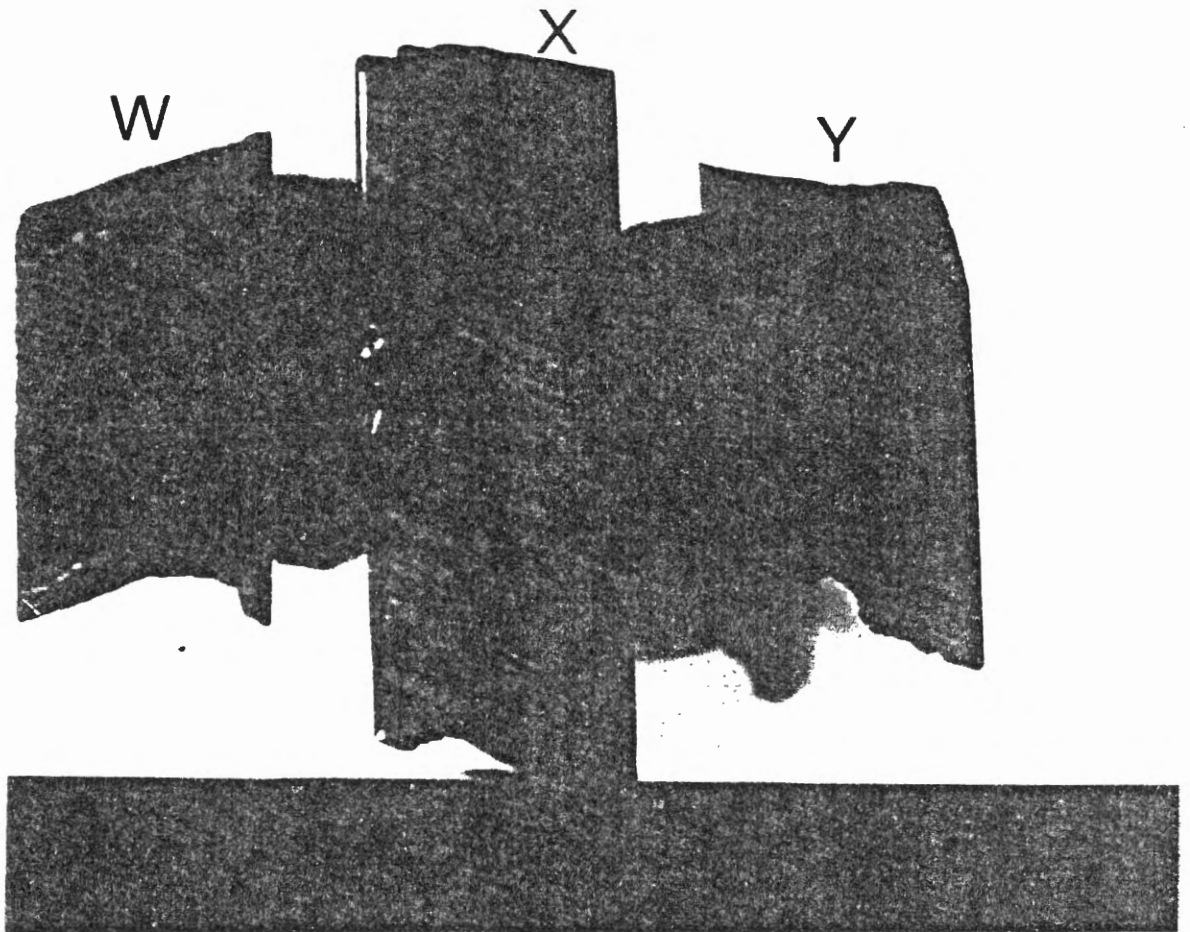
Figure 3.7 Styles of sulphide mineralization (cm scale is provided). (W) Bedded sulphides. (X) Pyrrhotite bed has been transposed along the foliation. (Y) Sphalerite and galena are shown in veinlets and open fractures.

in intergrowths with iron sulphides and galena, primarily in the Black Slate and Halifax Slate. One notable case found within the Halifax Slates consists of a 2 cm nodule with pyrrhotite, sphalerite, and carbonate in the core, rimmed by sphalerite, and by a second rim of pyrrhotite.

Disseminated pyrrhotite and pyrite occur predominantly as flecks within the MQM, BS, and HS. Sphalerite and lesser galena disseminations are found primarily in the more graphitic MZ sections and the BS and HS.

Many sulphide blebs, lenses, and beds are found to be transposed into the foliation, in cases to the extreme shown in Figure 3.7. Sphalerite is also found along kink bands, and as extensive smears along well developed cleavage surfaces.

The highest concentrations of sphalerite and galena exist in veins and fractures. Coarse grained sphalerite and galena are found in fractures; these in some samples join larger calcite veins. Pyrrhotite, pyrite, sphalerite, and galena also occur in quartz-feldspar veins.

It is noteworthy that vein and fracture related sulphide concentrations are highly dependent on the physical properties of the rock. For example, veins are not common in the Black Slate, presumably due to the ductile properties of this unit.

The most outstanding lead-zinc mineralization occurs where drill hole 28 transects the normal fault in the eastern section of the deposit. However, it appears that the

mineralization is concentrated within the competent blocks

of black slate rather than within the fault itself.

3.4 Discussion

The Goldenville units at Eastville represent a rather

rapid trend toward a more argillaceous, carbonaceous, thinly

bedded protolith, culminating in the composition of the

Black Slate. Even the Massive Quartz Metawacke contrasts

with the thickly bedded "typical" Goldenville quartzites

from Taylor Head described by Liew (1979). The buildup in

presumably pelagic organic material in the *BS* suggests that

this trend reflects a decreasing sedimentation rate toward

the top of the Goldenville in the GHT (ie. sediment

starved). The Halifax Slates seemingly represent a return to

higher sedimentation rates and a new sediment transport

mechanism or source owing to the high proportion of slate

compared to the *MQM*.

Coticule is a descriptive term used for spessartine

quartzites, such as the white beds found in the Manganese

Zone (Kramm, 1976; Schiller and Taylor, 1965) The literature

also reports that such coticules are generally highly

contorted. The genesis of coticules is under debate,

however, some preliminary ideas on the Eastville *MZ* can be

deduced at this point.

The contorted bedding and "blocky" beds represent a

structural problem. Ptygmatic folding would be expected in

the cores of concentric folds such as shown in Figure 3.3.

-27-

Boudinage in less ductile beds within such folds could have produced the garnet or carbonate "blocks" separated by infilled recrystallized quartz. However, it should be noted that the sharpness of the boundaries of the folded beds might indicate that the boudinage had occurred prior to the folding of the bed. A more detailed study of the microstructure would be needed to confirm the possibility of an earlier folding or extensional event.

The pre-tectonic growth of the spessartine garnets is indicated by the fact that the foliation wraps around the grains.The occurrence of both carbonate- and garnet-rich segments in similar "blocky" beds of the *MZ* suggests that carbonate is one of the reactants in the metamorphic growth of the spessartine garnet. The absence of carbonate in the Manganese horizon in the contact metamorphosed eastern cores might also reflect the metamorphic consumption of carbonate. A relationship with carbonaceous matter might be inferred from the presence of carbonate nodules and the carbonate rim surrounding one carbonaceous bleb (see Sec 4.3.3).

Inclusions of sulphides in garnet cores reflect their presence in the rocks before the metamorphic growth of the garnets. Stratiform and disseminated sulphides indicate a syn-sedimentary or diagenetic origin. However, much of the sphalerite and galena seem to have been remobilized into fractures and veins. This unfortunately makes studies of the the variation of Zn and Pb with respect to other metals in the original stratigraphy difficult.

Chapter 4

Geochemistry

Three areas of chemical analysis and study have been carried out on the Eastville drill core.

Bulk samples for consecutive 1-3m sections of the drill core from 25 of the bore holes were prepared by Sulpetro Minerals. Acid leachable Pb, Zn, Fe, Mn, As, Ba, and Sr were analysed using atomic absorption spectroscopy by Bondar-Clegg of Ottawa. Holes 24 and 25 were chosen for more detailed analysis on the assumption that they fell outside the metamorphic aureole of the pluton (see Cameron, 1985) . Whole rock analysis for 48 elements in fifty of the bulk powders from these two holes was performed by X-Ray Assay Laboratory of Toronto in 1983 (see Appendix 2).

A limited amount of mineral chemistry data were collected using the Electron Beam Microprobe in 1985.

Carbonate cements, veins, and blebs were analysed for C and O isotopes in 1984.

4.1 Bulk Geochemistry

4.1.1 Acid-Leach Data

Weighted averages based on the length of drill core sampled (to compensate for irregular sample intervals) for acid-leachable Zn and Pb over *all* (25) of the sampled drill holes are given in Table 4.1.

-29-

Table 4.1
Weighted averages for acid-leachable Zn and Pb.

Unit	Pb /ppm	Zn /ppm	Zn/Pb
Halifax and Black Slate	910	1950	2.1
Black Slate	460	1060	2.3
Manganese Zone	1400	3130	2.2
Interbedded Zone	1930	3570	1.8
Massive Quartz Metawacke	370	920	2.5

The data reveal a considerable enrichment in Zn and Pb in the upper Goldenville units. The entire section of GHT at Eastville is enriched by greater than an order of magnitude in these metals when compared with an average of ~84 ppm for Zn in "typical" slates and metawackes of the Goldenville at Taylor Head (Liew, 1979). In addition, the Zn:Pb ratio is remarkably constant at ~2.2 over the different units, reflecting the strong correlation between the two elements ($r > 0.95$ with $> 99.9\%$ confidence). Figure 4.1 reveals that, except for an increase near the pluton, the average Zn:Pb ratio for each drill hole remains close to 2.2 over the length of the deposit.

Acid-leach data for the same 50 samples as were analysed for whole rock chemistry are tabulated in Appendix 4.1, with summary statistics being presented in Appendix 4.2. The data reveal that Sr and Mn are strongly dependent on the stratigraphy (see also Fig. 4.2 and the next section). Sr increases by up to half an order of magnitude

-30-
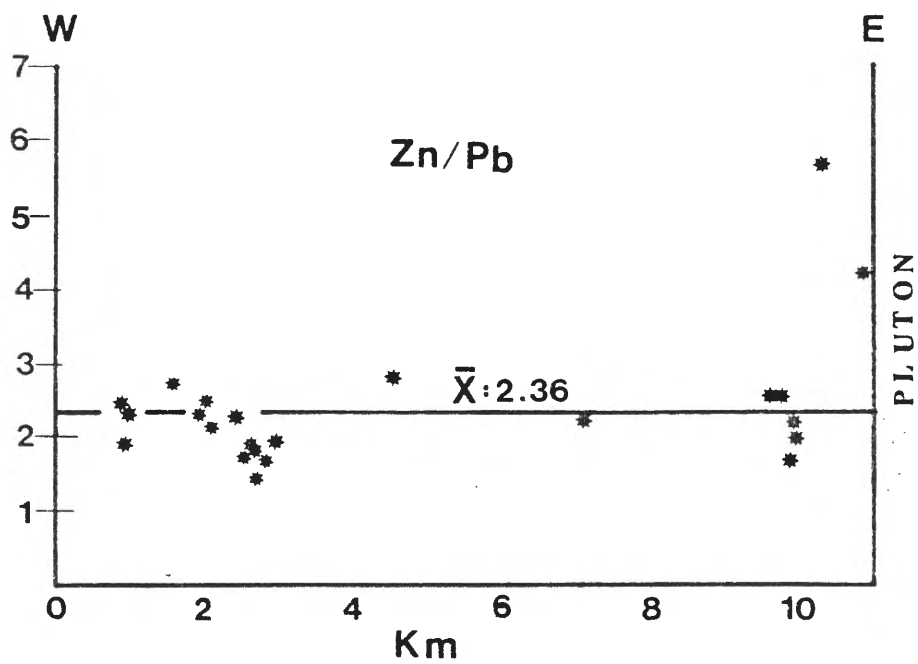
Figure 4.1 Zn/Pb ratios for each drill hole plotted against
the position of the hole relative to the pluton. With
the exception of the drill holes closest to the
granite, the ratios are very constant. The high values
could be due to the contact metamorphism.

in the Halifax Slates over its concentration in the underlying units. Mn is enriched (up to 2 Wt%) in the Manganese Zone, again by up to half an order of magnitude. The manganese contents are slightly lower near the pluton contact, but even a minimum of 0.30 Wt% for the *MZ* in the eastern drill holes constitutes an anomally over 0.09 Wt% (Liew, 1979) for the Goldenville at Taylor Head.

4.1.2 Whole-Rock Data

The results from the whole rock analyses for drill holes 24 and 25 are displayed in Appendix 4.3. Summary statistics are presented in Appendix 4.4, and mean values for selected elements from the Eastville units and some other study areas are found in Table 4.2.

It is noteworthy that, with the exception of manganese, the acid-leachable data are in strong agreement with the whole rock analyses. The whole rock analysis reveals a Mn content of one order of magnitude higher than that detected by the acid-leach method. It is probable that the acid-leach method excludes the element content of the more insoluble components of the rock, such as garnet. Hence, the correlation between the two analyses suggests that the elements Pb, Zn, Fe, As, Ba, and Sr are to a large degree confined to carbonates, sulphides, micas, and possibly oxides.

The variation in *whole rock* MnO, Sr, and Zn+Pb with respect to the stratigraphy is presented in Figures 4.2-4.4.

-32-

Table 4.2

Selected element averages for Eastville and comparison deposits.

Modersiebet (handwritten annotation above MZ/IZ)

	HS	BS	MZ	IZ	Gdv	Andros	Ardennes
SiO_2	59.14	54.88	49.71	60.59	76.62	63.56	70.49
TiO_2	1.05	1.03	0.99	0.88	0.59	0.46	1.17
Al_2O_3	22.53	20.45	17.42	19.92	11.99	9.97	17.50
Fe_2O_3*	8.75	12.04	13.97	8.63	4.18	7.23	0.79
MnO	0.32	1.96	9.68	0.72	0.05	13.67	5.61
MgO	2.13	2.34	3.20	2.74	1.28	1.16	1.03
CaO	0.80	2.33	2.63	1.11	0.28	2.30	0.45
Na_2O	1.13	0.61	0.11	0.74	2.88	1.41	1.13
K_2O	4.04	4.18	2.02	4.51	2.03	0.12	1.66
P_2O_5	0.11	0.19	0.27	0.15	0.10	0.11	0.16
TOTAL	100.00	100.00	100.00	100.00	100.00	100.00	100.00
n	23	5	8	14	4	5	3
Ni	56	80	116	62	20	19	99
Zn	3682	2290	1699	3770	60	57	89
Cr	145	156	151	116	74	59	NA
Y	14	18	16	7	22	43	NA
Zr	181	160	146	141	201	105	NA
Ba	947	1032	725	1253	518	177	1012
Cu	58	86	64	76	14	32	23
Pb	1558	995	483	1664	15	14	NA
Sr	347	174	28	61	182	53	278
Rb	155	148	58	140	74	4	98
V	138	176	89	156	82	76	NA
Th	11	10	9	9	6	6	NA
As	33	146	118	39	41	58	NA
Zn/Zn·Pb	0.70	0.70	0.78	0.69	0.80	0.80	

NOTES:

All major elements recalculated to 100% (volatile-free).

HS: Eastville Halifax Slate averages (see Appendix 4.4).

BS: Eastville Black Slate averages (see Appendix 4.4).

MZ: Eastville Manganese Zone averages (see Appendix 4.4).

IS: Eastville Interbedded Zone averages (see Appendix 4.4).

Gdv: Quartz metawackes from the New Harbour Member of the Goldenville Fm: Green Bay Nova Scotia (Zentilli, et. al., 1986).

Andros: Spessartine quartzite, from island of Andros, Cycladic Blueschist Belt, Greece (Reinecke, et. al., 1985).

Ardennes: Spessartine quartzites from Ardennes, Belgium (Kramm, 1976).

$Fe_2O_3* = $ total Fe expressed as Fe_2O_3.

Oxides given in Wt%.

Trace elements given in ppm.

DR. MARCOS ZENTILLI
DEPT. EARTH SCIENCES
DALHOUSIE UNIVERSITY
HALIFAX, N.S., B3H 3J5
CANADA

Figure 4.2 shows an almost identical variation in Mn with stratigraphy between the two drill holes. The 10-fold enrichment in Mn in the Manganese Zone (MZ) is most striking. It is also interesting that the lower portions of the Black Slate unit are also somewhat enriched in Mn.

The variation of Sr with stratigraphy (Fig. 4.3) is the opposite of that for MnO. Strontium is depleted in the MZ and rapidly increases by greater than a factor of 5 up section. The variation between drill holes is revealed by the fact that Sr increases more rapidly upward through the lower Halifax Slates followed by a gradual decline in concentration found in Hole 24, compared to the more gradual increase and higher peak value found in Hole 25. Available acid-leached samples indicate that further up section Sr does begin to decrease in Hole 25. This might indicate that the scale of some chemical variations (reflecting the scale of sedimentary depositional processes) changes laterally along the GHT at Eastville.

Similar to the acid-leach data, whole rock zinc and lead are very highly correlated. However, the variation in Zn+Pb with stratigraphy is very erratic, probably due to the fact that much of the concentration of sphalerite and galena appears to be structurally controlled. This is supported by the fact that the mean Zn and Pb for the MZ in Holes 24 and 25 combined (Table 4.2) has the lowest Zn and Pb content compared to the other units, while the MZ is the most enriched unit in Zn and Pb over the deposit as a whole

-34-
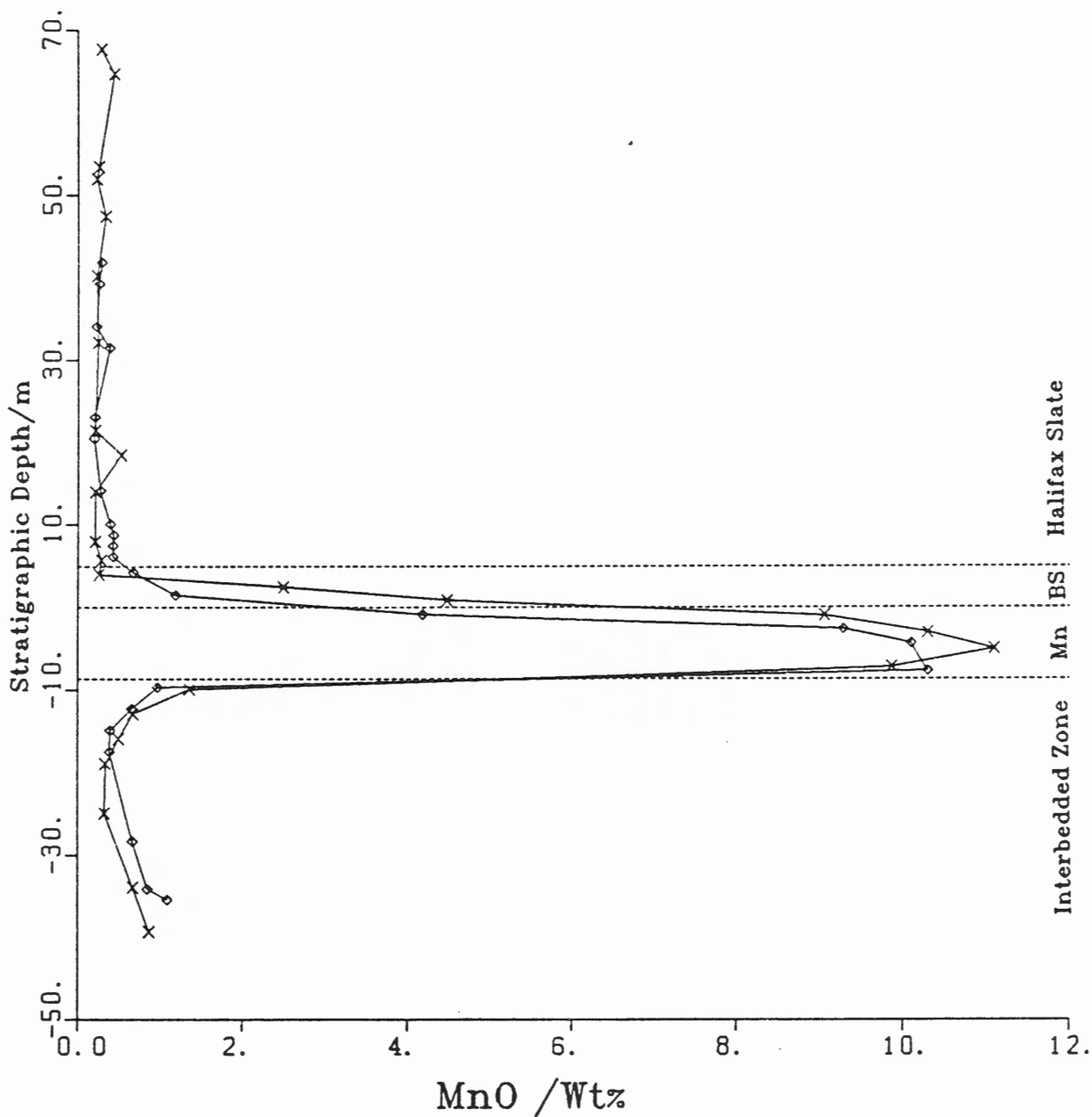
Figure 4.2 Variation in MnO with stratigraphy displays the
    order   of   magnitudeenrichment   in   manganese   in   the
    Manganese   Zone. Diamonds   denote   Hole   25   samples;
    crosses denote Hole 24.
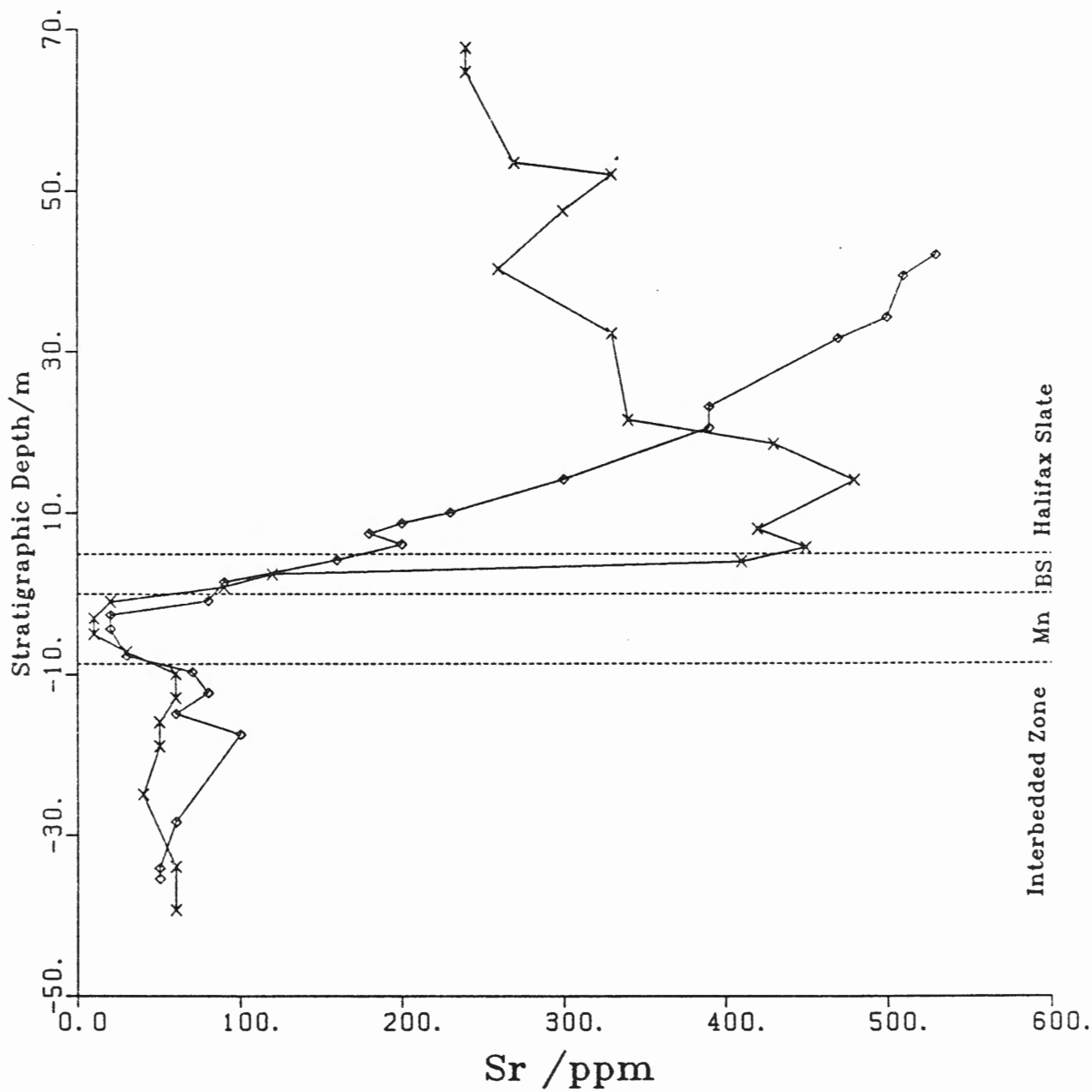
Figure 4.3 Variation in Sr with respect to the stratigraphy. Sr is lowest in the Manganese zone and increases rapidly upward through the Halifax Slate unit. In Hole 25 the increase is less rapid but does not reach a peak as is true for Hole 24. Diamonds denote Hole 25 samples; crosses denote Hole 24.
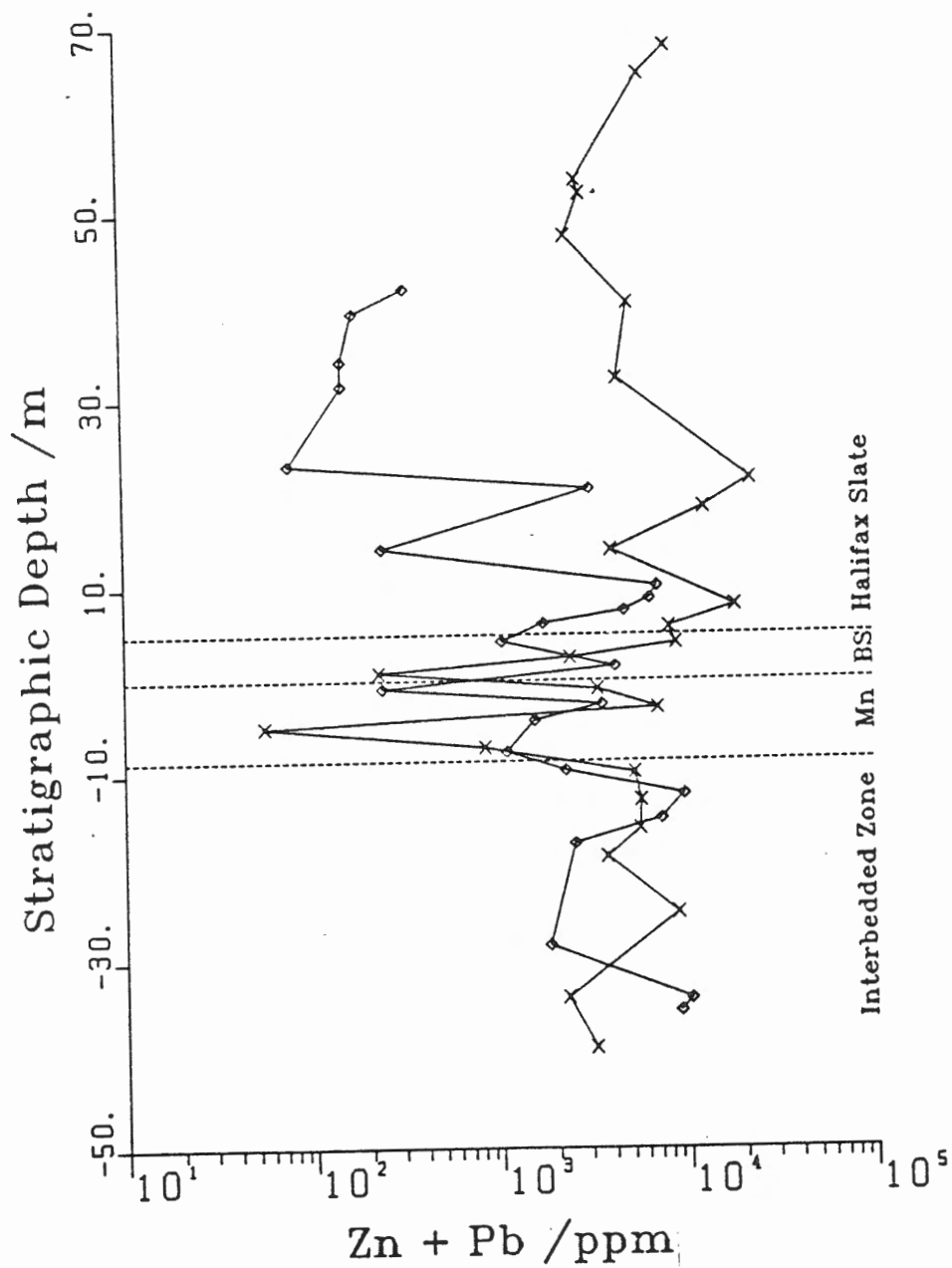
Figure 4.4 Variation of Zn+Pb with stratigrphy. There appears to be no direct relation between Zn+Pb and stratigraphy. Note the large difference in Zn+Pb values for the two drill holes, and the wide variation for samples within the same drill hole. Diamonds denote Hole 25 samples; crosses denote Hole 24.

(Table 4.1).

A triangular plot of SiO_2, Al_2O_3, and total iron expressed as Fe_2O_3* is given in Figure 4.5 as a means of comparing the Eastville Whole Rock composition to different sedimentary rock types. The Eastville rocks lie essentially along the mixing line between terrigenous shales, and quartz (ie. pure sandstone). It is reasonable that the original Eastville sediments were comprised of these components. In addition, the Manganese Zone and Black Slate display a mixing line with a pure, apparently non-detrital, Fe source.

The plot of Al_2O_3 against TiO_2 (Fig. 4.6) also reveals that the Eastville compositions lie near a mixing line for sandstone and pelagic clay and terrigenous material. However, the rocks are more aluminous than the "world" averages. The *MZ* compositions are consistently higher in Ti (for given Al contents) where an influence from the composition of Mid-Oceanic Ridge Basalts might be considered.

It is informative to normalize the data for each unit against a common reference Meguma rock in order to see how the composition of the GHT compares with that of the rest of the Meguma. An ideal reference would be quartz metawacke of the Goldenville Formation, taken stratigraphically well below the GHT. Such analyses are not available for Eastville, and Liew (1979) gives only an incomplete set of data. Hence, analyses from the New Harbour Member of the Goldenville Formation (Zentilli, *et. al.*, 1986) are used.
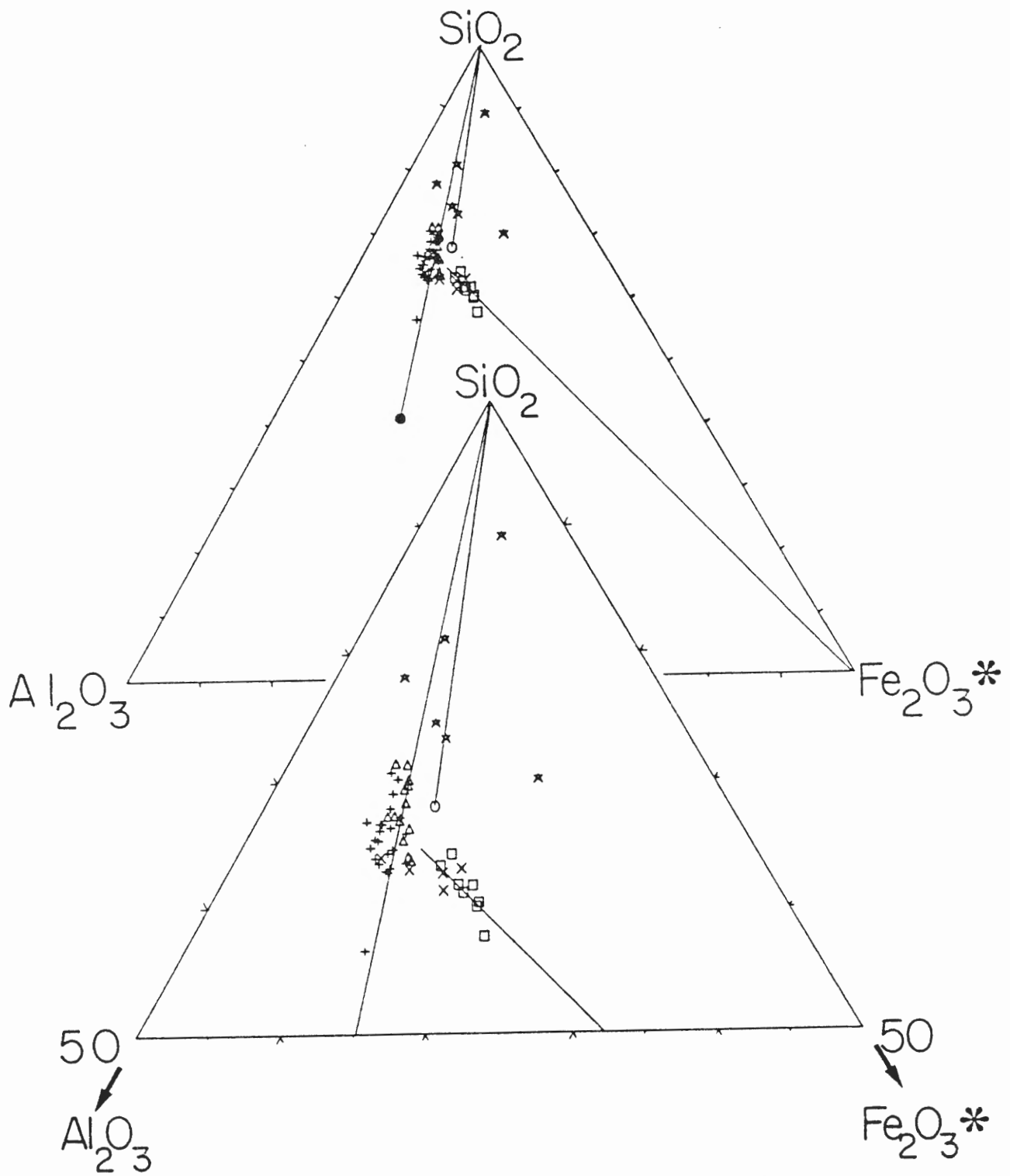
Figure 4.5 $SiO_2-Al_2O_3$-total Fe_2O_3 relations (inset is expanded to 50% SiO_2). Interbedded Zone = △ ; Manganese Zone = □ ; Black Slate = × ; Halifax Slate = + . Open circle is average pelagic clay, and closed circle is average terrigenous shale; both are taken from Turekian and Wedepohl (1961). Stars are spessartine quartzites from Andros, Greece (Reinecke, 1985). Note that the Eastville HS and IZ fall on the shale-quartz mixing line, while the MZ and BS appear to deviate from this trend by mixing with an iron-rich component.

-39-
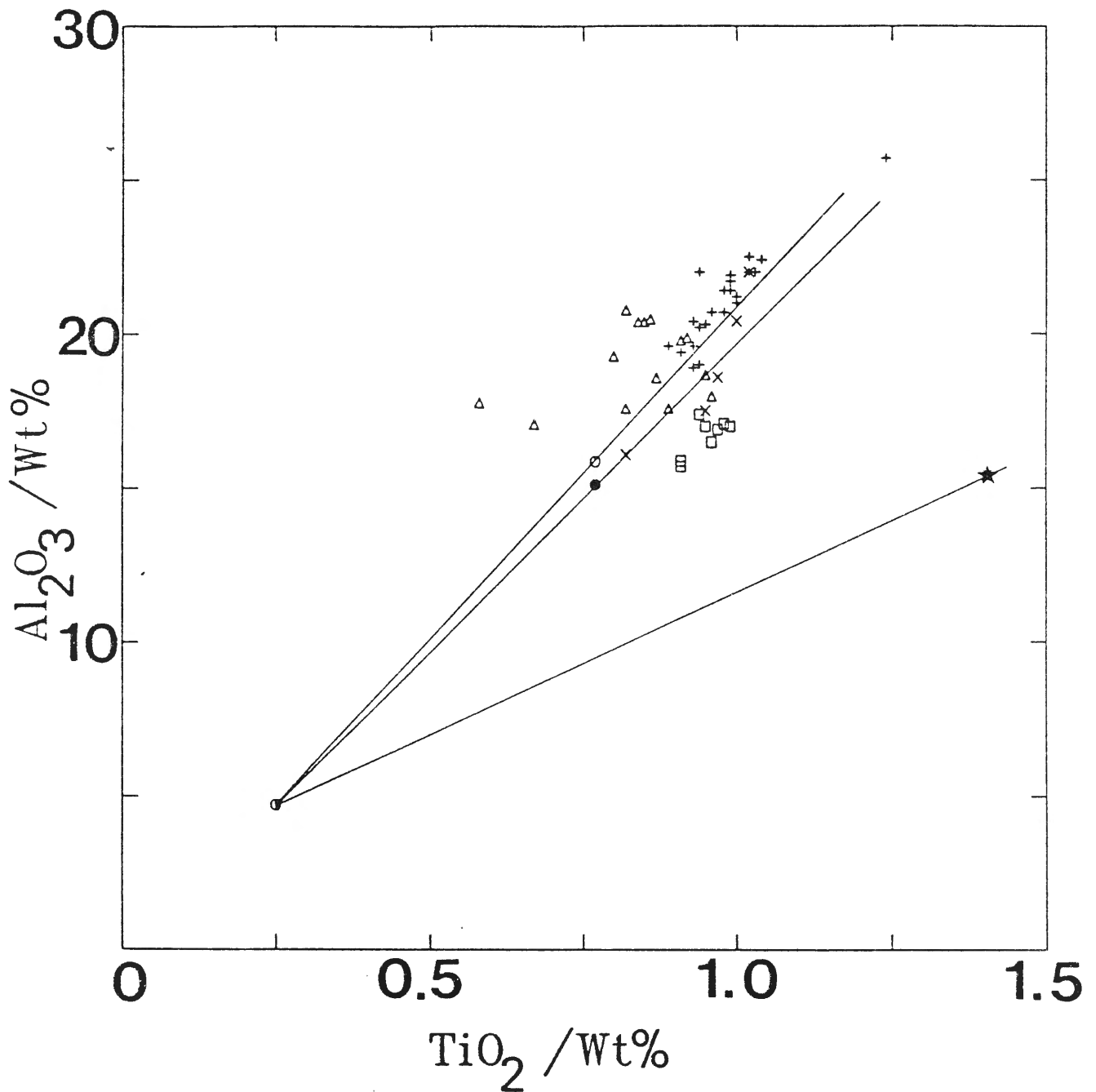
Figure 4.6 Al_2O_3 vs TiO_2. Interbedded Zone = △ ; Manganese Zone = □ ; Black Slate = × ; Halifax Slate = + . Open circle is average pelagic clay, and closed circle is average terrigenous shale, half-filled circle is average sandstone; all are taken from Turekian and Wedepohl (1961); star is average Mid Ocean Ridge Basalt (Reinecke, 1985). The Eastville samples are more aluminous than the references cited, but do line near the shale(and clay)-sand mixing line. Note that the MZ, and BS samples have lower Al (or higher Ti) than the other rock units.

The normalized data for each unit are displayed in Figures 4.7-4.10.

For the Interbedded Zone (Fig. 4.7), Mn is enriched by an order of magnitude, while Zn and Pb are each enriched by two orders of magnitude. There is also a slight enrichment in Ca and Cu, and slight depletion in Na, Y, and Sr.

In the Manganese Zone, Mn enrichment has risen to 2 orders of magnitude, with Ca, Zn, and Pb being an order of magnitude more concentrated than in the Goldenville. This unit also has noticeable enrichment in Ni and Cu. Strontium and Na are depleted by a factor of 10.

The Black Slate has greater than 10-fold enrichment in Mn, Zn, and Pb, and greater than 5-fold enrichment in Ca and Cu. Na is depleted by half an order of magnitude.

The Zn and Pb content of the Halifax Slate Unit is nearly 100 times that of the New Harbour Member, with Mn, and Cu still somewhat enriched. The Na depletion is less pronounced than in the other units.

Several interesting points are brought out in the normalized plots. The most obvious, is that the entire stratigraphic section at Eastville is anomalous in Mn compared to the Goldenville Formation. The Mn concentrating process must have been active at varying degrees of efficiency over the entire GHT in the deposit.

The enrichment in Ca within the *MZ* and *BS* reflects the presence of carbonate in these units. In fact, the abundance of carbonate and especially carbonaceous material is one of

-41-
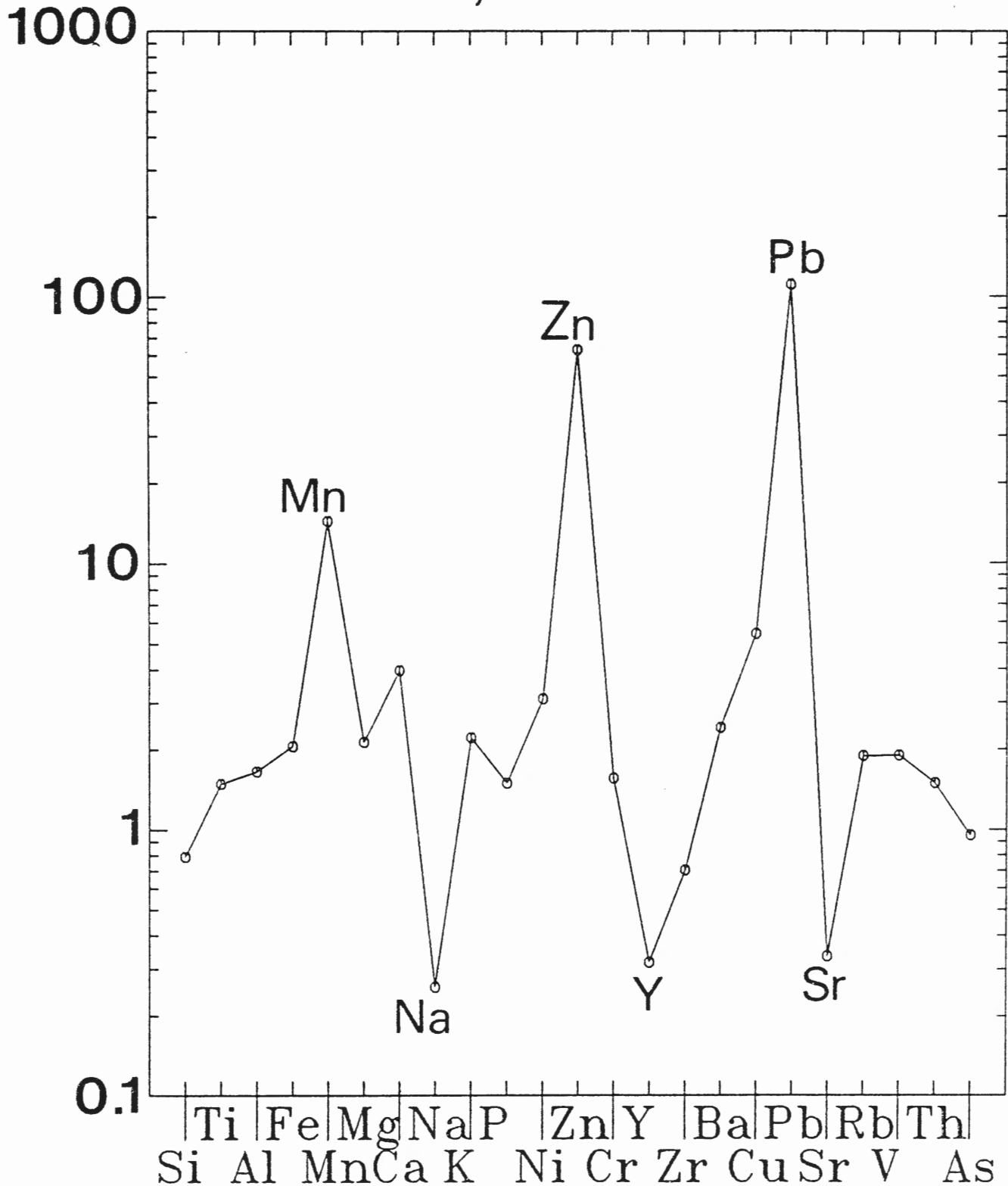
Figure 4.7 Average Interbedded Zone normalized to average metawacke composition for the New Harbour Member of the Goldenville Fm. (from Zentilli et al., 1986). Note that the IZ is enriched in Mn, Zn, and Pb, and slightly depleted in Na, Y, and Sr compared to the New Harbour metawackes.
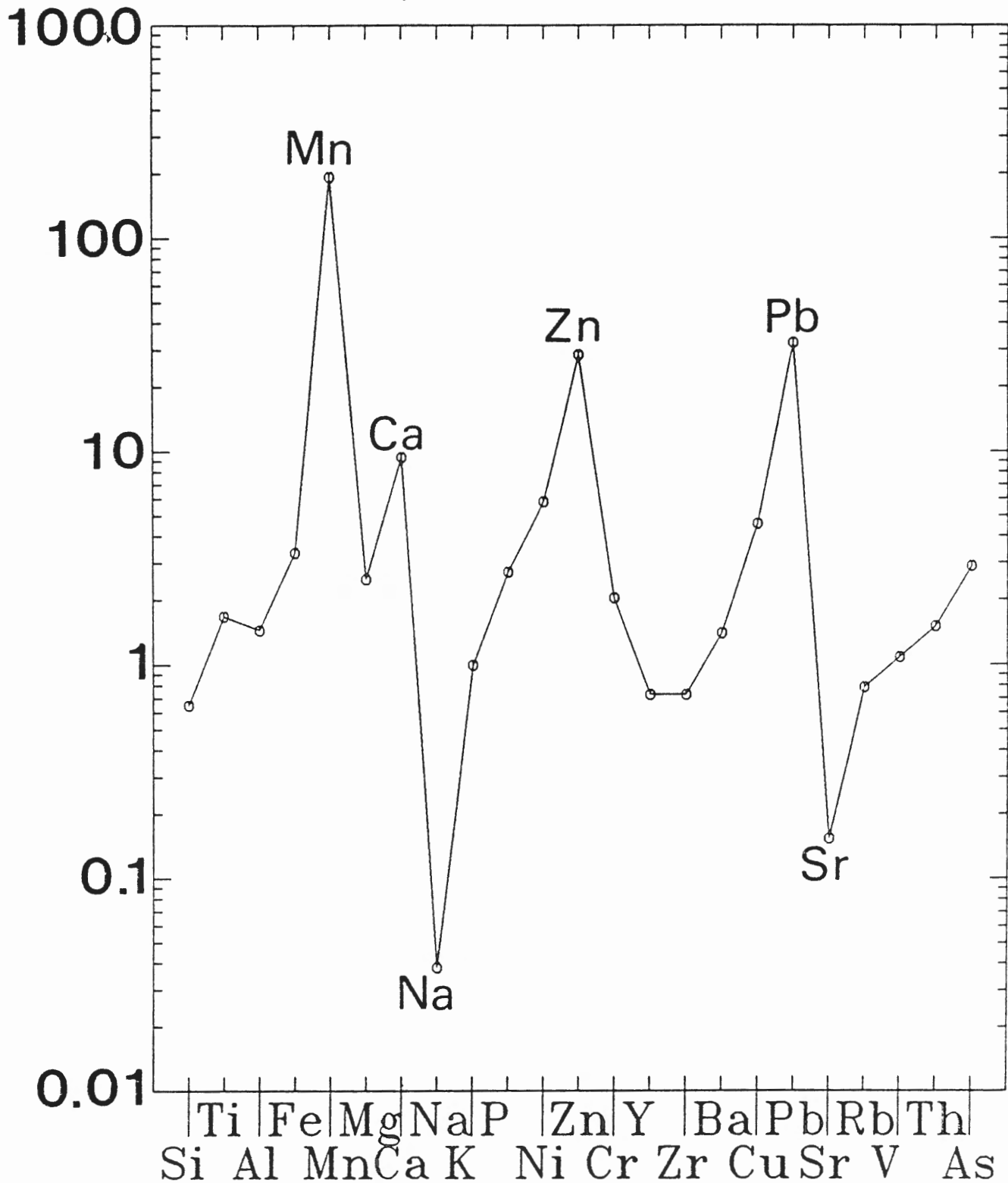
Figure 4.8 Average Manganese Zone normalized to average metawacke composition for the New Harbour Member of the Goldenville Fm. (from Zentilli et al., 1986). The MZ is enriched in Mn, Ca, Zn, and Pb, and depleted in Na and Sr.

BLACK SLATE / Gdv METAWACKE
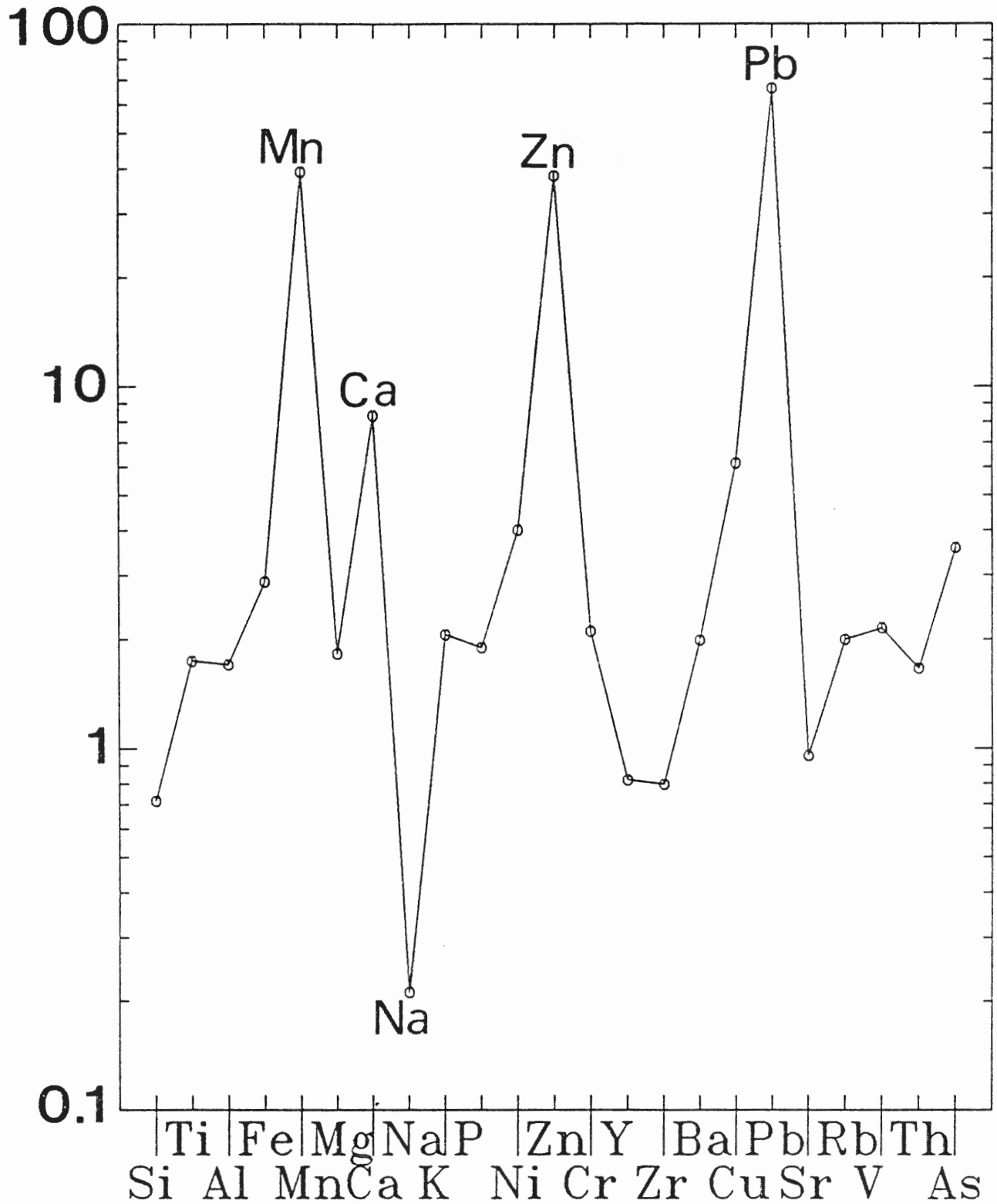
Figure 4.9 Average Black Slate normalized to average metawacke composition for the New Harbour Member of the Goldenville Fm. (from Zentilli et al., 1986). Note the enrichment in Mn, Ca, Zn, and Pb, and depletion in Na.
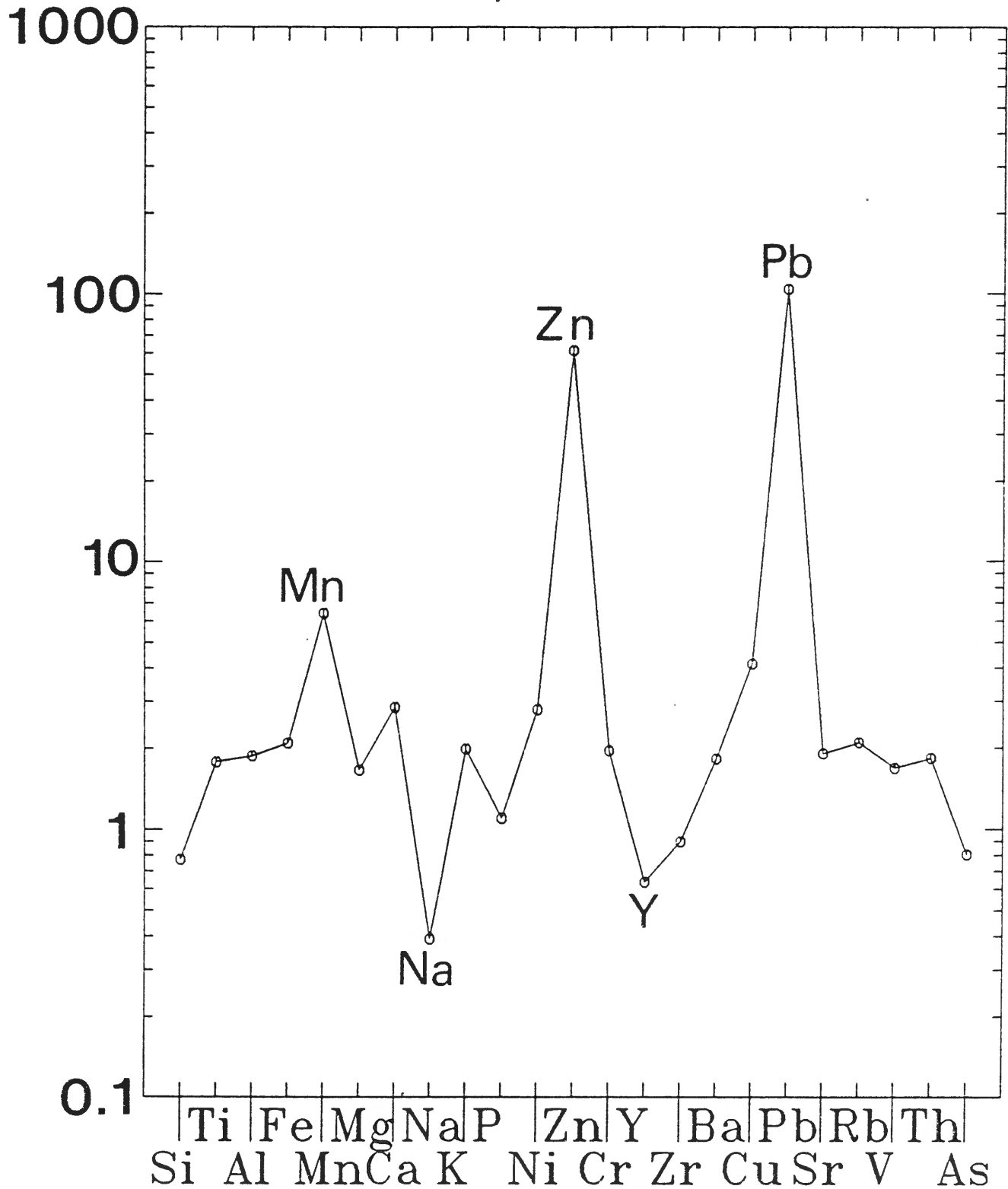
Figure 4.10 Average Halifax Slate unit normalized to average metawacke composition for the New Harbour Member of the Goldenville Fm. (from Zentilli et al., 1986). Zn and Pb are enriched by two orders of magnitude, while Mn is slightly enriched and Na is slightly depleted.

the most distinguishing features of the GHT at Eastville.

The higher Sr contents in the Halifax Slate unit appear to be more representative of Goldenville compositions. It is noteworthy that the depletion in Sr in the *MZ* is accompanied by a Na depletion. Strontium tends to substitute for calcium in plagioclase, suggesting that the Sr variation is at least in part caused by a reduced supply of detrital feldspars in the *IZ* and *MZ*.

While the Zn:Pb ratio for Holes 24 and 25 is 3:1, the enrichment over Goldenville metawackes is about two times greater for Pb than for Zn.

At this point it is useful to study the inter-element correlations within each unit. Chave and MacKenzie (1961) have shown that for deep sea muds, groups of elements which have high correlation coefficients (r) with each other tend to be present in the same minerals or group of minerals related by a common process. The application of this premise to metamorphosed sediments could theoretically reveal the element-mineral associations found in the sediments at the time of deposition, even though the mineral assemblage has changed. *However*, this requires that the diagenetic, and metamorphic changes must have been isochemical (ie. a closed system) on the scale at which the samples were taken. This is clearly not true for phases such as carbonates which have been re-distributed in veinlets, hence, some caution must be taken in interpreting the correlation data.

Spearman rank correlation coefficients (see Appendix 3)

-46-

were computed for all of the whole rock and acid-leach elements for each stratigraphic unit. The volume of resulting data is too large to be tabulated in this work, thus the diagramatic technique of Chave and MacKenzie (1961) is used. Elements exhibiting a high degree of correlation are joined by lines. These elements also tend to be intercorrelated with other elements thus forming a cluster of elements; it is this group of elements which is related to a common mineral or group of minerals. Differing levels of statistical significance for the correlations are indicated by different line types.

The correlation diagrams for each unit are displayed in the following Figures (4.11-4.14). A brief summary of each diagram will be included in the figure captions, and a general discussion of the observed trends in bulk geochemistry follows.

Following is a list of smectite minerals (from Deer *et al.*, 1966) which will be referenced in the discussion.

	Di-octahedral		
	Z	Y	X (exchange cations)
Montmorillonite	Si_8	$Al_{3.34}Mg_{0.66}$	$(\frac{1}{2}Ca,Na)_{0.66}$
Boidellite	$Si_{7.34}Al_{0.66}$	Al_4	$(\frac{1}{2}Ca,Na)_{0.66}$
Nontronite	$Si_{7.34}Al_{0.66}$	Fe_4^{+3}	$(\frac{1}{2}Ca,Na)_{0.66}$

	Tri-octahedral		
Saponite	$Si_{7.34}Al_{0.66}$	Mg_8	$(\frac{1}{2}Ca,Na)_{0.66}$
Hectorite	Si_8	$Mg_{5.34}Li_{0.66}$	$(\frac{1}{2}Ca,Na)_{0.66}$
Sauconite	$Si_{6.7}Al_{1.3}$	$Zn_{4-5}(Mg, Al, Fe^{+3})_{2-1}$	$(\frac{1}{2}Ca,Na)_{0.66}$

Figure 4.11

Correlation Diagram for Interbedded Zone

Unit 2

number of samples = 14
99.9% confidence limit (r > ~0.79)   _____
99.0% confidence limit (r > ~0.66)   _ _ _ _
elements preceded by "l" are acid-leached components.

(a) This group clearly represents the elements associated with the Zn and Pb minerals, primarily sphalerite and galena. Cadmium and to a lesser extent Ag have properties similar to Zn and Pb, hence their associatation with this group is not unexpected, however the correlation with Nb is difficult to explain.

(b) This poorly defined group might represent a clay grouping, possibly illite $(Al_4[Si_4O_{10}](OH)_8)$ and/or smectite (montmorillonite and others) due to the presence of the major elements Al, Fe, and K. Substitution for K by Th and the acid leachable fraction of Ba seems significant; the weaker correlation for whole rock Ba with K probably reflects the presence of non-leachable Ba in other minerals. The affiliation of Ba with Ag of Group a might indicate a barite association as found in some Pb-Zn deposits (Large, 1983). The correlation of the metals Cu, Co, and Ni with the apparent clay group is also of interest. It is possible that these metals were extracted from sea water at the time of deposition by adsorption to the clay minerals.

Figure 4.11
UNIT 2
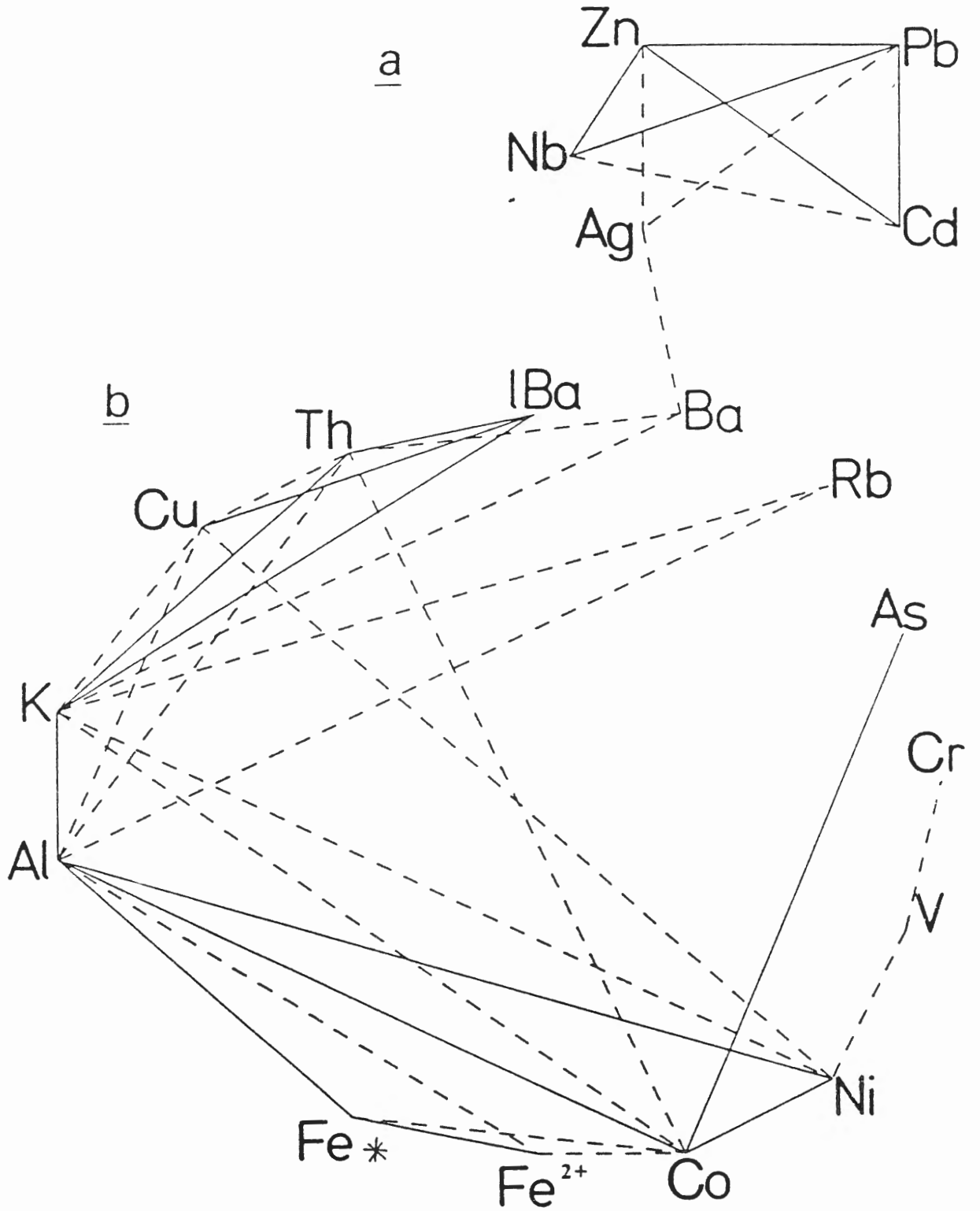
Figure 4.11 (continued)

Correlation Diagram for Interbedded Zone

Unit 2

```
number of samples = 14
99.9% confidence limit (r > ~0.79)     _____
99.0% confidence limit (r > ~0.66)     _ _ _ _
elements preceded by "l" are acid-leached components.
```

(c) This is a carbonate grouping. The source of the leachable Mn in the *IZ* is thus identified as manganiferous calcite. The total carbon content (C*) appears to be made up primarily of carbonate. The affiliation of B with CO_2 is possibly due to the fact that B is rather soluble in hydrothermal solutions, for example those forming the carbonate veinlets.

(d) No distinct association can be found in this group.

The lack of high correlation between sulphur and Fe^{2+} is unexpected in light of the abundance of pyrrhotite. Note that S is actually negatively correlated with Mn, and that Mn is not correlated with any element at this confidence level. *Group a*, presumably a sulphide group, also shows no correlation with S, but does have a negative correlation with Y. *Group b* is also negatively correlated with Groups *c* and *d*. Silicon exhibits a strong negative correlation with *Group b*, further substatiating this as a clay group, the concentration of which would be diluted by quartz in more sandy beds.

Figure 4.11
UNIT 2
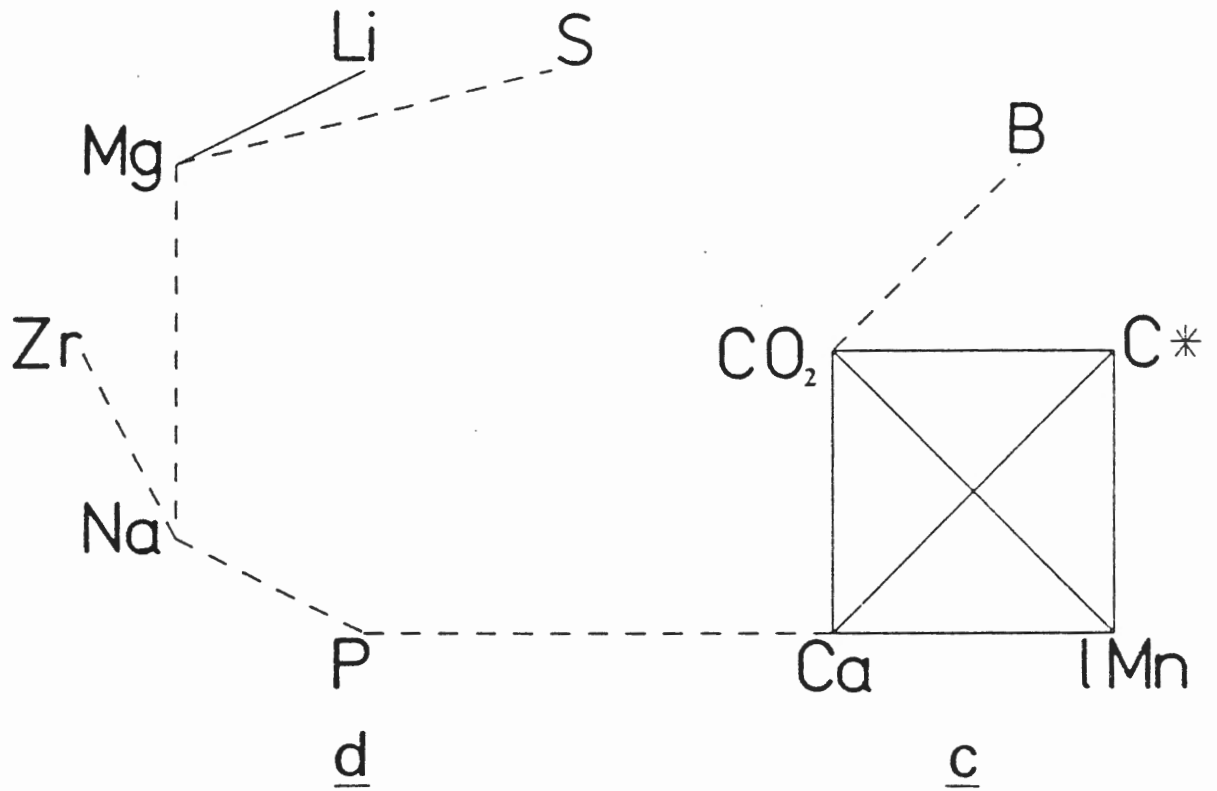
Figure 4.12

Correlation Diagram for Manganese Zone

Unit 3

number of samples = 8
99.9% confidence limit (r > ~0.93)   _____
99.0% confidence limit (r > ~0.84)   _ _ _ _
95.0% confidence limit (r > ~0.71)   __ __
elements preceded by "1" are acid-leached components.

(e) This group consists of several loosely correlated
groups. The V-Mo-Cu-S correlation probably indicates their
presence in sulphides, which appear to have been associated
with U-B-Sb. As for the *IZ*, Fe is not correlated with S even
though Fe-sulphides are abundant. There is a
Zr-K-Y-Sr-Ba-Rb-Th relation, however, it cannot be clearly
linked with any major mineral-forming elements. Again a
calcite grouping is found, but in this case total carbon
(C%) is more weakly correlated than in the *IZ*, probably due
to the higher proportion of carbonaceous matter. It appears
that the acid-leachable portion of Sr (ie. ~80% of the total
Sr) might be a constituent of the carbonates.

Figure 4.12
UNIT 3
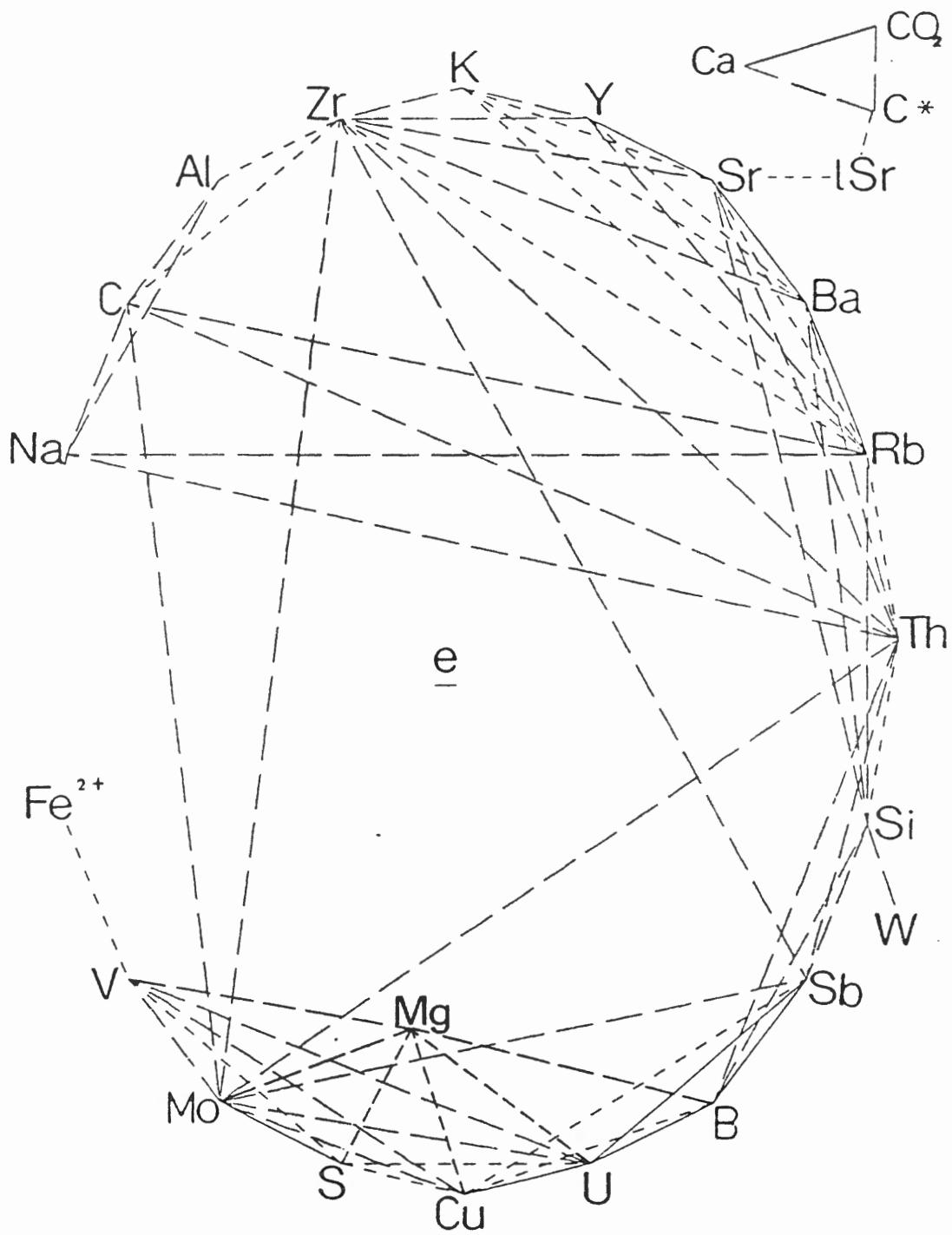
Figure 4.12 continued)

Correlation Diagram for Manganese Zone

Unit 3

```
number of samples = 8
99.9% confidence limit (r > ~0.93)     _____
99.0% confidence limit (r > ~0.84)     - - - -
95.0% confidence limit (r > ~0.71)     ___  ___
elements preceded by "l" are acid-leached components.
```

(f) This is primarily a group of Fe related metals. The correlations are not strong, and it is puzzling that the leachable fractions of Zn and Pb do not correlate with the Whole Rock contents. The implications behind the positive correlation of Mn with structurally bound H_2O and Mg are unclear.

The high correlation of Zn with Pb is in keeping with the previous observations. The low range in Sn contents makes the significance the Fe^{3+}-Sn relation questionable. The correlation of leachable manganese with Ti suggests that an acid-soluble, high Ti mineral is the source of this portion of the overall Mn content of the *MZ*.

Group f, including Mn and Mg, is anti-correlated with *Group e*. Both Ti and leachable Mn show negative correlations with CO_2, presumably indicating that the Ti-Mn mineral is incompatible with the existence of carbonate cements found in this unit.

Figure 4.12
UNIT 3
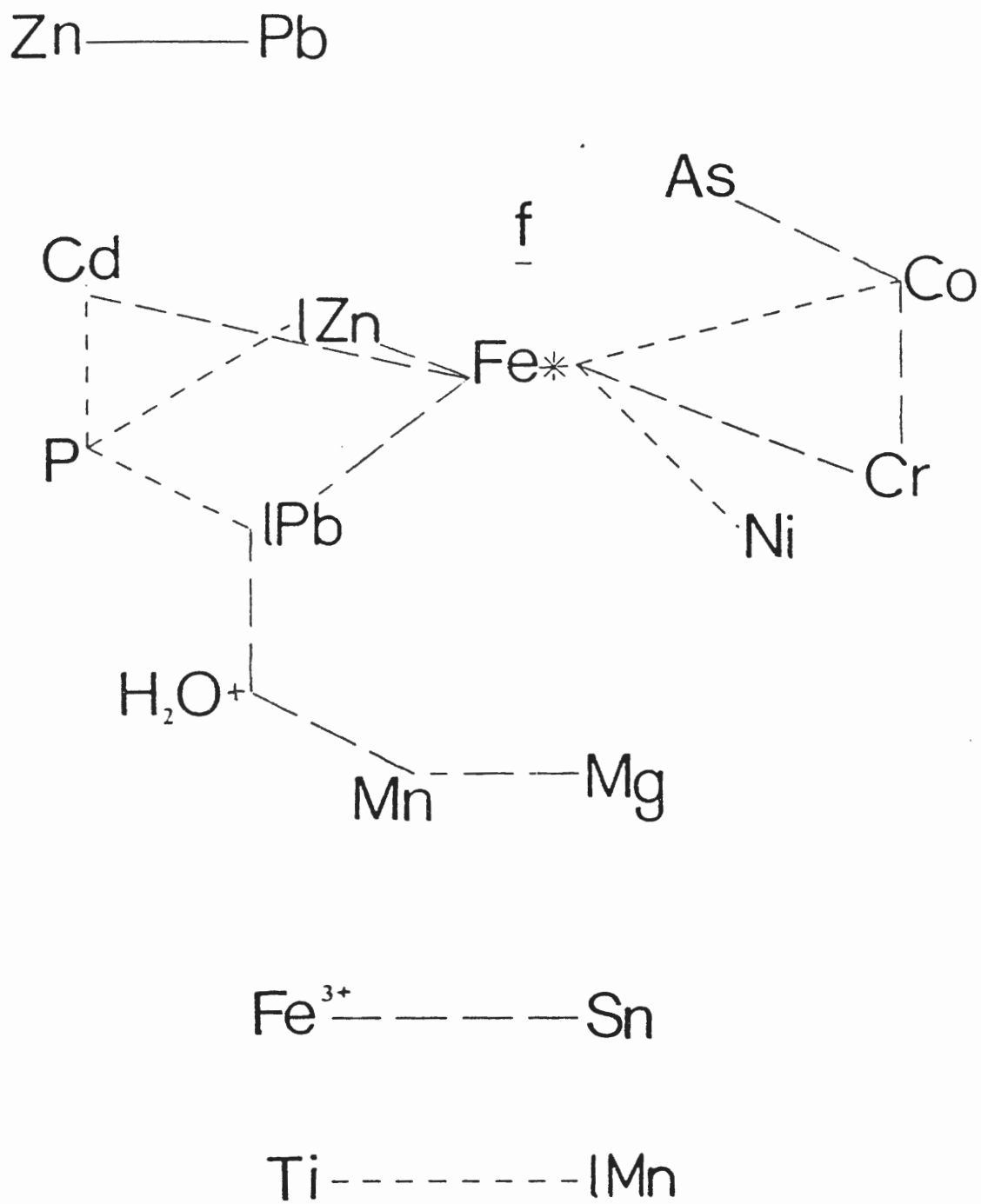
Figure 4.12
UNIT 3

Figure 4.13

Correlation Diagram for Black Slate

Unit 4

```
number of samples = 5
99.9% confidence limit (r > ~1.00)    _____
99.0% confidence limit (r > ~0.97)    _ _ _ _
95.0% confidence limit (r > ~0.89)    __  __
elements preceded by "l" are acid-leached components.
```

(g) This group demonstrates the coherent behaviour of Zn-Pb-Cd as in the *IZ* and *MZ*.

(h) The K-Ba-Rb-Th-Cu relation found in the underlying units is also present in the *BS*. If this represents elements contained in clays, the correlation of Cu with carbon is reasonable since fine grained clays and carbonaceous material would be expected to be deposited together. In addition, the affiliation of Cu, V, and especially uranium with carbon probably reflects the strong reducing conditions which would have been present in the carbonaceous sediments.

(i) The correlation of this aluminosilicate group with Na suggests that it might represent detrital plagioclase. However, the correlation with TiO_2 is uncharacteristic of plagioclase compositions. It is more probable that this represents detrital smectite which can contain significant quatities of Na and tetrahedral Ti substitution or even rutile inclusions (Deer *et al.*, 1966). It is interesting with respect to the rapid increase in Sr in the *BS* that in

the current (metamorphosed) mineralogy, leachable Sr also correlates with these elements.

Figure 4.13
UNIT 4
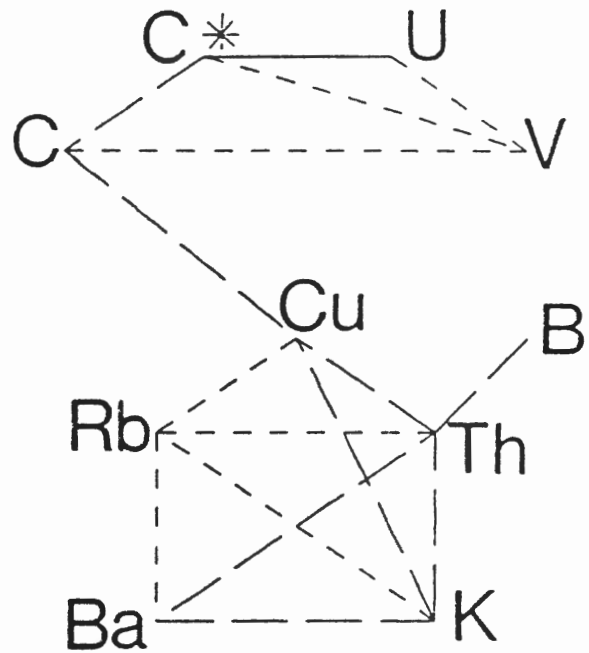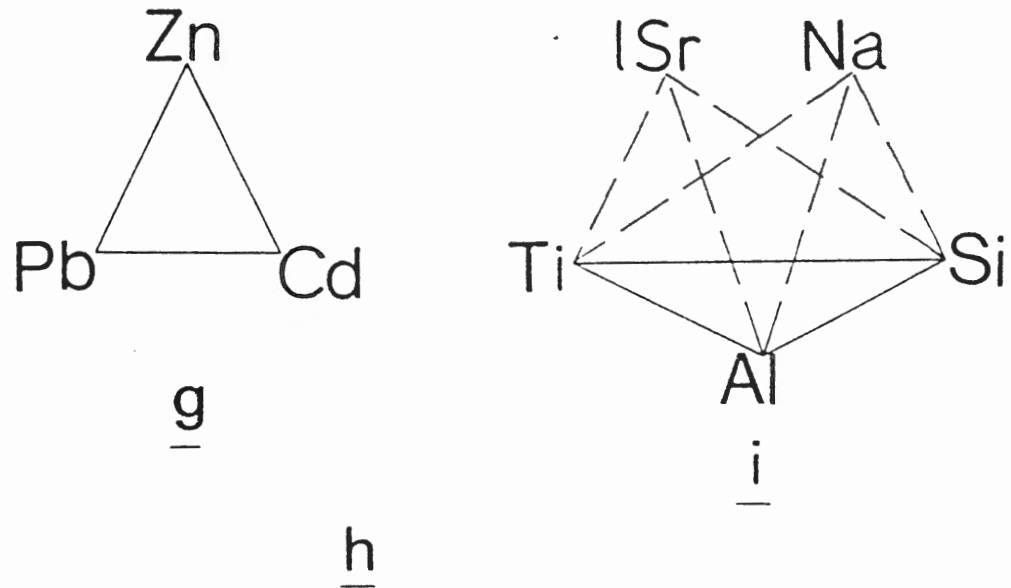
Figure 4.13 (continued)

Correlation Diagram for Black Slate

Unit 4

```
number of samples = 5
99.9% confidence limit (r > ~1.00)        _____
99.0% confidence limit (r > ~0.97)        _ _ _ _
75.0% confidence limit (r > ~0.89)        ___  ___
elements preceded by "l" are acid-leached components.
```

(*j*) This loosely correlated group seems to be centered around Fe sulphides and carbonates. Arsenic and W seem to be affiliated with a sulphide. Manganese, leachable Mn, Co, Ni, and W are probably found in calcite. It is significant that this is the only unit in which Whole Rock Mn exhibits reasonably strong correlation with several elements, including the acid-leached Mn.

Note that *Group j* is negatively correlated with *Group i*. Possibly the apparent clays in *Group i* in effect dilute the concentration of the chemical preciptates.

Figure 4.13
UNIT 4
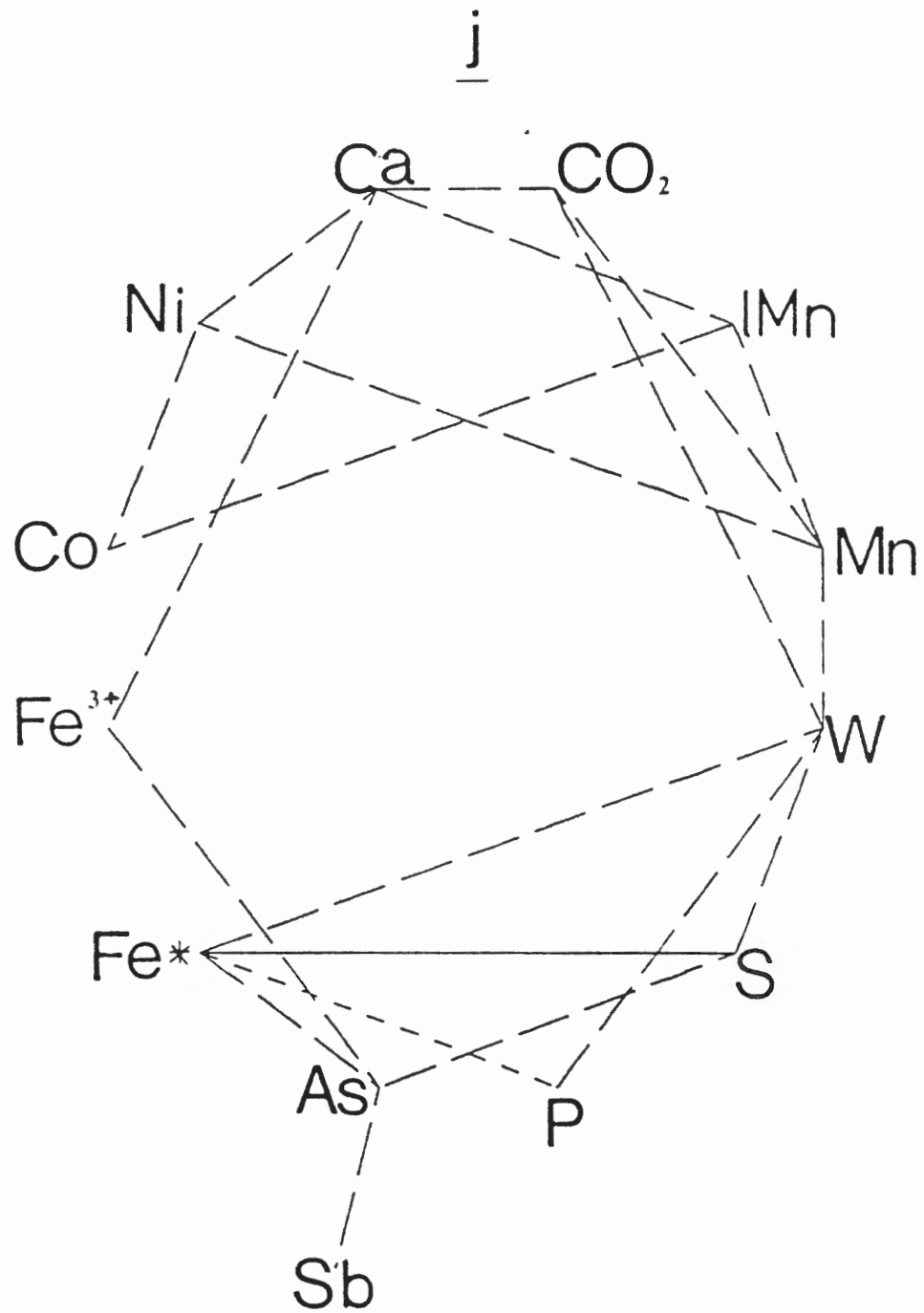
Figure 4.14

Correlation Diagram for Halifax Slate

Unit 5

number of samples = 23
99.9% confidence limit (r > ~0.64)   _____
99.0% confidence limit (r > ~0.53)   _ _ _ _
elements preceded by "l" are acid-leached components.

(k) This could conceivably represent components in one or more smectite clay minerals similar to that postulated for the BS. However, in this case, the element association is more convincing in light of the crystal chemistry indicated by Deer *et al.* (1966). Titanium is found in small quatities in the tetrahedral site in some smectites. Aluminium occurs in both tetrahedral and octahedral sites in these clays. Magnesium, Fe^{3+}, and Li can each be major constituents in the octahedral sites, while Ca, Na and presumably Sr are present in the interlayer portions of the crystal structure as a means of maintaining charge balance. Nickel (correlated from *Group I*) and other cations also substitute into the smectite structure.

It is proposed that the increase in Sr in the *HS* over the Goldenville units can be accounted for by higher shale:sand ratios, thereby increasing the smectite content of the deposited sediments.

(l) This is primarily an Fe-sulphide group. The elements Mo, Co, Ni, V, and Cu are all possible substituents for Fe^{2+}, in pyrite and pyrrhotite (Deer *et al.*, or else as

-61-

independent sulphide minerals (eg. chalcopyrite is seen in small quantities in thin section). The affiliated reduced carbon (ie. carbonaceous C) would provide the reducing conditions for sulphide formation. The association of C with uranium, which is immobile in the reduced state, is also reasonable.

However, the strong correlation of K, Rb, Ba, and B with Fe and S, which is more poorly defined in the *IZ* and very weakly in the *MZ*, is rather surprising. This elemental relation points to the depostion of the mineral jarosite, $KFe_3^{3+}(SO_4)_2(OH)_6$, a product of sub-aerial wethering, in the orginal sedimentts (Hurlbut and Klein, 1977).

Figure 4.14
UNIT 5
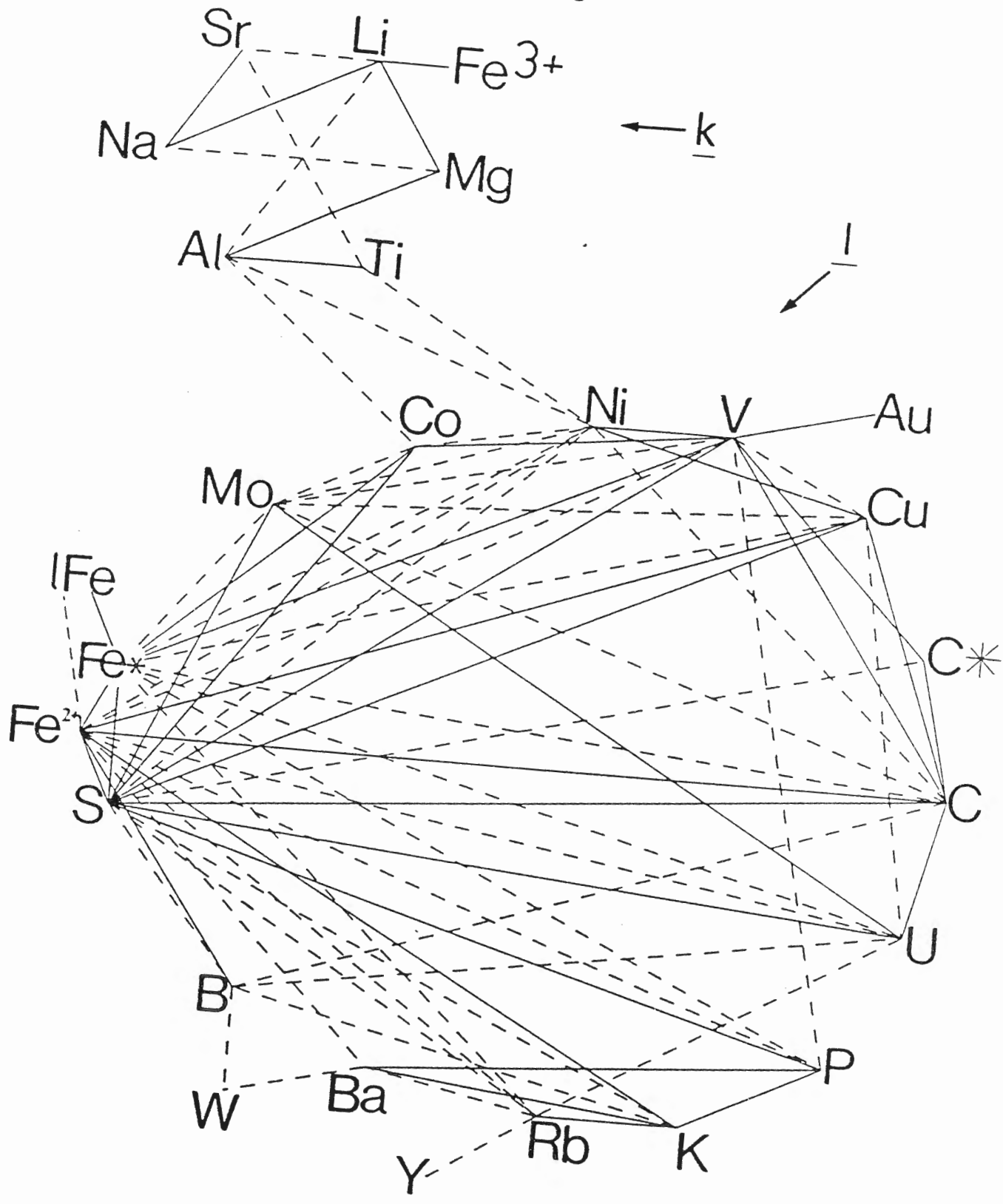
Figure 4.14 (continued)

Correlation Diagram for Halifax Slate

Unit 5

```
number of samples = 23
99.9% confidence limit (r > ~0.64)        _____
99.0% confidence limit (r > ~0.53)        _ _ _ _
elements preceded by "l" are acid-leached components.
```

(m) The substitution of Th for Zr in the mineral zircon (Zr[SiO$_4$]) could explain this relation. Zircon, with a density of ~4.6, would be expected to concentrate in more sandy beds (ie. quartz-rich). This is substantiated by strong negative correlations with the apparent fine grained groups *k and l*.

(n) The Zn-Pb-Cd-Ag correlation seen in the underlying units is prominent in the *HS*. This group is anti-correlated with Y and Zr.

Other significant negative correlations occur, such as, Fe^{3+} with Fe^{2+} and B, Li with B, and Sr with Ba. Others include Sb with Y, Co with CO_2, Mo and U with leachable Mn, and Cd with Rb and Th.

Figure 4.14
UNIT 5

Zr

Th - - - Si

m

Zn ———— Pb

Ag ———— Cd

n
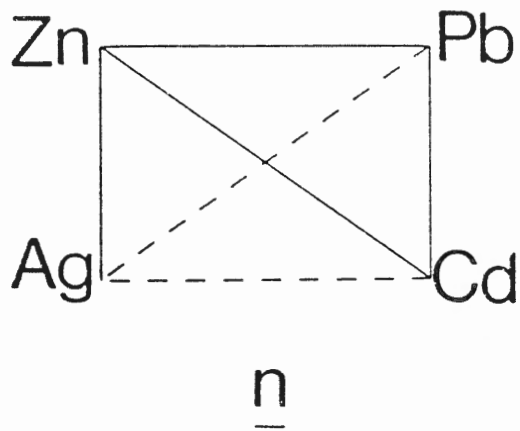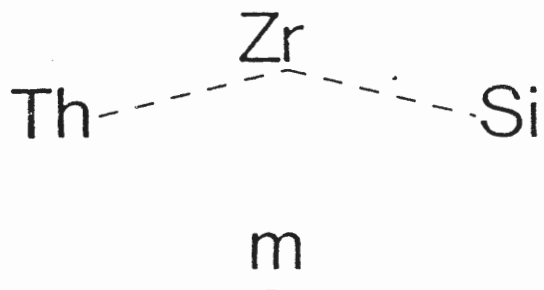
4.1.3 General Discussion of Bulk Geochemistry

Several important facts have been drawn from the bulk chemical analyses. The rocks fall compositionally between terriginous shales and sandstones based on Si-Al-Fe ratios, but are noticeably enriched in Al and Ti over the world averages cited for such rocks. The GHT at Eastville is anomalous in Mn, Zn, Pb, Sr, and to a lesser degree Ca, Na, Y, Ni and Cu, compared to the compositions for rocks found at lower stratigraphic levels in the Goldenville Formation (ie. massive sandstones and thick Bouma turbidite sequences as in Liew (1979)).

The rocks of the *MZ* and *BS* are the most outstanding in a chemical sense. An additional source of Fe separates these units from the shale-sandstone mixing line on the Si-Al-Fe diagram. The lack of correlation between Mn and other elements, and its remarkable degree of enrichment restricted to such a narrow horizon at the scale of the study area point to a synsedimentary or diagenetic enrichment for the manganese. On this basis these units can be considered as a primary ferromanganese deposit. The abundance of carbonate and reduced carbon in these adjacent units promotes the idea that oxidation-reduction relations must have been important in the genesis of the deposit.

The strong inter-correlation between Zn, Pb, and Cd, plus the consistency of these relations (Zn/Pb ~2.2) over the length of the deposit implies that the Zn-Pb

concentration process was operating at a rather large scale.
Otherwise fractionation of these metals based on their
individual chemical properties would be observed. The lack
of correlation between this group and other elements
probably reflects the fact that the sphalerite and galena
have been remobilized under the structural controls of vein
and foliation development. Hence, any elemental associations
characteristic of the method of Zn-Pb deposition in the
sediments have been lost, severely hampering attempts to
model this process.

The correlation diagram analysis as a tool for
predicting the source of metals gives remarkable results
considering the degree of metamorphic mineral growth in the
rocks. The smectite clays, and possibly illite, appear to
have been important components of the sediments being
deposited at Eastville. The cation exchange properties of
these minerals would make them excellent sources of metals
(in this case notably Ni and Co), either as transported from
the continent from which they were weathered or as
adsorption traps for aqueous metals given sufficient
exposure to sea and pore waters. These aluminous clays were
the precursors to the abundent micas and garnet found in the
present mineralogy.

The implied presence of jarosite in the original
sediments is also of considerable interest. It is reasonable
that the sulphate and ferric components of jarosite would be
reduced by carbonaceous material within the sediments to

-67-

produce pyrite. The degree of the contribution of Fe and S to the sediments by jarosite is uncertain. The presence of large blebs of pyrite and pyrrhotite, and the association of metals such as Cu which are not highly correlated with K suggests that reduction of sea water sulphate by pelagic carbonaceous material and/or in bacterial metabolism is also a major source for the sulphides. A study of sulphur isotopes might be of value in this problem.

4.2 Mineral Chemistry

The very fine grained nature of the lower grade metamorphic rocks at Eastville has made accurate analysis of mineral chemistry difficult, even by electron beam microprobe. However, the new, more advanced *JEOL* microprobe at Dalhousie might make a more comprehensive study feasible in the future.

Cameron (1985) detailed the variation in mineral chemistry with increasing degrees of contact metamorphism in the deposit. Some of the Cameron (1985) and other data taken in the same analysis session are presented in Appendix 5, and are discussed below with reference to the current distribution of elements and its implications on the early history of the deposit.

4.2.1 Garnet

Cameron (1985) identified two types of garnet in the deposit. Almandine garnets appear in the contact aureole of

-68-

the pluton, while the previously described regional metamorphic garnets are *spessartine* $(Mn_3Al_2Si_3O_{12})$ rich, having up to 30 Wt% MnO.

The abundance of spessartine garnet in the rocks indicates that it is the primary manganese mineral. Since garnet is not readily soluble in hot acid, the low acid-leach Mn values are explained.

Cameron (1985) interpreted the garnets as having formed in conjunction with biotite growth at the expense of chlorite and muscovite. It is noted that spessartine garnets grow at temperatures below the garnet zone of regional metamorphism, especially in the presence of a high concentration of Mn (Loomis *et al.*, 1982). However, Cameron's (1985) analyses show less than 1 Wt% MnO for chlorite and muscovite. Even after the formation of spessartine garnet, some manganiferous chlorites should be found. Hence, while the aluminum in the spessartine has come from chlorite and muscovite, much of the Mn has come from another mineral.

4.2.2 Carbonates

The abundant carbonate cements from the Manganese Zone were in general too fine grained to obtain accurate microprobe analyses. However, a set of analyses were obtained from a carbonate rich block similar to those described in *Chapter 3*. Contents of up to 5.8 Wt% MnO were found. Carbonates found in veins are virtually free of Mn,

CARBONATE
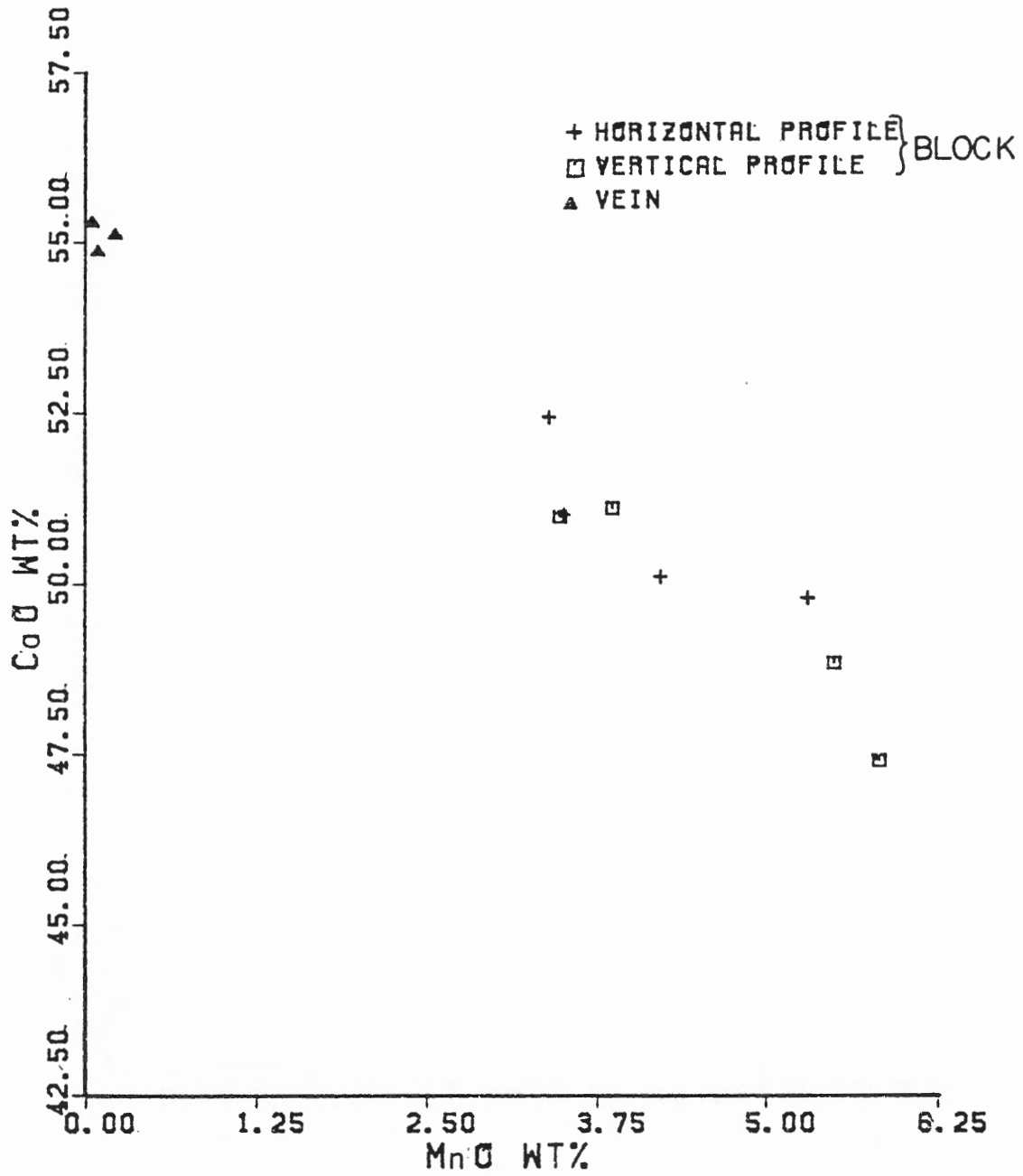
Figure 4.15 Ca — Mn plot for analysed carbonates at Eastville. The "block" refers to a carbonate-rich boudin as described in Chapter 2. Note that calcium and manganese appear to be substituting for each other.

the difference being taken up by calcium (Fig. 4.15).

It can be argued that the present manganese-bearing carbonates are the residue from a manganese-rich carbonate (*rhodochrosite*) which has supplied the Mn for garnet growth. This is substantiated by the fact that, in manganiferous sections of lower metamorphic grade GHT at other locations, manganese-rich carbonate is the major manganese mineral. Hingston (1985) found that garnet appears at the expense of rhodochrosite in more metamorphosed sections of the Lake Charlotte deposit.

It is possible that the present-day calcite is derived from the calcite component in impure rhodochrosite. It is also possible that CO_2 released in the reaction of rhodochrosite to form garnet would pick up Ca released by albitization of plagioclase (> ~200°C). Excess CO_2 from garnet formation was probably removed from the system as bicarbonate anions formed in the structural water released in the breakdown of muscovite and chlorite.

4.2.3 Sulphides

A limited number of analyses of sulphide minerals have been undertaken. About 5 Wt% Fe has been found in the sphalerite, hence explaining the greenish to amber colour of sphalerite under transmitted light (Deer *et al.*, 1966).

The existence of 1 Wt% Mn in sphalerite at the core of a spessartine garnet, as well as the small quantities of Mn in pyrrhotite, is interesting. These sulphides are found

prominently at the core of spessartine garnets or "clumps" of garnets. It seems logical that with the onset of metamorphism, the sulphides would begin to release Mn, thus catalysing the early nucleation and growth of garnet.

In some sections of the drill core, carbonate rims surrounding disseminated pyrrhotite blebs are observed. These carbonates can be interpreted as forming by the oxidation of carbonaceous material in the formation of the sulphides (D.E. Large, personal communication). If such carbonates were manganiferous, the formation of garnet clumps might be favoured. Hence, the degree of Mn contribution to garnet formation from sulphides is uncertain, but was probably more important in the sulphide-rich Black Slate unit.

The simple presence of Mn in the sulphides is important. High concentrations of Mn^{2+} must have been present at the time of sulphide deposition considering the low stability of Mn sulphides (Roy, 1981).

4.2.4 Oxides

The only oxides found in the rocks are rutile, and the more abundant ilmenite. Lateral X-ray dispersion into adjacent grains due to small grain sizes was again a hindrance in obtaining accurate analyses.

Blood red rutile (TiO_2) flecks were found to contain about 2 Wt% FeO impurity, thus explaining the red colour (Deer, *et al.*, 1966). However, some opaque laths are

comprised of pure TiO2. Thus a difficulty arises in distinquishing rutile from ilmenite by microscopy alone.

The ilmenite (FeTiO$_3$) laths were found to contain significant quantities of manganese (from 6 to 30 Wt% MnO). Cameron (1985) found that the manganese content decreased compared to this range in the contact metamorphosed rocks. Thus, it is probable that the release of Mn from ilmenite was a source for the manganese content of metamorphic minerals, especially at higher temperatures. The degree of contribution to spessartine garnets is again questionable for no concentration of garnet growth or clumping was found to be related to the presence of ilmenite.

The origin of the rutile and ilmenite is uncertain. The laths are oriented with the foliation, thus pre-dating the folding event. The idioblastic crystal shape suggests metamorphic or diagenetic growth rather than as a detrital component in the original sediments. The possibility that these minerals are the partially reduced artifacts of fossil Mn-Fe-Ti oxy-hydroxides, as found in nodules and crusts in deep sea ferromanganese deposits, is intriguing. However, confirmation of this speculation is difficult.

4.2.5 General Discussion of Mineral Chemistry

Manganese plays a major role in the mineralogy of the deposit. Due to regional metamorphism, spessartine garnet is the major Mn mineral. The evidence, and comparison with similar less metamorphosed sections of the GHT, point to a

manganese-rich carbonate and possibly Mn-rich sulphides and ilmenite as the source for the Mn in the spessartine garnets.

The ilmenite and rutile in the rocks seem to be diagentic or metamorphic in origin, although the precursor to these minerals is open to speculation. The exact degree to which ilmenite has contributed Mn to the garnets, or other minerals, is uncertain.

The presence of Mn in sphalerite infers a relation between the syngenetic or diagentic deposition of the Zn sulphides and the Mn concentration process. The occurrence of Mn in the sulphides and carbonates testifies to the aqueous rather than detrital origin for the manganese.

3.3 Stable Isotope Geochemistry

The origin of the carbonates at Eastville is of considerable importance in understanding the genesis of the deposit. The first question to be answered involves the fact that the carbonates are present in rocks which were presumably deposited below the Carbonate Compensation Depth in a deep-water fan, thus restricting the precipitation of carbonates. Understanding the carbonates is also of importance considering its concentration in such a limited stratigraphic interval (primarily the MZ), and the possibility that carbonates contained a major portion of the manganese before the metamorphic growth of garnet. The presence of remobilized sphalerite and galena in calcite

-74-

veins is also of interest.

One means of studying the chemistry of the carbonates involves the use of carbon and oxygen stable isotopes from the carbonates. A brief introduction to the principles of isotope effects is given below. For more information, the reader is referred to the literature used: Henley *et al.* (1984), Anderson and Arthur (1983), Hoefs (1980), O'Neil (1979), and Faure (1977).

4.3.1 Stable Isotope Theory

Stable isotopes are non-radioactive atoms of an element, by definition having a set number of protons, which have different number of neutrons, and hence a different atomic mass. Certain chemical and physical properties, such as reaction rates and bond energies, are affected by these mass differences; these changes are called *isotope effects*.

There are three main types of isotope effects. All three types serve to fractionate the heavy and light isotopes (ie. changing their ratios) and are thus of use in tracing the physical and chemical changes involved in geological processes. In the equilibrium exchange of isotopes of a particular element between to two species (say CO_2 and HCO_3^-) the heavier isotope will be preferentially retained in the species in which it is more strongly bonded. The equilibrium constant (K_{eq}) for such isotope exchange depends on temperature, and therefore is useful in geothermometry. In disequilibrium reactions, bonds involving

the lighter isotope are weaker and are broken more readily. As a result of this kinetic isotope effect the lighter isotope will be enriched in the products of a unidirectional reaction if it does not go to completion. In isotopic diffusion, the lower kinetic energy required to move the lighter isotope results in a residual buildup of the heavier isotope in the source material.

The relative abundances of the three oxygen isotopes are:

^{16}O = 99.7630%
^{17}O = 0.0375%
^{18}O = 0.1995%

while the natural abundances for the two stable carbon isotopes are:

^{12}C = 98.89%
^{13}C = 1.11%   .

These abundances indicate that the ratios $^{18}O/^{16}O$ and $^{13}C/^{12}C$ can be most easily measured. Hence, changes in the isotopic composition of two carbonate-bearing samples due to geochemical processes can be detected by differences in these isotope ratios. For consistency, all measured isotope ratios are reported as the parts per thousand (*per mil*, or $^{o}/_{o}$) deviation of the sample compared to an international standard. This is the δ (*del*) notation; differences between Rd for samples is a direct measure of the degree of isotope fractionation. Carbon isotope ratios are referenced to the *PDB* standard as $\delta^{13}C_{PDB}$. Oxygen is referenced against present day *Standard Mean Ocean Water* as $d^{18}O_{SMOW}$. Hence, a

sample having an identical $^{18}O/^{16}O$ ratio as *SMOW* would have $d^{18}O_{SMOW}$ = 0 $^{oo}/_{o}$. A sample having positive $d^{18}O_{SMOW}$ would be relatively more enriched in ^{18}O than *SMOW*.

The $\delta^{18}O_{SMOW}$ for several oxygen-bearing substances is shown in **Figure** 4.16. Figure 4.17 shows the isotopic composition for carbon in different rock types. For reference, the order of increasing depletion in ^{13}C in carbon-bearing species in geological systems is:

$CaCO_3 > HCO_3^- > CO_3^{2-} > H_2CO_3 \sim CO_2(g) >> CH_4$

in which the bicarbonate anion (HCO_3^-) is the most common species in geological fluids (Anderson and Arthur, 1983). Figure 4.18 shows the that $\delta^{13}C$ for carbonates decreases with increasing temperature and thermal metamorphism. A similar effect is true for oxygen

4.3.2 Results

The sample preparation method and analytical procedure are outlined in Appendix 6 along with sample descriptions. Samples were grouped into the following categories:

1. Typical calcareous quartz metawacke and slate.
2. Fine laminated or contorted calcareous quartz metawacke and slate, presumably more manganiferous beds.
3. Unmineralized carbonate veins.
4. Carbonate veins mineralized with sphalerite and galena.
5. Carbonates showing some spatial relation to current or possibly previous concentrations of carbonaceous material.

The carbon and oxygen isotopic compositions for the Eastville carbonates are displayed in Table 4.3. The data are plotted according to the sample categories in Figures

4.19-4.21, with suitable comments on the observed trends included in the figure captions.

The general comment which applies to all of the data (with the exception of some of the mineralized samples) is that the samples are extremely depleted in ^{13}C ($\delta^{13}C$ PDB < -9 $^{oo}/_o$) compared to average values for Cambro-Ordovician marine carbonates.
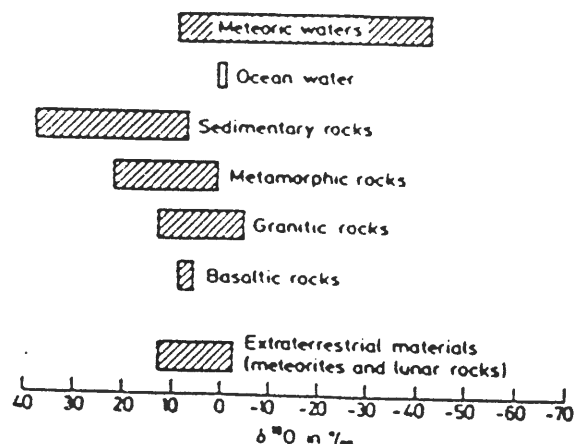
Figure 4.16 $\delta^{18}O_{SMOW}$ for some naturally occurring oxygen-bearing substances. (from Hoefs, 1980, p36)
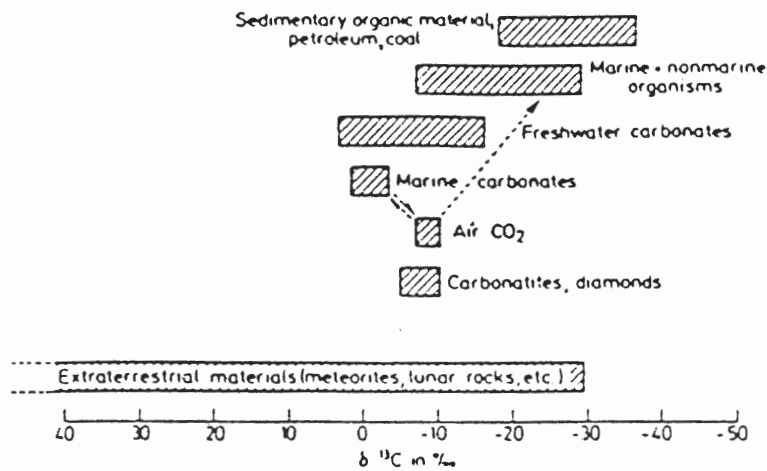
Figure 4.17 $\delta^{13}C_{PDB}$ for some important carbon compounds. (from Hoefs, 1980, p32)
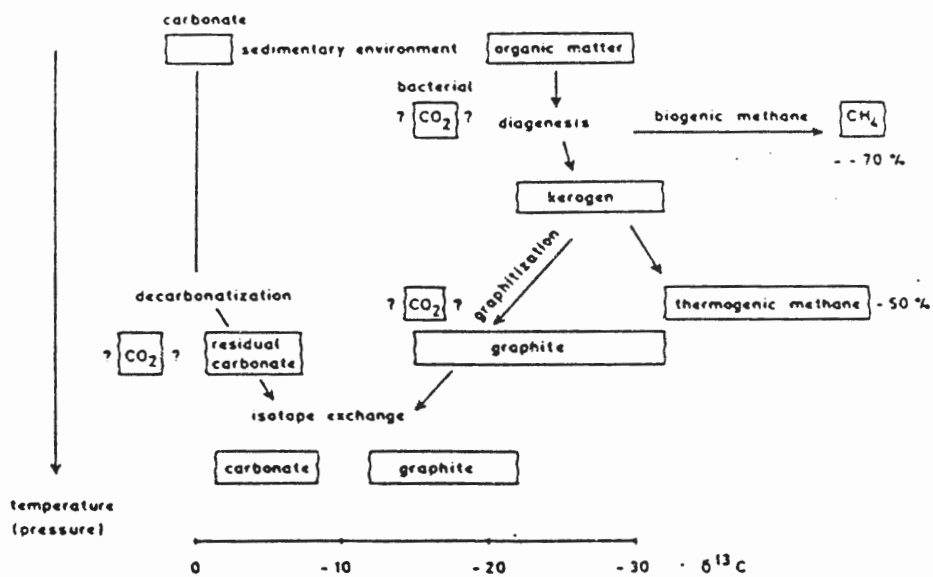
Figure 4.18 Schematic diagram of the evolution of $\delta^{13}C$ (carbonate) and $\delta^{13}C$ (organic) with increasing temperature. (from Hoefs, 1982, p107)

Table 4.3

C and O Isotope Results

SAMPLE	DRILL DEPTH	STRATI-GRAPHIC DEPTH	HOLE	UNIT	TYPE	$\delta^{13}C_{PDB}$	$\delta^{18}O_{SMOW}$
23.5	59.30	83.70	15	5	4	-9.85	23.61
51.1	59.95	--	28	2	1	-16.84	18.92
67.5	223.56	-16.16	27	3	1	-17.60	13.25
68.2	223.89	-16.49	27	3	1	-16.77	15.56
70.2	227.12	-19.72	27	3	2	-18.57	22.02
70.4	227.12	-19.72	27	3	5	-18.20	23.60
73.1	232.89	-25.42	27	3	3	-17.16	11.42
73.4	232.89	-25.42	27	3	1	-16.67	13.56
75.1	237.91	-30.51	27	2	3	-16.43	9.57
112-A	155.56	-6.34	15	3	3	-17.72	14.00
112-B	155.56	-6.34	15	3	5	-17.87	15.95
126-A	176.32	-37.69	16	1	3	-18.04	7.52
126-B	176.32	-39.02	16	1	1	-17.07	14.16
131	100.10	-3.86	17	3	4	-10.45	24.95
132	102.90	-6.57	17	3	2	-18.72	17.30
140	72.56	-7.11	18	3	2	-19.61	15.18
151	105.21	-20.65	19	2	5	-13.90	16.41
166	40.32	-23.68	10	2	3	-10.76	14.07
169	58.24	-5.76	10	2	4	-14.23	20.92
174	23.98	-0.48	12	3	3	-15.20	21.55
175.5	36.68	-13.18	12	2	3	-15.32	17.88
176.5	45.80	-22.30	12	1	1	-14.00	15.29
186-A	46.83	-6.67	14	2	4	-19.79	20.14
186-B	46.83	-6.67	14	2	1	-18.87	20.39
187	49.04	-9.54	14	2	3	-15.82	23.18
189	73.48	-30.92	14	1	1	-15.44	19.38
197	68.71	-14.76	2	2	4	-0.35	23.78
208	50.60	-11.29	6	2	1	-12.61	19.41
210-A	87.69	-48.37	6	2	3	-16.19	14.22
210-B	87.69	-48.37	6	2	1	-17.34	15.12
215-A	60.50	35.82	7	5	3	-9.77	24.05
215-B	60.50	35.82	7	5	1	-15.14	15.91
232	214.42	-12.92	23	2	3	-16.04	19.35
235	129.44	17.26	24	5	4	-14.58	25.33
238	147.36	-0.66	24	3	2	-16.97	16.67
240	160.10	-13.40	24	2	3	-16.41	17.68
248	106.66	-11.96	25	2	5	-15.28	18.27
252	86.77	--	26	1	3	-14.00	19.56

Figure 4.19

C and O Isotopes in Carbonate Cements

Average composition for Cambro-Ordovician marine carbonate (Anderson and Arthur, 1983). ★

Carbonate veins containing scheelite (tungsten) mineralization at the GHT at various locations in Nova Scotia (Fisher, 1984).

The carbonate cements are characterized by a strong depletion in ^{13}C compared to the average for Cambro-Ordovician marine carbonates. Many of the cements actually have $\delta^{13}C$ values closer to those for Cambro-Ordovician organic matter ($\sim -26^{o}/_{o}$). The greatest ^{13}C depletion appears to be correlated with the contorted and fine laminated rock types, suggesting a relation with manganese concentrations in the host rock. Notice that the cements have a relatively narrow range in isotopic composition (especially compared to the vein carbonates in Fig 4.21).

EASTVILLE CARBONATE CEMENTS

+ —in Qtz Metawacke and Slate
□ —in Contorted Qtz Metawacke and Slate
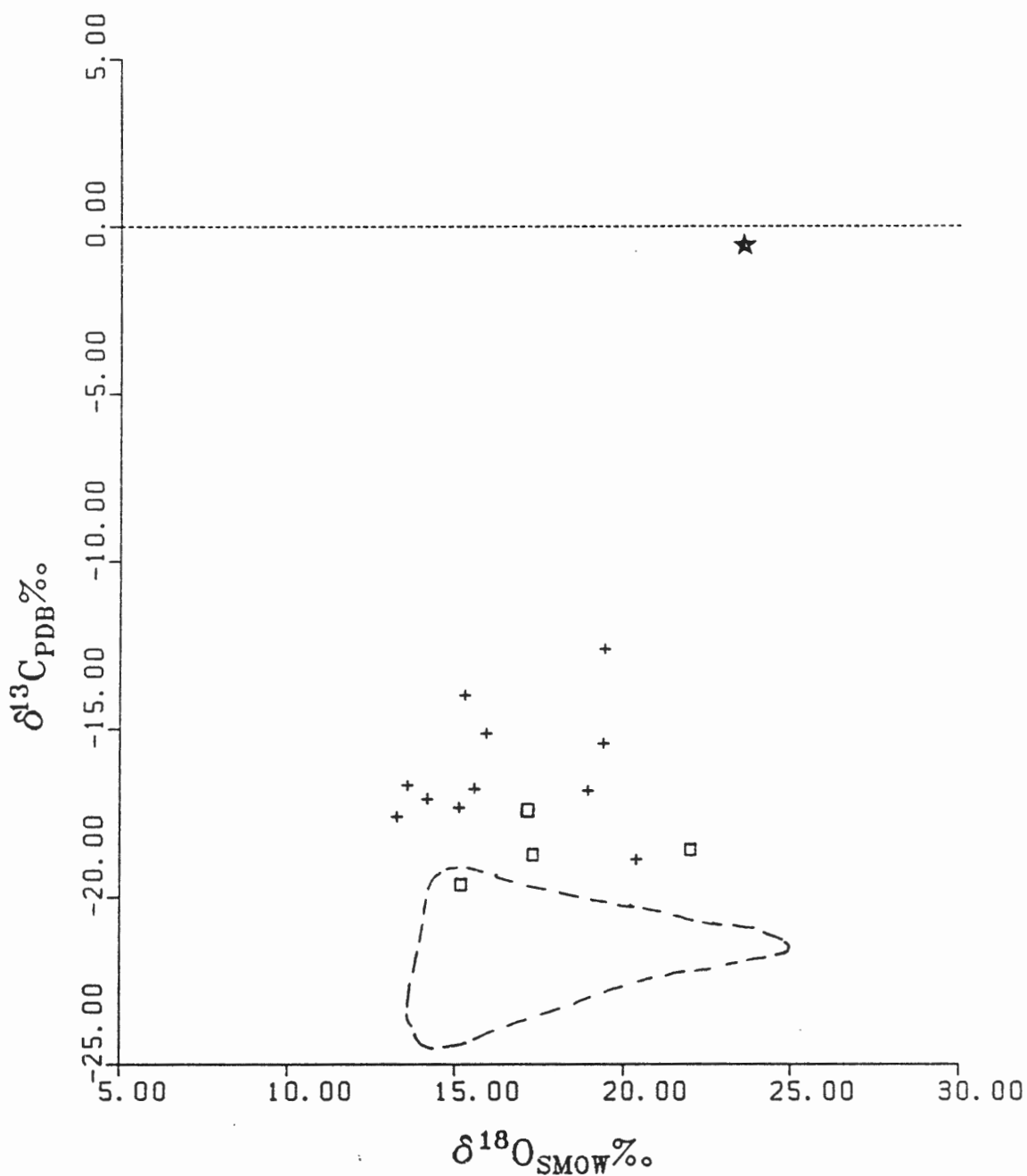
Figure 4.20

C and O Isotopes in Carbonate Blebs and Rims

Average composition for Cambro-Ordovician marine carbonate (Anderson and Arthur, 1983). ★

Carbonate veins containing scheelite (tungsten) mineralization at the GHT at various locations in Nova Scotia (Fisher, 1984).

The isotopic compositions of carbonates found in nodular blebs and in a rim surrounding a carbonaceous lens are similar to those of the cements displayed in Figure 4.19.

OTHER EASTVILLE CARBONATES

○ —in Blebs
△ —in Rims Around Dark Blebs
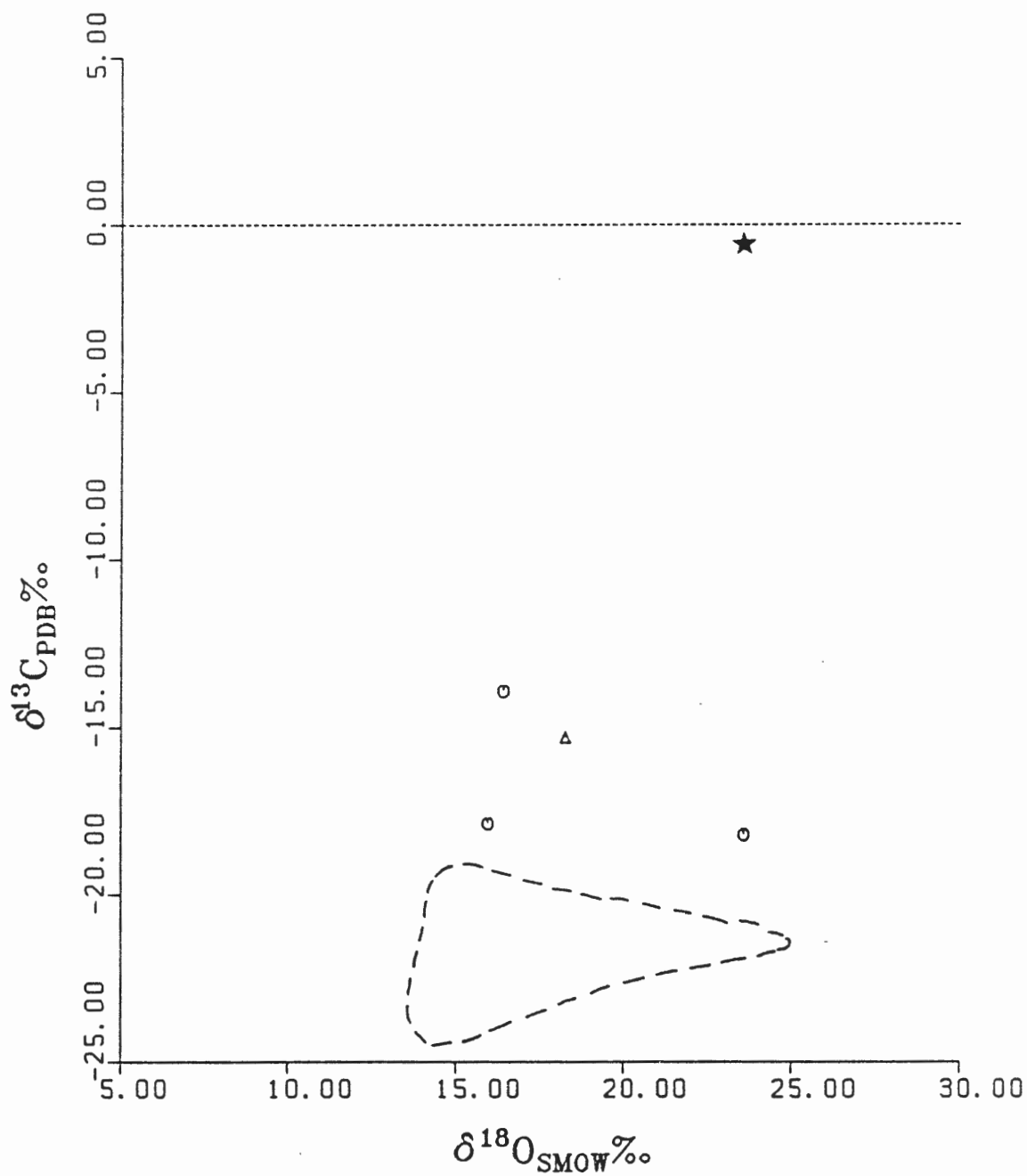
Figure 4.21

C and O Isotopes in Carbonate Veins

Average composition for Cambro-Ordovician marine carbonate (Anderson and Arthur, 1983). ★

Carbonate veins containing scheelite (tungsten) mineralization at the GHT at various locations in Nova Scotia (Fisher, 1984).

The veins which are barren of sphalerite and galena mineralization show a remarkably linear trend compared to the cluster of the cements and blebs. Decreasing $\delta^{18}O$ correlates positively with decreasing $\delta^{13}C$. The two unmineralized samples with considerably higher $\delta^{13}C$ are unexplained, however, they do define the same slope.

The mineralized veins show a very different trend in isotopic composition. These samples are confined to higher $\delta^{18}O$ values (20.14 to 25.33 $^{\circ\circ}/_{\circ}$) compared to the other samples (7.52 to 24.05 $^{\circ\circ}/_{\circ}$), and is close to the Cambro-Ordovician average. In contrast to their narrow $\delta^{18}O$ range, the mineralized veins range from the highest to the lowest values for $\delta^{13}C$ in the deposit. Note that the anomalous unmineralized vein sample 215-A mentioned above does in fact contain pyrite cubes.

EASTVILLE VEIN CARBONATE

× −Unmineralized
◇ −Mineralized with Sphalerite and Galena
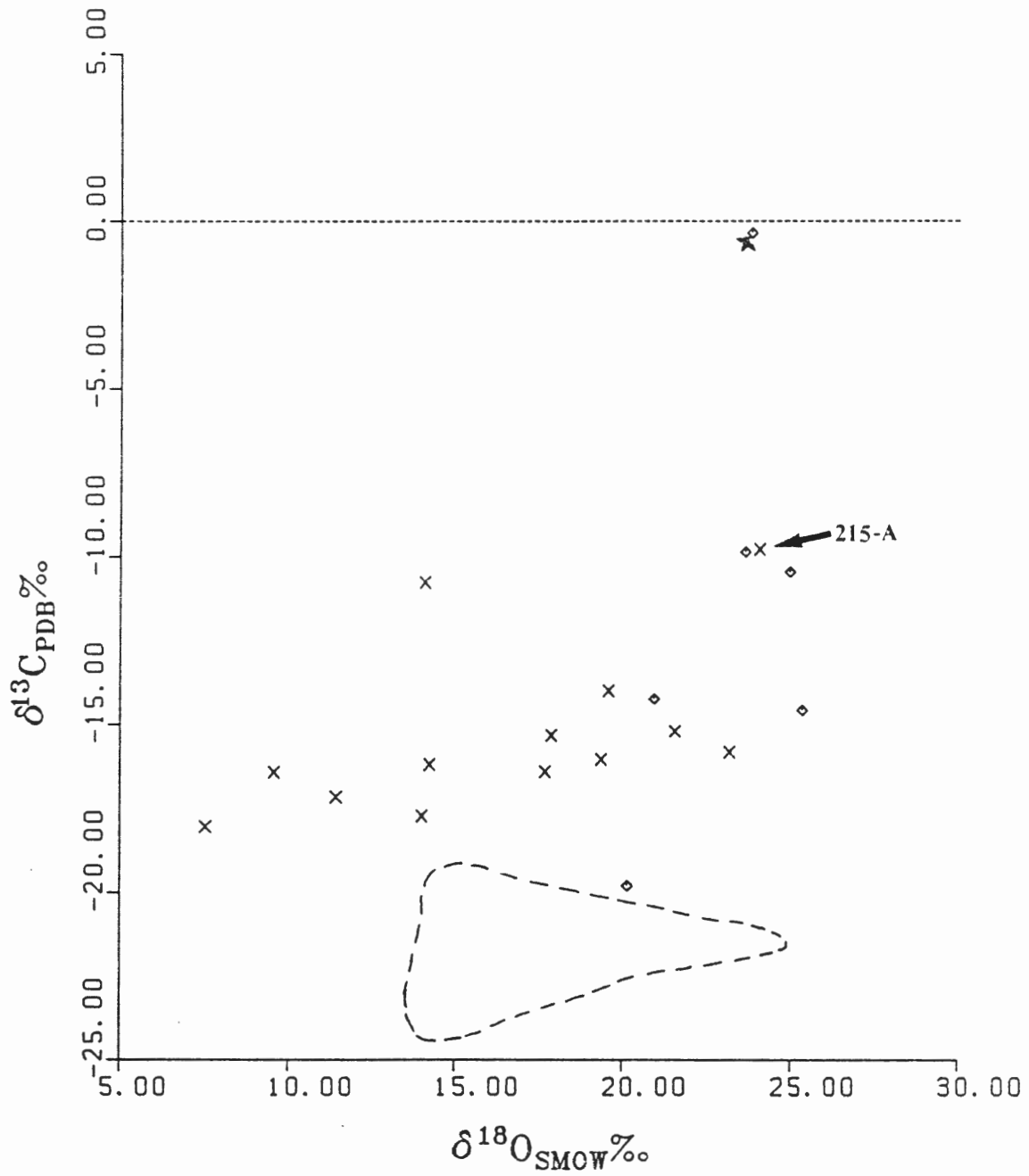
4.3.3 Discussion of Carbon and Oxygen Isotopes

The isotope data presented in Figures 4.19-4.21 indicate that the Eastville carbonates have not been formed by precipitation from Cambro-Ordovician sea water. The presence of carbonaceous material in the rocks, and the similarity in the $\delta^{13}C$ values to Cambro-Ordovician organic matter, suggests that the carbonates have been derived from biogenic carbonaceous material. It is thus not surprising that strong depletion in $\delta^{13}C$ is considered indicative of carbonate formation from organic material (Hoefs, 1982; Ohmoto and Rye, 1979).

The conversion of organic matter to carbonate involves *(1)* oxidation-reduction reactions at temperatures below about 300°C, as well as *(2)* hydrolysis reactions at higher temperatures (*ox* is any oxidizing agent):

(1) $C + ox \longrightarrow CO_2$
(2) $2C + 2H_2O \longrightarrow CO_2 + CH_4$ (methane)
          (Ohmoto and Rye, 1979).
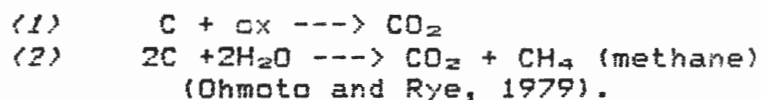
The oxidation of organic matter to produce authigenic carbonates is thought to be an important process in the diagenesis and early metamorphism of organic carbon-bearing sedimentary rocks (Anderson and Arthur, 1983), and in the genesis of metalliferous (Mn and other transition metals) sediments, (Bender and Heggie, 1984; Graybeal and Heath, 1984; Kalhorn and Emerson, 1984; Anderson and Arthur, 1983). There are generally several oxidizing agents present in

sediments, being removed in the reduction of organic material in the order of decreasing yield of Gibb's free energy:

O_2, NO_3^-, MnO_2, Fe_2O_3, SO_4^{2-}

(Bender and Heggie, 1984).

Hence, it is reasonable that the Eastville carbonates have formed from the diagenetic oxidation of organic material within the original sediments while suitable oxidants were still available. The abundant evolution of bicarbonate in association with high concentrations of Mn^{2+} or Ca^{2+} in the pore fluids, would promote carbonate formation even below the carbonate compensation depth.

However, the degree to which each oxidizing agent was involved is not known. The presence of unstable Mn-Fe-Ti oxyhydroxides would serve both as the oxidizing agent and as the Mn source to fix the CO_2 into carbonate before it could escape by diffusion. This could be backed up by the fact that the contorted (presumably more manganiferous) cements have the lowest $\delta^{13}C$, implying the highest degree of oxidation. However, the abundance of sulphides in the deposit suggests that large quantities of organic material must have been oxidized in the reduction of sulphate to sulphide.

The similar depletion in ^{13}C in tungsten veins in the GHT elsewhere in the Meguma (Fisher, 1983) could indicate that such oxidation is a dominant factor in the concentration of metals in the GHT.

The linear variation in the isotopic composition of the unmineralized carbonate veins is probably dependent on the stage in the hydrothermal event at which the carbonate precipitated. At early stages, hydrothermal fluids would precipitate carbonates enriched in the more reactive lighter isotopes (^{16}O, and ^{12}C). Subsequent enrichment of the heavy isotope in the late stage fluids and the lower temperatures of precipitation, would result in late stage carbonates being enriched in the heavy isotopes. Fractionation factors for carbon are lower than those for oxygen, thereby explaining the smaller changes in $\delta^{13}C$. Increasing temperature as well as the associated release of ^{18}O-poor water from clays has also probably served to decrease the $\delta d^{18}O$ and $\delta^{13}C$ values (Faure, 1977). Fractionation factors for carbon are lower than those for oxygen, thereby explaining the smaller changes in $\delta^{13}C$.

However, significant isotope fractionation requires that the carbonates must be accessible to fluids. Sediment compaction during lithification and the filling of pore spaces by the carbonate cement would reduce rock permeability, and thus fluid movement. In fact, Rye and Ohmoto (1974) have indicated that carbonates formed at low temperatures often show little or no isotopic fractionation at higher metamorphic temperatures. Hence, the cluster of cement compositions is probably close to the composition at the time of oxidation and precipitation.

The different trend in the sphalerite and galena

bearing carbonate veins is interesting. The high $\delta^{18}O$ could be explained by precipitation of calcite in the late stage of ore deposition, but this could not account for the extreme range in $\delta^{13}C$ (Rye and Ohmoto, 1974). Rye and Ohmoto (1974) have explained such occurrences by considering the oxygen fugacity of the fluid. At certain low levels of oxygen fugacity very large ranges (20 - 25 $^{oo}/_o$) in $\delta^{13}C$ of the precipitated carbonates are possible. In addition, the minimum $\delta^{13}C$ value for precipitated carbonate can be no more than 1 $^{oo}/_o$ lower than that of the original fluid (ie. falling in the range of the other samples in this case). This results from the fact that decreases in fO_2 would decrease the CO_2/CH_4 ratio and hence increase $\delta^{13}C$ for CO_2 due to the strong partitioning of ^{12}C into methane. The presence of Zn and Pb sulphides, and pyrite in sample 215-A, suggest low oxygen fugacities in the fluids, thus fitting the proposal of Rye and Ohmoto (1974).

Chapter 5

General Discussion

The following section presents a summary of the geological history of the deposit based on the discussions given in the previous sections.

5.1 Geological History of the Deposit

The GHT at Eastville seems to represent a period of sediment starvation in the sedimentary history of the Meguma Group. The buildup of the products of terrigenous weathering, such as jarosite and clay minerals such as smectites would be possible under these conditions, thus contributing to the aluminous nature of the rocks. The strong adsorption of metals on these minerals could account for a portion of the metal contents of the rocks, the most notable case being the apparent relation between Sr and smectite.

Oxidation of jarosite could explain part of the Fe-sulphide content, however, a sulphur isotope study might show that reduction of sea water sulphate by bacterial action or by the abundant carbonaceous material was a more important mechanism in the syngenetic or diagenetic formation of Fe, Zn, and Pb sulphides. Another indication of the importance of the oxidation of the organic component of the sediments is depletion in ^{13}C for the carbonates. It is

highly probable that carbonates derived by carbon oxidation were the major bearers of the anomalous quantities of manganese in the Manganese Zone. Thus, the state of non-sedimentation with subsequent buildup of carbonaceous material in the sediments was conceivably the critical factor in the retention of the anomalous metals Mn, Fe, Zn, and Pb in the sediments.

The late stages of diagenesis and early metamorphism probably saw the conversion of clays to muscovite and chlorite. The manganese for the metamorphic growth of spessartine garnet was probably supplied to a large degree by Mn-rich carbonates. Garnet nucleation might have been favoured by the release of Mn^{2+} from sulphides.

Garnet growth was followed by folding of the rocks and development of a foliation. Sphalerite and galena remobilization along the foliation, in open fractures, and in quartz and calcite veins must have occurred during or after the folding. Low oxygen fugacities in fluids carrying Zn and Pb in solution could have precipitated carbonates having a wide range in ^{13}C.

The higher grade metamorphic history of the GHT rocks at Eastville have been detailed by Cameron (1985).

5.2 Origin of Metals at Eastville

While the abundance of organic carbon in the newly deposited sediments can be seen to have been an important factor in the trapping of metals in the newly deposited

sediments, it does not directly explain where the metals came from.

One model for the development of metalliferous sediments is from hydrothermal solutions of volcanogenic origin (Bonatti, 1975). These solutions include those emanating from "black smokers" at rifting or spreading centres, and fossil deposits are commonly associated with ophiolites. Sulphide deposits form in the reducing conditions beneath spreading centres. Upon entering oxygenated water at the sea floor, water soluble Mn^{2+} and Fe^{2+} begin to form insoluble oxides. Fe^{2+} oxidizes more easily, hence becoming fractionated from Mn.

Characteristically, such oxide deposits form rapidly, thereby preventing excessive scavenging of other metals such as Cu, Co, and Ni. All of the Eastville data plots in the hydrothermal field of a NiCoCu-Fe-Mn diagram (Fig. 5.1). This is probably more indicative of the fact that even the limited sedimentation rate of the GHT would bury Fe and Mn minerals too quickly for "scavenging" of metals from sea water, rather than a volcanogenic Fe and Mn source. Similarly, a plot of U against Th (generally lower in rapidly formed hydrothermal deposits) places the Eastville rocks in the range of pelagic sediments (Fig. 5.2).

The lack of any indication of nearby volcanic activity within the Meguma Group, and the failure of standard geochemical comparisons indicates that a volcanogenic hydrothermal source for the Eastville metals is unlikely.

-93-
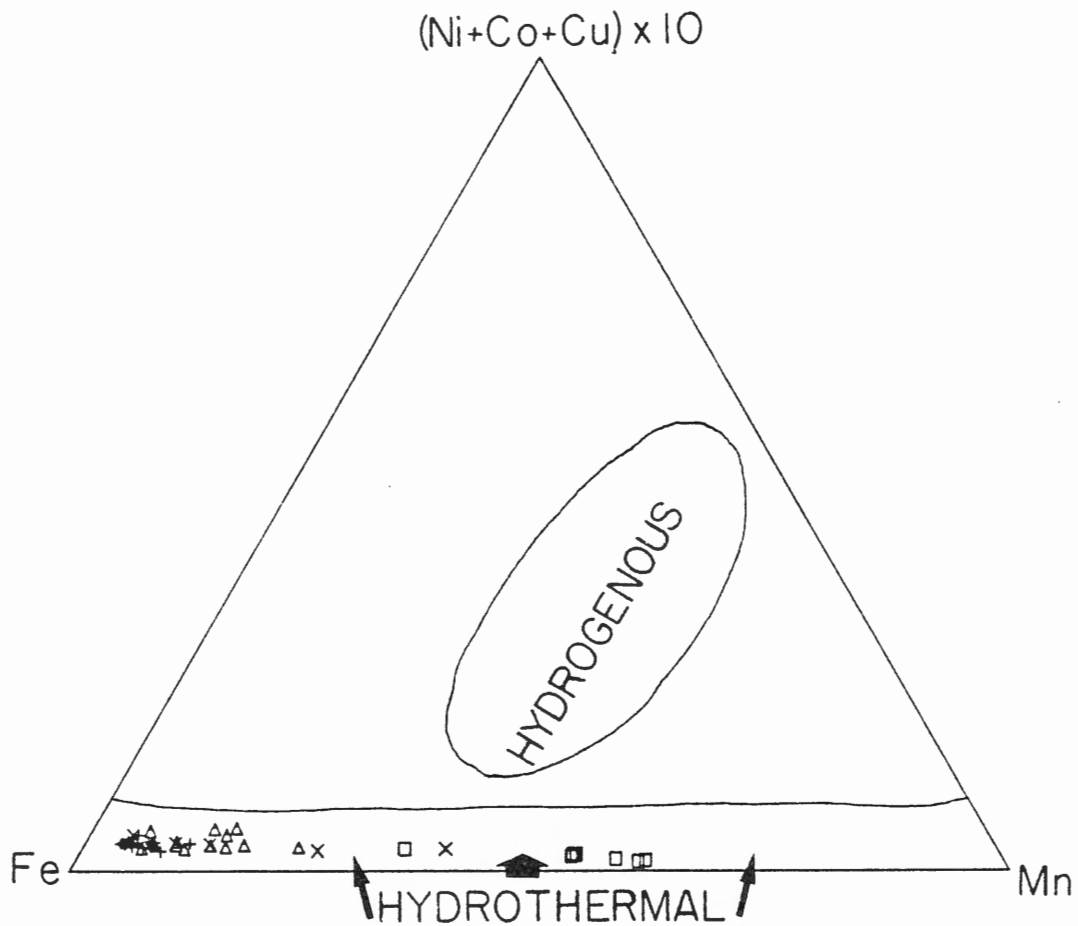
Figure 5.1 Fe-Mn-(Ni+Co+Cu) plot of the Eastville samples.
Hydrogenous and hydrothermal fields are taken from
Bonatti, 1975. All concentrations are in ppm.
Interbedded Zone = Δ ; Manganese Zone = □ ; Black Slate
= X ; Halifax Slate = +
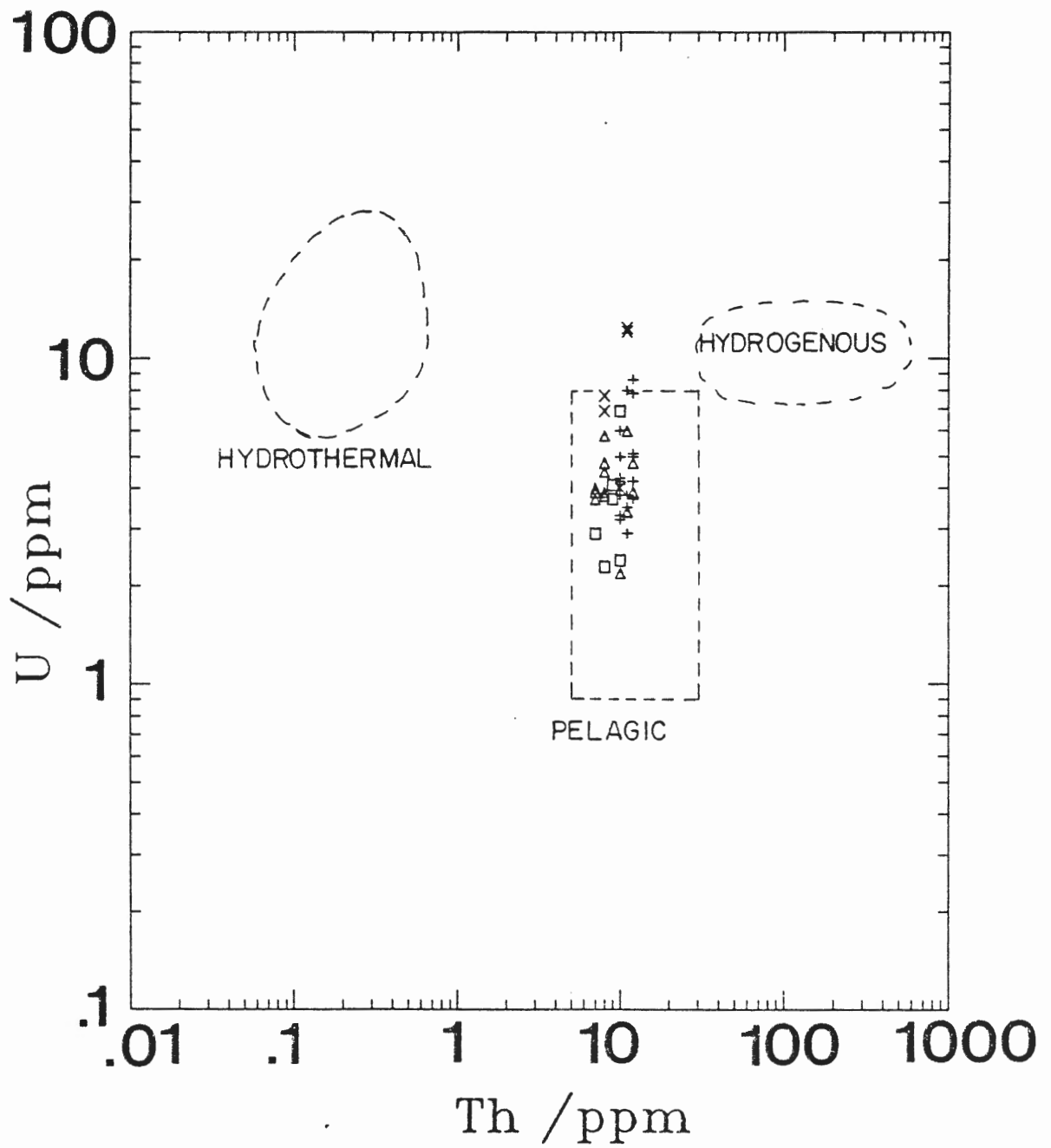
Figure 5.2 Uranium - Thorium plot. Pelagic, hydrogenous and hydrothermal fields are from Bonatti, 1975. Interbedded Zone = △ ; Manganese Zone = □ ; Black Slate = × ; Halifax Slate = +

Hydrogenous deposits form by the slow precipitation of metals dissolved in sea water (Dymond, *et al.*, 1984; Bonatti, 1975). In this case the metals have been produced by continental weathering. These deposits occur in areas with little or no terrigenous sediment input. This is clearly not the case at Eastville, and is supported by the discriminating plot in Figures 5.1, and 5.2.

Processes involved in the formation of diagenetic deposits seem much more comparable to those postulated for Eastville's early history. These processes take place in hemipelagic (low sedimentation rate) sediments having a relatively high rate of organic matter deposition (Dymond, *et al.*, 1984; Bonatti, 1975). Oxy-hydroxides of Mn and Fe, containing other metals such as Zn, Cu, Ni, Co, and Ti, are deposited in the oxygenated upper few mm to cm of sediment (Graybeal and Heath, 1984; Dymond *et al.*, 1984) (some type of bottom current would be necessary to maintain an oxygenated sediment-water interface).

After being covered by new influxes of sediment to the depth of a few cm, the oxy-hydroxides are involved in oxidation-reduction reactions with carbonaceous material. The insoluble Mn^{4+} oxides are converted to Mn^{2+} in solution (similarly $Fe^{3+} \rightarrow Fe^{2+}(aq)$). The aqueous species then percolate back up to the oxidizing zone and are re-precipitated (Greybeal and Heath, 1984; Roy, 1981).

This cycle will tend to concentrate Mn, Fe and other metals near the sediment-water interface. However, at a

certain point the concentration of metals in the reducing zone will be sufficient that they will start to precipitate (with anions) or become adsorbed to minerals such as smectites.

In the Manganese Zone at Eastville, the precipitates appear to have been Mn-rich carbonate and Fe-sulphides. Excess Mn present at the sediment-water interface in the extremely reducing conditions of carbonaceous buildup of the Black Slate might be forced to form Mn-sulphide mixtures with co-precipitating pyrrhotite or sphalerite.

However, the degree to which diagenesis contributed to the actual *enrichment* in Mn, Fe, Zn, and Pb is indeterminable. Note also that the while Zn mobility would be controlled by diagenesis, Pb distribution would be more strongly controlled by its ready adsorption to, and complexing with, organic material. Constant Zn:Pb ratios would not be maintained if the elements were predominantly involved in these two independent processes. Co-precipitation of sphalerite and galena was probably a dominant factor in the highly reducing black slate beds, but again the extent of enrichment is not known.

Thus, another, external source of metal enrichment such as sedimentary exhalative hydrothermal fluids might have been important. Lydon, *et al.*, (1985) have developed a model for sedimentary exhalative deposits having considerable lateral extent and relatively constant ratios between elements (ie. similar to Eastville). Overpressured pore

fluids resulting from clay de-watering in sandy rocks situated deep in the sediment pile would leach Zn and Pb. Formation of synsedimentary faults would release these fluids to fill anoxic pools in which sulphide deposition could occur. A good deal of caution must be taken in applying this model to the Eastville deposit where no synsedimentary fault has been identified.

Chapter 6

Conclusions

1. The increasingly fine bedding, and higher contents of
    carbonaceous material toward the top of the Goldenville
    and in the Black Slate unit imply a state of sediment
    starvation in the Goldenville-Halifax Transition at
    Eastville.

2. The section is enriched in Mn, Zn, and Pb, and to a
    lesser degree Ca, compared to typical sections of the
    Goldenville Formation. The Manganese Zone and the Black
    Slate are particularly enriched in Mn and Ca, while Zn
    and Pb distributions are erratic.

3. Manganese is found in spessartine garnet, ilmenite,
    manganiferous calcite, and in small quantities in
    sulphides. Most of the Mn is concentrated in spessartine
    garnet, which in their growth appear to have derived the
    Mn from manganese-rich carbonates, and possibly
    manganiferous sulphides.

4. Zinc and lead are found in a 2:1 ratio (by weight in
    the whole rock) contained in sphalerite and galena,
    predominatly in cross-cutting veins, fractures,
    transposed along the foliation, and to a lesser degree in
    disseminated and bedded blebs. It is believed that
    all of the Zn and Pb is of syngenetic or diagenetic
    origin, with remobilization in low oxygen fugacity

fluids, or transposition along cleavage planes, accounting for the structurally controlled cases.

5. Inter-element correlations reveal that several terrigenous "clay" minerals were probably important bearers of some metals when the sediments were deposited. For instance, it appears that the abundance of smectite minerals in the original detritus controls the present-day variation in Sr contents, and jarosite might have contributed to the abundance of Fe-sulphides. However, correlation coefficients do not point to any detrital minerals as the source for the Mn, Zn, and Pb, hence suggesting deposition as chemical precipitates

6. Carbon isotopes for the carbonates indicate that they have formed by the oxidation of the resident carbonaceous material. This, combined with the apparent low sedimentation rate, and abundance of carbonaceous matter, suggests that diagenetic processes could have been an important enrichment mechanism for the Mn and Zn. Adsorption to the organic matter could have concentrated Pb from the available sea water.

7. It is not known if the diagenetic and adsorption processes could have produced the observed metal content or the consistent Zn:Pb ratios. Another possible metal source could be sedimentary exhalative hydrothermal solutions.

Chapter 7

Recommendations

1. The samples prepared for rare earth element analysis should be run commercially or at St. Mary's if the equipment is repaired. REE's might give more information on the sea water or hydrothermal solutions involved in the deposition of the Mn, Zn, and Pb.

2. Sulphur isotopes might reveal the contribution to the sulphides by jarosite, and carbon or bacterial reduction of sea water.

3. Whole rock analysis at a smaller scale (eg. hand samples rather than the metre scale) might provide better resolution in the inter-element correlation analysis.

4. A more sophisticated statistical method such as factor analysis might be attempted for comparison with the correlation diagram method used here.

5. More microprobe analyses are needed to better define the distribution of manganese.

6. A detailed study of the structural history of the area is required for a better understanding of the remobilization of the sphalerite and galena, and to determine the economic potential of this deposit and similar deposits which might be discovered elsewhere in the Meguma.

7. An understanding of the tectonics and sedimentation of

the Meguma are required to determine the reason for the
sudden halt in sediment supply in the GHT, and for the
wide regional extent of metalliferous GHT. A better
understanding of the depositional environment of the GHT
is needed to determine if factors such as the time scale
between sediment injections, and oxygen and sea water
circulation would be sufficient for diagenetic processes
to concentrate significant quantities of metals. The
identification of synsedimentary faults or feeder zones
in the Meguma might be instrumental in confirming a
sedimentary exhalative contribution to the metal content
of the GHT.

References

Anderson, T.F.; and Arthur, M.A.   1983.
     Stable isotopes of oxygen and carbon and their
application to sedimentation and paleoenvironmental
problems.
     in: Stable isotopes in sedimentary geology, SEPM Short
Course, 10, Dallas, Chapter 1, 151pp.

Bender, M.L.; and Heggie, D.T.   1984.
     Fate of organic carbon reaching the deep sea floor: a
status report.
     in: Geochim. Cosmochim. Acta, 48, 977-986.

Binney, W.P.   1979.
     Report on 1979 diamond drilling, Gold Brook - Project
224 for St. Joseph Explorations Limited. (Confidential
Report)

Bonatti, E.   1975.
     Metallogenesis at ocean spreading centers.
     in: Review of Earth and Planetary Sciences, 3, 401-431.

Burke, W.E.F.   1983.
     Geophysical analysis of field and laboratory
measurements at the Eastville lead-zinc deposit,
Colchester County, Nova Scotia.
     Unpublished B.Sc. Thesis, Dalhousie University,
Halifax, Nova Scotia, 60pp

Cameron, B.I.   1983.
     The contact metamorphic effects of a granitoid pluton
on zinc-lead mineralization in the manganiferous
metasediments of the Meguma Group, Eastville, Colchester
County, Nova Scotia.
     Unpublished B.Sc. Thesis, Dalhousie University,
Halifax, Nova Scotia, 104pp

Chave, K.E., and MacKenzie, F.T.   1961.
     A statistical technique applied to the geochemistry of
pelagic muds.
     in: J. Geol., 69, 572-582.

Clarke, D.B.; and Halliday, A.N.   1985.
    Sm/Nd isotopic investigation of the age and origin of
  the Meguma Group metasedimentary rocks.
    in: CJES, 22, 102-107.

Clarke, D.B.; and Halliday, A.N.   1980.
    Strontium isotope geology of the South Mountain
  Batholith, Nova Scotia.
    in: Geochim. Cosmochim. Acta, 44, 1045-1058.

Deer, W.A.; Howie, R.A.; and Zussman, J.   1972.
    An introduction to the rock forming minerals.
  Longman Group Ltd., Toronto, 527pp.

Dymond, J.; Lyle, M.; Finney, B.; Piper, D.Z.; Murphy, K.;
  Conard, R.; and Pisias, N.   1984.
    Ferromanganese nodules from MANOP Sites H, S, and R -
  control of mineralogical and chemical composition by
  multiple accretionary processes.
    in: Geochim. Cosmochim. Acta, 48, 931-949.

Faure, G.   1977.
    Principles of Isotope Geology.
    Wiley, Toronto, 464pp.

Fisher, B.E.   1984.
    A regional investigation of scheelite occurrences in
  the Meguma Group of Nova Scotia.
    Unpublished   B.Sc.   Thesis,   Dalhousie   University,
  Halifax, Nova Scotia, 106pp

Fletcher, H.; and Faribault, E.R.   1903.
    Eastville sheet # 48, Geological Survey of Canada,
    Map 633

Fyson, W.K.   1966.
    Structures in the Lower Paleozoic Meguma Group, Nova
  Scotia.
    in: GSA Bull., 77, 931-944.

Graves, M.C.; and Zentilli, M.   1982.
    A review of the geology of gold in Nova Scotia.
    in: CIM Special Paper 23, 233-242.

Greybeal, A.L.; and Heath, G.R.   1984.
    Remobilization of transition metals in surficial
pelagic sediments from the Eastern Pacific.
    in: Geochim. Cosmochim. Acta, 48, 965-975.

Henley, R.W.; Truesdell, A.H.; and Barton, P.B. Jr.   1984.
    Fluid-mineral equilibria in hydrothermal systems.
    in: Reviews in Econ. Geol., 1, 267pp., Society of Econ.
Geologists, Elpaso, USA.

Hoefs, J.   1982.
    Isotope geochemistry of carbon, p103-113.
    in: Stable Isotopes, H.L, Schmidt; Forstel, H; and
Heinzinger, K (eds.), Analytical Chemistry Symposia
Series, 11, Elesvier Scientific Publishing Company,
Amsterdam, 775pp.

Hoefs, J.   1980.
    Stable Isotope Geochemistry.
    Springer-Verlag, New York, 208pp.

Hurlbut, C.S.; and Klein, C.   1977.
    Manual of Mineralogy.
    19th ed., Wiley, Toronto, 532 pp.

Jenner, K.A.   1982.
    A study of sulphide mineralization in the Meguma Group
sediments, Gold Brook, Colchester County, Nova Scotia.
    Unpublished B.Sc. Thesis, Dalhousie University,
Halifax, Nova Scotia, 60pp

Kalhorn, S.; and Emerson, S.   1984.
    The oxidation state of manganese in surface sediments
of the deep sea.
    in: Geochim. Cosmochim. Acta, 48, 897-902.

Keppie, J.D.   1982.
    The Minas Geofracture.
    in: Major structural zones and faults of the northern
Appalachians. ed. P. St. Julien and J. Beland. GAC,
Special Paper 24, 263-280.

Kramm, U.   1976.
    The coticule rocks (spessartine quartzites) of the
Venn-Stavelot, a volcanoclastic sediment?
    in: CMP, 6, 135-155.

Liew, M.   1979.
     Geochemical studies of the Goldenville Formation at
Taylor Head, Nova Scotia.
     Unpublished   M.Sc.   Thesis,   Dalhousie   University,
Halifax, Nova Scotia.

Lydon, J.W.; Goodfellow, W.D.; and Jonasson, I.R.   1985.
     A general genetic model for stratiform baritic deposits
of the Selwyn Basin, Yukon Territory and District of
MacKenzie.
     in: Current Research, Part A, Geological Survey of
Canada, Paper 85-1A, 651-660

MacMicheal, T.P.   1975.
     The origin of the lead-zinc-silver ores and   the
alteration of the surrounding granites at the Dunbrack
mine, Musquodoboit Harbour. Nova Scotia.
     Unpublished B.Sc. Thesis Dalhousie University, Halifax,
N.S.

O'Neil, J.R.   1979.
     Stable isotope geochemistry of rocks and minerals,
p235-265.
     in: Lectures in Isotope Geology. Jager, E, and
Hunziker, J.C. (eds.), Springer-Verlag, New York, 329pp.

Ohmoto, H.; and Rye, R.O.   1979
     Isotopes of sulphur and carbon, p 509-567.
     in: Geochemistry of hydrothermal ore deposits (2nd
Ed.), Barnes, H.L. (ed.), Wiley, Toronto, 798pp.

Poole, W.H.   1971.
     Graptolites, copper, and potassium-argon in Goldenville
Formation, Nova Scotia.
     in: Report of Activities, part A, Geological Survey of
Canada, Paper 71-1A, 9-11.

Poole, W.H.; Sanford, B.V.; Williams, H.; Kelley, D.G. 1970.
     Geology of southeastern Canada.
     in: Geology and Economic Minerals of Canada, ed. R.J.W.
Douglas. GSC, Economic Geology Report 1, 229-304.

Poole, W.H.   1967.
    Tectonic evolution of the Appalachian region of Canada.
    in: Geology of the Atlantic region. ed. E.R.W. Neale,
    and H. Williams. GAC, Special Paper, 4, 9-51.

Reinecke, T.; Okrusch, M.; and Richter, P.   1985.
    Geochemistry of ferromanganoan metasediments from the
    island of Andros, Cyladic Blueschist Belt, Greece.
    in: Chem. Geol. , 53, 249-278.

Reynolds, P.H.; Zentilli, M.; and Muecke, G.K.   1981.
    K-Ar and $^{40}Ar/^{39}$ geochronology of granitoid rocks from
    southern Nova Scotia: it's bearing on the geological
    evolution of the Meguma Zone of the Appalachians.
    in: CJES, 18, .386-394.

Reynolds, P.H.; Zentilli, M.; Elias, PM.; Muecke, G.K. 1984.
    The southwestern Meguma Zone, Nova Scotia: an argon age
    study of regional cooling and Hercynian mineralization.
    in: Geol. Ass. of America, Northeastern Section,
    Abstracts with Programs, 16, 59.

Reynolds, P.H.; and Muecke, G.K.   1978.
    Age studies on slates: applicability of the $^{40}Ar/^{39}Ar$
    stepwise outgassing method.
    in: EPSL, 40, 111-118.

Reynolds, P.H.; Kublick, E.E.; and Muecke, G.K.   1973.
    Potassium-argon dating of slates from the Meguma Group,
    Nova Scotia.
    in: CJES, 10, 1059-1067.

Roy, S.   1981.
    Manganese Deposits.
    Academic Press, London, 451pp.

Rye, R.O.; and Ohmoto, H.O.   1974.
    Sulfur and carbon isotopes and ore genesis: a review.
    in: Econ. Geol., 69, 826-842.

Schenk, P.E.   1983.
     The Meguma Terrane of Nova Scotia - an aid to trans-
Atlantic correlation.
     in: Regional Trends in the Geology of the
Appalachian-Caledonian-Hercynian-Mauritanide Orogen, ed.
P.E. Schenk, NATO ASI Series C, 116, 121-130.

Schenk, P.E.   1981.
     The Meguma Zone of Nova Scotia - a remnant of Western
Europe, South America, or Africa?
     in: Geology of the North Atlantic Borderlands, ed. J.M.
Kerr and A.J.Ferguson, Can. Soc. Petroleum Geol. Mem. 7,
119-148.

Schenk, P.E.   1970.
     Variation of the flysh-like Meguma Group (Lower
Paleozoic) of Nova Scotia compared to the Recent
sedimentation off the Scotian Shelf.
     in: Geol. Ass. Can. Special Paper 7, 127-153.

Schiller, E.A. and; Taylor, F.C.   1965.
     Spessartine-quartz rocks (coticules) from Nova Scotia.
     in: Am. Min., 50, 1477-1481.

Taylor, F.C.; and Schiller, E.A.   1966.
     Metamorphism of the Meguma Group of Nova Scotia.
     in: CJES, 3, 959-974.

Turekian, K.K.; and Wedepohl, K.H.   1961.
     Distribution of the elements in some major units of the
earth's crust.
     in: Geol. Soc. Am. Bull., 72, 175-192.

Wolfson, I.K.   1983.
     A study of the tin mineralization and lithogeochemistry
in the area of the Wedgeport Pluton, southwestern Nova
Scotia.
     Unpublished M.Sc. Thesis, Dalhousie University,
Halifax, Nova Scotia, 396pp.

Zentilli, M.; Graves, M.C., Mulja, T.; MacInnis, I.N.   1986.
     Geochemical characterization of the Goldenville-Halifax
transition of the Meguma Group of Nova Scotia: preliminary
report.
     in: Current Research, Part A, Geological Survey of
Canada, Paper 86-1a, 423-428.

Zentilli, M.; Wolfson, I.; Shaw, W.; and Graves, M.C.   1984.
    The Goldenville-Halifax transition of the Meguma Group
as control for metallic mineralization.
    in: Geological Society of America, Abstracts with
Programs, 16, 73.

Zentilli, M.; and MacInnis, I.N.   1983.
    Geochemical   investigation   of   manganiferous   beds
associated with strata-bound lead-zinc mineralization in
the Meguma Group.
    in: Nova Scotia Dept. of Mines and Energy Information
series, 6, 65-68.

Zentilli, M.; and Graves, M.C.   1977.
    Evolution of metallogenic domains in Nova Scotia.
    in: CIM Bull., 70, 69 (abstract).
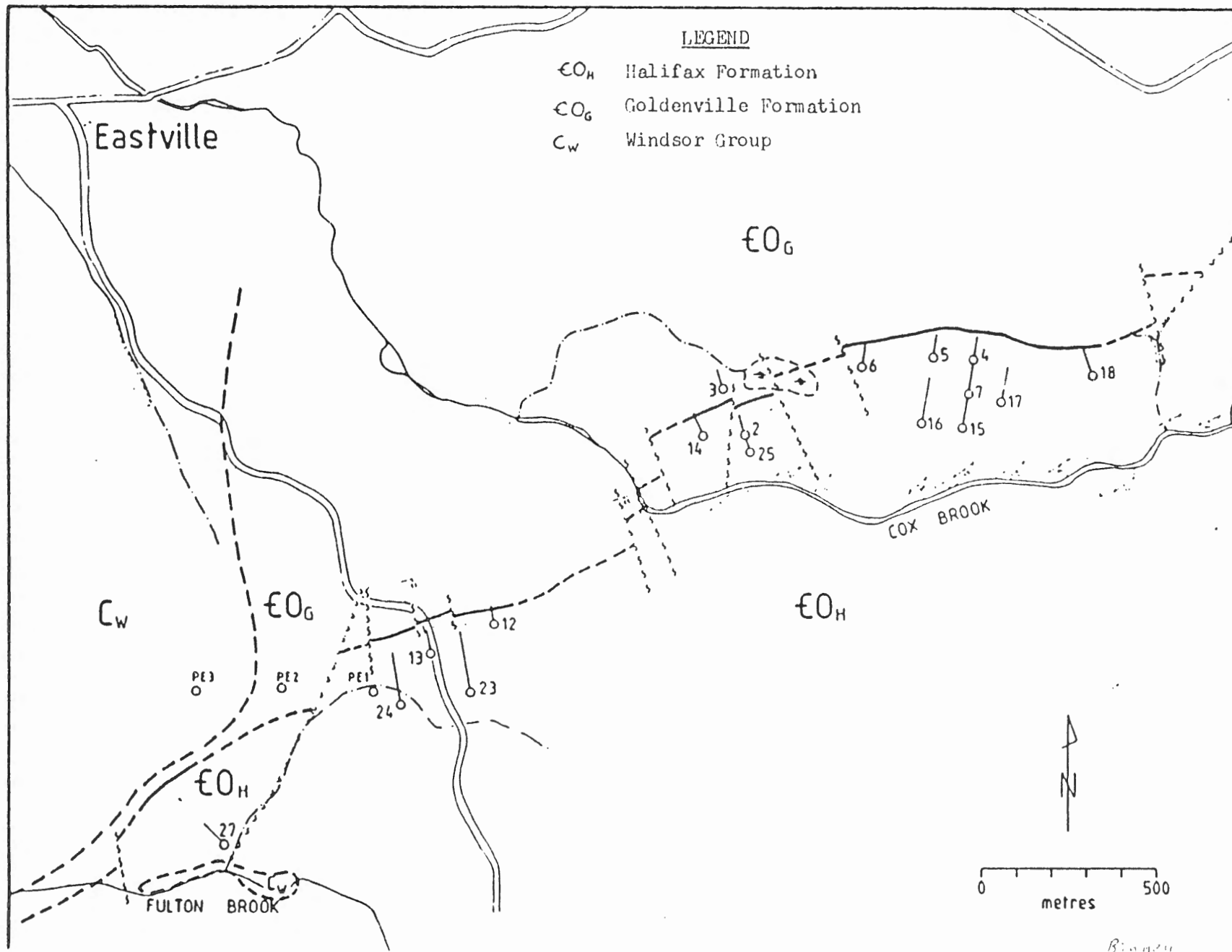
LEGEND

€O$_H$ Halifax Formation

€O$_G$ Goldenville Formation

C$_W$ Windsor Group

Eastville

€O$_G$

€O$_G$

C$_W$

€O$_H$

€O$_H$

COX BROOK

FULTON BROOK

PE3

PE2

PE1

N

0   500
metres

LEGEND

€O$_H$ Halifax Formation

€O$_{HA}$ Contact Aureole

€O$_G$ Goldenville Formation

DC$_G$ Granitoid
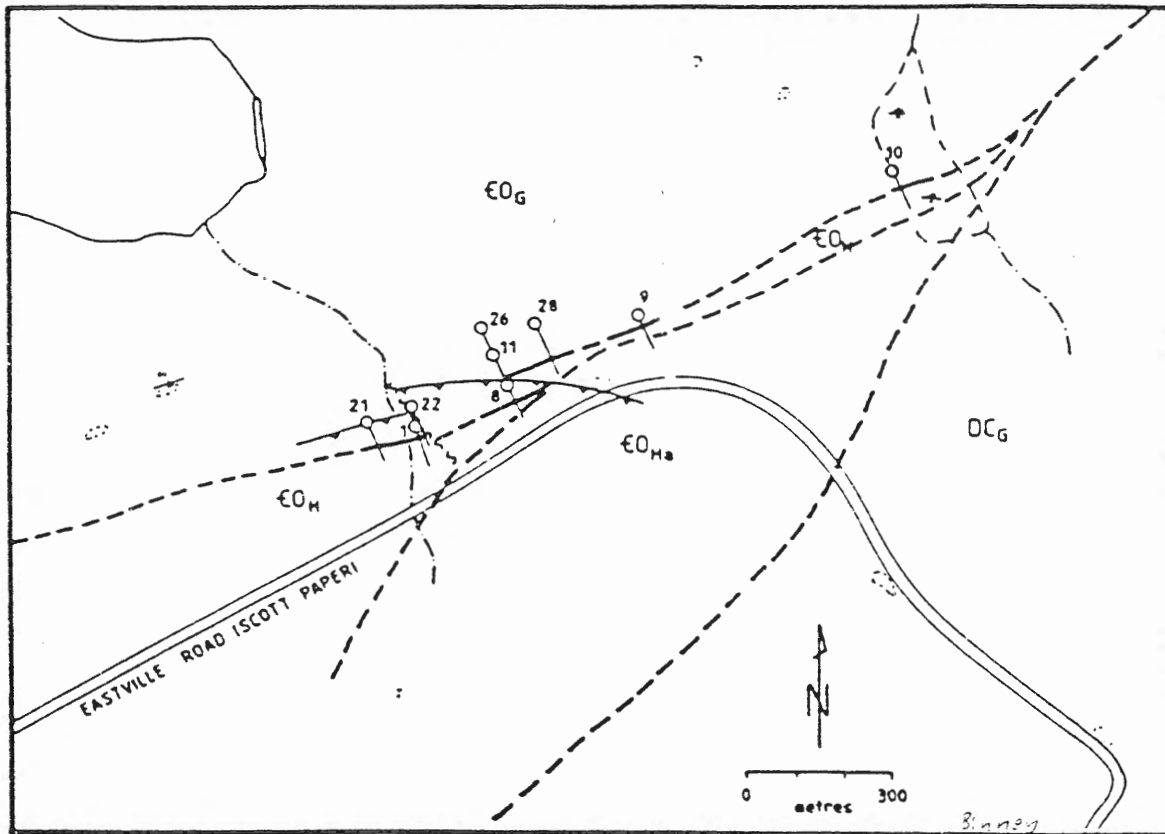
APPENDIX 2 - Comment on Data Quality

The exact method of dissolution for the acid-leach samples is not known. The accuracy of the data also is unknown, but the error can be assumed to be high (> 10%) considering the volume of samples analysed for the Eastville deposit (~1000).

The isotope analysis was made with about 0.02°/oo accuracy.

Wolfson (1983) reported good accuracy for interenational standards analysed at X-Ray Labs (<5% error for major elements; <10% error for trace elements). Following is the list of instrumental methods used. Note that all Bi fell below the detection limits. Values for Zn and Pb which were above the analysis limit (4000 ppm) were substituted with acid leach values since both analytical methods gave reasonably consistent results.

	METHOD	DETECTION LIMIT
AU PPB	FANA	1.000
LI PPM	A4	1.000
BE PPM	DCP	10.000
B PPM	DCP	10.000
WRMIN PPM	XRF	10.000
CO2 %	WET	0.100
WRMAJ %	XRF	0.010
S %	XRF	0.002
CL PPM	XRF	50.000
V PPM	DCP	2.000
MO PPM	DCP	1.000
CR PPM	DCP	2.000
FEO %	WET	0.100
CO PPM	NA	5.000
NI PPM	DCP	1.000
CU PPM	DCP	0.500
ZN PPM	DCP	0.500
GE PPM	DCP	10.000
AS PPM	NA	1.000
AG PPM	DCP	0.500
CD PPM	DCP	1.000
SN PPM	EMS	3.000
SB PPM	NA	0.200
C %		0.010
W PPM	NA	1.000
HG PPB	WET	10.000
PB PPM	DCP	2.000
BI PPM	EMS	10.000
U PPM	DNC	0.100
TH PPM	NA	1.000

APPENDIX 3 - Comment on Statistical Methods

Values which fell below the detection limit were omitted from all statistical analyses, since this study was oriented towards the trends in element contents rather than actual concentrations

In order to avoid preforming data transformation to achieve normal Gaussian data distributions Spearman rank correlation coefficients were obtained rather than Pearson correlations. The Spearman program also provided 2-tailed significance levels (here confidence = (1-sig)*100%).

All statistics were carried out using the Statistical Package for the Social Sciences (SPSS) program on Dalhousie's CDC Cyber 170/740. Plots were made using ZETA plotting routines in FORTRAN 5.

APPENDIX 4.1
ACID-LEACHABLE METAL CONTENTS FOR HOLES 24 AND 25

SAMPLE	HOLE	UNIT	DEPTH /m	Pb /ppm	Zn /ppm	MnO /Wt%	FeO* /Wt%	As /ppm	Ba /ppm	Sr /ppm
1659	24	5	67.70	2000	6500	0.03	6.69	19	938	199
1660	24	5	64.70	1500	4300	0.03	6.04	12	812	194
1543	24	5	53.45	680	2400	0.02	5.02	14	884	214
1544	24	5	51.95	720	2100	0.02	4.63	5	899	250
1547	24	5	47.45	540	1900	0.03	5.27	15	963	231
1552	24	5	40.20	1500	4000	0.02	4.89	3	765	189
1665	24	5	32.20	1300	3180	0.02	6.04	15	776	239
1557	24	5	21.45	8200	14000	0.02	4.37	38	862	246
1635	24	5	18.45	3800	9200	0.05	3.99	20	712	323
1638	24	5	13.95	1200	3200	0.02	4.76	17	819	366
1561	24	5	7.95	6800	11200	0.02	4.76	46	815	288
1562	24	5	5.70	2300	5700	0.02	6.04	25	755	311
1563	24	4	3.95	3000	5800	0.02	5.40	25	870	303
1640	24	4	2.45	740	1900	0.07	5.66	222	824	88
1667	24	4	0.85	75	128	0.12	8.23	26	916	74
1668	24	3	-1.00	935	2450	0.12	7.59	55	857	31
1669	24	3	-3.00	1600	5600	0.12	8.49	82	646	20
1670	24	3	-5.00	1250	2650	>2.00	7.07	4	692	30
1671	24	3	-7.20	130	710	>2.00	6.43	82	848	47
1672	24	2	-9.90	1280	3750	0.11	5.40	16	1058	56
1673	24	2	-12.90	1700	3500	0.06	4.50	13	1078	58
1674	24	2	-15.90	1700	4100	0.05	5.66	12	955	52
1675	24	2	-18.90	900	3000	0.03	6.56	8	895	50
1677	24	2	-24.90	2980	5600	0.02	5.79	29	1063	12
1680	24	2	-33.90	420	2000	0.06	6.82	43	1063	49
1682	24	2	-39.28	860	2550	0.03	6.56	59	1115	42
1683	25	5	41.87	32	288	0.03	8.23	11	895	394
1684	25	5	39.27	18	120	0.02	6.94	5	719	385
1686	25	5	34.08	9	110	0.02	7.20	-1	841	405
1687	25	5	31.48	8	108	0.02	6.56	16	727	342
1614	25	5	23.04	2600	5200	0.02	4.89	55	821	306
1616	25	5	20.44	840	2200	0.02	5.14	17	895	294
1690	25	5	14.16	44	168	0.02	5.14	37	740	222
1643	25	5	10.05	2000	5200	0.02	4.63	88	962	162
1644	25	5	8.75	2000	4400	0.01	5.79	51	1113	164
1645	25	5	7.45	1300	3600	0.01	5.40	8	1074	142
1691	25	5	6.15	430	1500	0.01	7.07	90	963	161
1692	25	4	4.20	235	880	0.01	8.23	3	967	137
1693	25	4	1.45	1200	3100	0.03	9.13	260	1072	90
1618	25	3	-.87	60	140	0.09	7.46	64	991	89
1619	25	3	-2.59	800	2800	0.09	6.17	113	840	30
1620	25	3	-4.33	320	1400	0.12	6.82	113	785	27
1622	25	3	-7.65	240	800	0.13	5.27	75	909	43
1694	25	2	-9.66	420	1925	0.03	5.27	17	1064	69
1695	25	2	-12.25	3200	6180	0.05	5.02	38	1086	70
1696	25	2	-14.85	200	5200	0.03	6.17	10	1102	67
1697	25	2	-17.45	640	2000	0.03	5.14	78	780	87
1700	25	2	-28.28	435	1400	0.02	6.82	21	1111	56
1626	25	2	-34.12	3800	6600	0.02	4.63	116	1290	51
1627	25	2	-35.42	3200	5800	0.03	6.82	52	1217	47

APPENDIX 4.2
GENERAL STATISTICS FOR ACID-LEACHABLE METALS - DDH24 AND 25

ALL UNITS

	Pb /ppm	Zn /ppm	MnO /Wt%	FeO* /Wt%	As /ppm	Ba /ppm	Sr /ppm
VALID	50	50	50	50	49	50	50
MEAN	1443	3451	0.0396	6.052	45.78	916.9	156.0
STDEV	1629	2846	0.0351	1.209	51.69	145.5	119.5
MIN	8	108	0	3.99	3	646	12
MAX	8200	14000	0.13	9.13	260	1290	405

HALIFAX SLATE - UNIT 5

	Pb /ppm	Zn /ppm	MnO /Wt%	FeO* /Wt%	As /ppm	Ba /ppm	Sr /ppm
VALID	23	23	23	23	22	23	23
MEAN	1731	3938	0.0216	5.630	27.59	858.7	262.0
STDEV	2073	3608	0.0091	1.077	24.79	108.9	80.88
MIN	8	108	0.01	3.99	3	712	142
MAX	8200	14000	0.05	8.23	90	1113	405

BLACK SLATE - UNIT 4

	Pb /ppm	Zn /ppm	MnO /Wt%	FeO* /Wt%	As /ppm	Ba /ppm	Sr /ppm
VALID	5	5	5	5	5	5	5
MEAN	1050	2362	0.0503	7.330	107.2	929.8	138.4
STDEV	1176	2223	0.0454	1.687	123.2	95.61	95.03
MIN	75	128	0.01	5.40	3	824	74
MAX	3000	5800	0.12	9.13	260	1072	303

MANGANESE ZONE - UNIT 3

	Pb /ppm	Zn /ppm	MnO /Wt%	FeO* /Wt%	As /ppm	Ba /ppm	Sr /ppm
VALID	8	8	8	8	8	8	8
MEAN	666.9	2069	0.5838	6.912	73.50	821.0	39.63
STDEV	568.1	1737	0.8742	0.9812	34.91	111.9	21.74
MIN	60	140	0.09	5.27	4	646	20
MAX	1600	5600	>2.00	8.49	113	991	89

INTERBEDDED ZONE - UNIT 2

	Pb /ppm	Zn /ppm	MnO /Wt%	FeO* /Wt%	As /ppm	Ba /ppm	Sr /ppm
VALID	14	14	14	14	14	14	14
MEAN	1553	3829	0.0406	5.796	36.57	1063	54.71
STDEV	1241	1772	0.0234	0.8295	31.13	124.8	17.02
MIN	200	1400	0.02	4.50	8	780	12
MAX	3800	6600	0.11	6.82	116	1290	87

APPENDIX 4.3
ANALYSES FOR HALIFAX SLATE - UNIT 5

SAMPLE	HOLE	UNIT	DEPTH /m	SiO$_2$ /Wt%	Al$_2$O$_3$ /Wt%	CaO /Wt%	MgO /Wt%
1659	24	5	67.70	54.40	22.50	0.47	2.07
1660	24	5	64.70	56.30	22.00	0.51	2.13
1543	24	5	53.45	58.70	20.20	0.49	1.84
1544	24	5	51.95	56.00	22.00	0.47	1.82
1547	24	5	47.45	55.00	21.70	0.48	2.09
1552	24	5	40.20	61.30	18.90	0.37	1.84
1665	24	5	32.20	56.60	21.40	0.46	2.10
1557	24	5	21.45	55.50	21.20	0.50	2.19
1635	24	5	18.45	49.90	20.30	4.61	2.03
1638	24	5	13.95	54.10	22.50	0.35	2.11
1561	24	5	7.95	56.10	20.70	0.33	2.07
1562	24	5	5.70	52.60	21.90	0.96	2.27
1683	25	5	41.87	47.10	25.70	0.43	2.40
1684	25	5	39.27	53.70	22.40	0.51	2.09
1686	25	5	34.08	53.80	22.00	0.42	2.08
1687	25	5	31.48	56.90	20.70	1.12	1.87
1614	25	5	23.04	60.00	19.60	0.49	1.79
1616	25	5	20.44	57.80	21.40	0.56	1.79
1690	25	5	14.16	61.50	19.00	1.09	1.70
1643	25	5	10.05	56.50	19.40	0.98	1.89
1644	25	5	8.75	52.90	20.40	0.43	1.99
1645	25	5	7.45	55.50	19.60	0.84	1.95
1691	25	5	6.15	54.50	21.00	0.35	1.92

DEPTH /m	Na$_2$O /Wt%	K$_2$O /Wt%	Fe$_2$O$_3$ /Wt%	FeO /Wt%	Fe$_2$O$_3$* /Wt%	MnO /Wt%	TiO$_2$ /Wt%
67.70	0.91	3.95	2.60	5.10	8.27	0.29	1.02
64.70	1.06	3.74	2.17	5.20	7.95	0.44	0.94
53.45	0.96	3.43	2.75	4.40	7.64	0.25	0.94
51.95	0.95	3.83	2.44	4.70	7.66	0.23	1.02
47.45	1.04	3.67	2.18	6.00	8.85	0.33	0.99
40.20	0.97	3.07	2.30	4.40	7.19	0.23	0.93
32.20	0.98	3.62	2.66	4.50	7.66	0.24	0.99
21.45	1.24	3.45	1.05	4.80	6.38	0.21	1.00
18.45	1.60	3.06	1.88	4.50	6.88	0.52	0.95
13.95	1.17	3.69	3.21	4.90	8.66	0.21	1.02
7.95	1.30	3.32	2.33	4.60	7.44	0.21	0.96
5.70	1.38	3.36	2.87	5.80	9.32	0.28	0.99
41.87	1.25	4.42	0.18	9.20	10.40	0.28	1.24
39.27	1.33	3.63	0.84	7.60	9.29	0.25	1.04
34.08	1.27	3.68	0.87	7.70	9.43	0.22	1.03
31.48	1.21	3.45	0.66	6.80	8.22	0.38	0.98
23.04	0.96	3.52	0.45	6.20	7.34	0.20	0.93
20.44	0.94	4.10	0.54	6.30	7.54	0.19	0.98
14.16	0.94	3.90	0.08	5.80	6.53	0.27	0.94
10.05	0.82	4.29	0.61	6.90	8.28	0.39	0.91
8.75	0.65	4.64	1.33	7.80	10.00	0.43	0.93
7.45	0.84	4.46	0.0	8.70	9.16	0.42	0.89
6.15	0.61	4.84	0.69	7.40	8.91	0.42	1.00

ANALYSES FOR HALIFAX SLATE - UNIT 5   (continued)

DEPTH /m	P_2O_5 /Wt%	LOI /Wt%	H_2O+ /Wt%	S /Wt%	Cl /ppm	C /Wt%	CO_2 /Wt%
67.70	0.12	6.23	4.00	1.73	150.00	0.64	0.30
64.70	0.11	5.47	2.70	1.12	<50.00	0.56	0.30
53.45	0.09	5.62	2.80	1.37	<50.00	0.79	0.60
51.95	0.10	6.47	2.10	1.43	<50.00	1.14	0.60
47.45	0.11	6.00	2.90	1.55	<50.00	0.91	0.50
40.20	0.09	5.31	3.00	1.28	<50.00	0.78	0.70
32.20	0.11	6.16	2.30	1.45	50.00	0.97	0.40
21.45	0.10	6.31	2.70	1.35	<50.00	0.98	0.60
18.45	0.10	7.08	3.10	1.41	<50.00	1.17	3.60
13.95	0.10	6.62	3.50	1.94	<50.00	0.95	0.50
7.95	0.10	6.00	2.50	1.72	<50.00	0.95	0.60
5.70	0.10	6.47	3.10	2.00	<50.00	1.16	0.90
41.87	0.11	6.93	3.70	2.13	<50.00	1.49	0.30
39.27	0.11	5.85	3.80	1.77	<50.00	1.18	0.30
34.08	0.10	5.77	2.60	1.65	<50.00	1.32	0.30
31.48	0.09	4.77	2.80	1.55	<50.00	1.11	0.80
23.04	0.10	5.00	2.80	1.58	<50.00	0.99	0.30
20.44	0.10	5.16	2.20	1.56	<50.00	0.79	0.50
14.16	0.09	4.39	2.50	1.36	<50.00	0.70	0.80
10.05	0.12	5.93	2.50	2.52	<50.00	1.27	0.50
8.75	0.13	7.31	2.50	3.46	<50.00	1.74	0.40
7.45	0.14	6.31	2.00	2.98	<50.00	1.56	0.70
6.15	0.16	6.62	2.70	2.41	<50.00	1.89	0.40

DEPTH /m	C^* /Wt%	Au /ppb	As /ppm	Li /ppm	B /ppm	V /ppm	Mo /ppm
67.70	0.72	23	26	110	90	130	6
64.70	0.64	12	19	120	80	130	2
53.45	0.95	1	10	110	90	110	6
51.95	1.30	6	10	110	80	120	9
47.45	1.05	10	19	120	80	110	4
40.20	0.97	6	6	110	90	100	7
32.20	1.08	12	23	130	90	140	5
21.45	1.14	10	45	120	80	120	5
18.45	2.15	63	23	110	90	150	4
13.95	1.09	31	20	130	80	170	9
7.95	1.11	13	64	120	90	130	7
5.70	1.41	7	22	140	100	150	9
41.87	1.57	41	9	130	140	190	9
39.27	1.26	40	8	110	90	160	6
34.08	1.40	21	3	110	100	160	6
31.48	1.33	5	11	99	100	140	4
23.04	1.07	6	77	95	110	120	5
20.44	0.93	<1	15	96	120	110	4
14.16	0.92	14	28	80	120	100	4
10.05	1.41	14	150	78	140	130	8
8.75	1.85	18	74	82	130	170	19
7.45	1.75	16	7	72	140	160	17
6.15	2.00	25	91	61	150	170	17

DEPTH /m	Cr /ppm	Co /ppm	Ni /ppm	Cu /ppm	Zn /ppm	Pb /ppm	Cd /ppm
67.70	140	32	57	54	6500	2000	17
64.70	125	22	42	33	4300	1800	12
53.45	140	18	46	46	2200	570	7
51.95	140	24	58	52	2200	700	6
47.45	130	25	57	51	1900	500	5
40.20	150	20	42	50	3800	1300	13
32.20	135	25	50	48	3200	1200	9
21.45	150	21	62	59	14000	8200	44
18.45	150	23	51	49	9200	3300	23
13.95	165	29	65	51	3000	970	9
7.95	145	20	57	59	11200	6800	32
5.70	145	28	56	97	5700	2300	21
41.87	185	31	68	61	280	48	<1
39.27	140	26	68	60	140	32	<1
34.08	130	27	63	64	120	28	<1
31.48	135	24	57	56	120	28	<1
23.04	150	26	52	56	50	26	18
20.44	125	22	52	56	2300	770	10
14.16	130	15	41	36	180	56	<1
10.05	150	24	46	51	5200	1700	14
8.75	165	32	70	83	4400	1900	14
7.45	170	22	61	81	3400	1200	14
6.15	135	26	60	73	1300	410	4

DEPTH /m	Ag /ppm	Sb /ppm	W /ppm	U /ppm	Th /ppm	Rb /ppm	Sr /ppm
67.70	1.50	4.00	<1	3.80	10	150	240
64.70	1.00	1.70	4	2.90	11	130	240
53.45	<0.50	2.00	5	3.50	11	140	270
51.95	<0.50	2.10	3	5.10	12	160	330
47.45	<0.50	2.40	4	3.50	11	170	300
40.20	1.00	3.10	4	4.20	12	150	260
32.20	1.00	3.80	6	4.10	10	160	330
21.45	1.50	3.50	2	3.30	10	120	340
18.45	2.50	2.50	4	3.20	10	110	430
13.95	1.00	4.10	1	3.80	11	170	480
7.95	1.50	4.30	3	4.20	10	140	420
5.70	1.00	3.30	2	4.30	10	110	450
41.87	<0.50	2.30	10	5.00	12	200	530
39.27	<0.50	1.90	4	4.10	10	150	510
34.08	<0.50	1.80	3	5.00	10	170	500
31.48	<0.50	1.80	6	4.20	10	160	470
23.04	1.00	6.10	4	3.80	11	140	390
20.44	0.50	2.30	4	3.70	12	170	390
14.16	<0.50	1.60	8	3.80	11	150	300
10.05	1.00	3.90	4	6.00	10	160	230
8.75	1.00	4.40	9	7.80	12	180	200
7.45	<0.50	3.50	7	8.00	11	170	180
6.15	<0.50	1.90	5	8.60	12	200	200

| DEPTH | Ba | Y | Zr | Nb | Ge | Hg | Sn |
/m	/ppm	/ppm	/ppm	/ppm	/ppm	/ppb	/ppm
67.70	1010	0	160	20	10	10	3
64.70	960	0	160	20	10	10	<3
53.45	910	20	220	20	10	20	3
51.95	980	40	190	20	10	<10	3
47.45	960	10	170	40	20	<10	3
40.20	810	0	230	0	<10	<10	5
32.20	950	10	160	40	20	10	2
21.45	930	0	160	20	10	<10	3
18.45	730	0	150	20	20	<10	<3
13.95	900	10	170	30	20	10	<3
7.95	810	0	160	10	20	<10	3
5.70	790	0	140	20	20	<10	3
41.87	1010	50	200	20	<10	10	3
39.27	920	40	160	30	<10	<10	<3
34.08	920	40	190	10	<10	<10	3
31.48	890	10	200	30	<10	<10	3
23.04	880	0	210	20	20	20	5
20.44	970	10	200	30	10	10	<3
14.16	1020	40	230	20	<10	<10	3
10.05	1000	0	170	10	20	10	<3
8.75	1080	0	160	20	10	<10	3
7.45	1110	10	180	20	10	<10	<3
6.15	1230	30	190	30	<10	<10	3

SAMPLE	HOLE	UNIT	DEPTH /m	SiO_2 /Wt%	Al_2O_3 /Wt%	CaO /Wt%	MgO /Wt%
1563	24	4	3.95	54.10	22.00	0.54	2.20
1640	24	4	2.45	48.60	16.10	5.06	2.18
1667	24	4	0.85	49.10	17.50	3.66	2.32
1692	25	4	4.20	52.40	20.40	0.46	2.06
1693	25	4	1.45	49.70	18.60	1.05	2.05

DEPTH /m	Na_2O /Wt%	K_2O /Wt%	Fe_2O_3 /Wt%	FeO /Wt%	Fe_2O_3* /Wt%	MnO /Wt%	TiO_2 /Wt%
3.95	1.20	3.85	3.18	4.80	8.51	0.25	1.02
2.45	0.35	2.92	6.84	5.00	12.40	2.50	0.82
0.85	0.21	3.39	3.81	7.10	11.70	4.48	0.95
4.20	0.67	4.71	0.73	8.70	10.40	0.67	1.00
1.45	0.38	4.47	3.92	7.90	12.70	1.18	0.97

DEPTH /m	P_2O_5 /Wt%	LOI /Wt%	H_2O+ /Wt%	S /Wt%	Cl /ppm	C /Wt%	CO_2 /Wt%
3.95	0.10	6.31	3.20	1.86	50.00	0.98	0.30
2.45	0.20	7.39	3.30	3.35	50.00	1.66	3.70
0.85	0.20	6.54	2.80	3.34	50.00	0.80	3.00
4.20	0.19	7.39	2.90	2.70	<50.00	2.71	0.40
1.45	0.21	8.77	2.70	3.73	<50.00	2.87	0.90

DEPTH /m	C* /Wt%	Au /ppb	As /ppm	Li /ppm	B /ppm	V /ppm	Mo /ppm
3.95	1.06	7	35	110	90	140	6
2.45	2.67	19	280	71	90	170	27
0.85	1.62	7	40	63	70	140	55
4.20	2.82	20	5	70	150	200	28
1.45	3.12	10	370	65	140	230	28

DEPTH /m	Cr /ppm	Co /ppm	Ni /ppm	Cu /ppm	Zn /ppm	Pb /ppm	Cd /ppm
3.95	150	25	66	92	5800	2900	20
2.45	200	40	85	64	1700	670	5
0.85	165	52	110	83	140	86	1
4.20	135	23	64	94	810	220	2
1.45	130	49	77	97	3000	1100	8

DEPTH /m	Ag /ppm	Sb /ppm	W /ppm	U /ppm	Th /ppm	Rb /ppm	Sr /ppm
3.95	1.50	3.70	4	4.00	10	150	410
2.45	1.50	4.00	7	7.70	8	110	120
0.85	<0.50	2.40	7	6.90	8	120	90
4.20	0.50	1.80	5	12.10	11	180	160
1.45	1.00	4.20	7	12.40	11	180	90

DEPTH /m	Ba /ppm	Y /ppm	Zr /ppm	Nb /ppm	Ge /ppm	Hg /ppb	Sn /ppm
3.95	920	0	140	20	10	10	3
2.45	760	20	140	20	20	10	2
0.85	910	30	180	20	10	10	<2
4.20	1230	40	180	20	10	<10	3
1.45	1340	0	160	30	20	<10	3

SAMPLE	HOLE	UNIT	DEPTH /m	SiO_2 /Wt%	Al_2O_3 /Wt%	CaO /Wt%	MgO /Wt%
1668	24	3	-1.00	47.90	17.00	1.87	2.76
1669	24	3	-3.00	44.50	17.00	1.86	3.47
1670	24	3	-5.00	44.70	15.90	3.96	3.27
1671	24	3	-7.20	48.10	15.70	4.00	3.57
1618	25	3	-0.87	49.50	17.40	2.89	2.21
1619	25	3	-2.59	49.10	16.50	1.63	2.60
1620	25	3	-4.33	48.50	16.90	1.59	2.91
1622	25	3	-7.65	48.80	17.10	2.37	3.73

DEPTH /m	Na_2O /Wt%	K_2O /Wt%	Fe_2O_3 /Wt%	FeO /Wt%	Fe_2O_3* /Wt%	MnO /Wt%	TiO_2 /Wt%
-1.00	0.16	1.99	1.84	10.40	13.40	9.06	0.99
-3.00	0.08	1.35	3.04	11.30	15.60	10.30	0.95
-5.00	0.01	1.20	2.35	10.30	13.80	11.10	0.91
-7.20	0.02	1.97	2.10	8.10	11.10	9.87	0.91
-0.87	0.16	3.67	1.42	10.60	13.20	4.18	0.94
-2.59	0.11	1.83	2.45	10.30	13.90	9.28	0.96
-4.33	0.02	1.55	3.34	10.40	14.90	10.10	0.97
-7.65	0.32	1.91	3.20	7.20	11.20	10.30	0.98

DEPTH /m	P_2O_5 /Wt%	LOI /Wt%	H_2O+ /Wt%	S /Wt%	Cl /ppm	C /Wt%	CO_2 /Wt%
-1.00	0.29	4.23	2.90	1.89	<50.00	0.21	0.90
-3.00	0.29	3.85	3.60	0.79	<50.00	0.13	0.70
-5.00	0.28	4.54	3.20	0.33	<50.00	0.14	2.30
-7.20	0.22	4.77	2.50	0.20	100.00	0.07	3.40
-0.87	0.22	4.77	2.00	3.62	50.00	0.78	2.30
-2.59	0.28	3.23	2.30	1.69	<50.00	0.17	0.60
-4.33	0.27	2.93	2.50	0.81	50.00	0.09	0.60
-7.65	0.22	2.85	2.90	0.18	50.00	0.36	0.10

DEPTH /m	C* /Wt%	Au /ppb	As /ppm	Li /ppm	B /ppm	V /ppm	Mo /ppm
-1.00	0.46	9	76	69	40	110	10
-3.00	0.32	12	110	77	30	90	5
-5.00	0.77	8	160	55	20	78	<1
-7.20	1.00	10	84	63	20	56	1
-0.87	1.41	27	88	50	90	160	57
-2.59	0.33	8	220	55	50	84	8
-4.33	0.25	18	130	200	50	84	8
-7.65	0.39	10	74	67	40	50	<1

DEPTH	Cr	Co	Ni	Cu	Zn	Pb	Cd
/m	/ppm	/ppm	/ppm	/ppm	/ppm	/ppm	/ppm
-1.00	165	64	120	75	2400	950	7
-3.00	150	70	140	61	5600	1300	16
-5.00	155	78	97	46	43	12	8
-7.20	120	42	72	39	660	170	3
-0.87	145	54	120	87	170	64	2
-2.59	165	68	150	78	2700	790	8
-4.33	170	99	150	70	1200	320	4
-7.65	140	41	76	56	820	260	3

DEPTH	Ag	Sb	W	U	Th	Rb	Sr
/m	/ppm	/ppm	/ppm	/ppm	/ppm	/ppm	/ppm
-1.00	<0.50	1.00	3	3.70	9	60	20
-3.00	<0.50	0.90	4	2.90	7	30	10
-5.00	0.50	0.50	4	2.30	8	30	10
-7.20	0.50	0.60	5	2.30	8	50	30
-0.87	<0.50	2.30	12	6.90	10	130	80
-2.59	<0.50	1.70	7	4.10	9	50	20
-4.33	<0.50	1.00	6	3.70	9	40	20
-7.65	<0.50	1.00	4	2.40	10	70	30

DEPTH	Ba	Y	Zr	Nb	Ge	Hg	Sn
/m	/ppm	/ppm	/ppm	/ppm	/ppm	/ppb	/ppm
-1.00	760	10	150	0	<10	10	3
-3.00	550	0	140	30	20	<10	3
-5.00	580	0	120	20	20	<10	3
-7.20	770	30	140	10	20	<10	3
-0.87	930	40	180	10	20	<10	3
-2.59	730	0	140	20	10	<10	3
-4.33	670	20	140	10	20	<10	5
-7.65	810	30	160	10	20	<10	5

SAMPLE	HOLE	UNIT	DEPTH /m	SiO_2 /Wt%	Al_2O_3 /Wt%	CaO /Wt%	MgO /Wt%
1672	24	2	-9.90	59.10	17.60	1.75	2.83
1673	24	2	-12.9	60.20	17.80	1.96	2.51
1674	24	2	-15.9	59.20	17.60	1.68	2.81
1675	24	2	-18.9	58.10	18.70	0.96	2.84
1677	24	2	-24.9	57.50	19.90	0.37	2.91
1680	24	2	-33.9	56.10	19.30	2.14	2.40
1682	24	2	-39.3	56.50	20.50	0.34	2.27
1694	25	2	-9.66	59.90	18.60	0.73	2.73
1695	25	2	-12.3	60.00	17.10	1.54	2.55
1696	25	2	-14.9	57.30	19.80	0.53	3.01
1697	25	2	-17.5	59.40	18.00	1.74	2.62
1700	25	2	-28.3	55.50	20.80	0.55	2.60
1626	25	2	-34.1	57.60	20.40	0.29	2.03
1627	25	2	-35.4	54.20	20.40	0.31	2.53

DEPTH /m	Na_2O /Wt%	K_2O /Wt%	Fe_2O_3 /Wt%	FeO /Wt%	Fe_2O_3* /Wt%	MnO /Wt%	TiO_2 /Wt%
-9.90	0.53	3.78	1.65	5.30	7.54	1.35	0.89
-12.9	0.57	4.12	1.49	4.30	6.27	0.67	0.58
-15.9	0.82	3.76	1.78	5.20	7.56	0.49	0.82
-18.9	1.14	3.95	2.29	5.30	8.18	0.33	0.95
-24.9	0.68	4.51	2.11	5.30	8.00	0.32	0.92
-33.9	0.35	4.40	1.86	6.60	9.19	0.67	0.80
-39.3	0.18	5.04	2.44	6.30	9.44	0.86	0.86
-9.66	0.90	4.20	1.20	5.90	7.76	0.96	0.87
-12.3	0.89	3.89	0.87	5.50	6.98	0.65	0.67
-14.9	1.29	4.25	1.48	6.30	8.48	0.39	0.91
-17.5	1.82	3.60	1.23	5.90	7.79	0.38	0.96
-28.3	0.31	4.90	1.96	7.50	10.30	0.66	0.82
-34.1	0.27	5.18	1.28	5.70	7.61	0.84	0.85
-35.4	0.21	4.78	1.51	8.00	10.40	1.08	0.84

DEPTH /m	P_2O_5 /Wt%	LOI /Wt%	H_2O+ /Wt%	S /Wt%	Cl /ppm	C /Wt%	CO_2 /Wt%
-9.90	0.13	4.16	3.30	0.66	<50.00	0.08	1.90
-12.9	0.33	3.85	1.80	0.56	50.00	0.17	1.20
-15.9	0.14	4.00	4.00	0.91	<50.00	0.11	1.50
-18.9	0.14	4.16	3.30	1.01	50.00	0.01	1.10
-24.9	0.13	4.54	3.00	0.91	<50.00	0.12	0.30
-33.9	0.14	4.00	1.80	0.37	<50.00	0.08	1.60
-39.3	0.10	4.16	3.20	0.82	<50.00	0.18	0.20
-9.66	0.13	3.54	3.10	0.62	<50.00	0.07	0.80
-12.3	0.16	4.08	2.90	0.87	<50.00	0.17	1.20
-14.9	0.14	4.16	3.30	0.94	<50.00	0.15	0.40
-17.5	0.15	3.47	2.30	0.91	<50.00	0.18	1.20
-28.3	0.13	4.16	3.40	0.65	<50.00	0.12	0.40
-34.1	0.10	4.08	3.10	0.64	<50.00	0.15	0.40
-35.4	0.12	4.47	3.50	0.70	<50.00	0.0	0.40

DEPTH /m	C* /Wt%	Au /ppb	As /ppm	Li /ppm	B /ppm	V /ppm	Mo /ppm
-9.90	0.60	13	9	67	40	150	5
-12.9	0.50	12	10	65	40	100	5
-15.9	0.52	44	12	72	60	160	6
-18.9	0.31	11	6	71	70	180	2
-24.9	0.20	18	28	72	60	190	3
-33.9	0.52	22	49	65	60	130	<1
-39.3	0.23	16	66	54	70	200	23
-9.66	0.29	10	11	65	60	150	9
-12.3	0.50	13	20	64	60	120	7
-14.9	0.26	11	6	74	70	160	3
-17.5	0.51	13	85	53	90	150	4
-28.3	0.23	11	21	62	80	140	2
-34.1	0.26	20	140	51	80	180	4
-35.4	0.09	14	77	61	70	180	4

DEPTH /m	Cr /ppm	Co /ppm	Ni /ppm	Cu /ppm	Zn /ppm	Pb /ppm	Cd /ppm
-9.90	105	23	57	58	3800	1400	12
-12.9	80	19	39	45	3800	1800	11
-15.9	115	25	52	51	3800	1700	14
-18.9	130	24	53	39	2900	770	10
-24.9	130	27	79	99	5600	3100	17
-33.9	115	30	62	44	1800	460	5
-39.3	125	43	87	140	2300	860	5
-9.66	115	26	61	56	1800	430	4
-12.3	120	24	51	49	6180	3200	22
-14.9	125	26	63	62	5200	1900	16
-17.5	120	30	55	43	1800	670	4
-28.3	105	31	59	110	1400	410	3
-34.1	130	36	64	130	6600	3500	21
-35.4	115	34	86	140	5800	3100	15

DEPTH /m	Ag /ppm	Sb /ppm	W /ppm	U /ppm	Th /ppm	Rb /ppm	Sr /ppm
-9.90	0.50	0.40	6	3.90	7	140	60
-12.9	0.50	0.50	7	5.80	8	130	60
-15.9	0.50	0.90	4	3.90	8	120	50
-18.9	<0.50	0.90	6	4.00	7	150	50
-24.9	1.50	1.10	3	3.90	8	130	40
-33.9	0.50	0.70	3	2.20	10	150	60
-39.3	1.00	0.90	5	6.00	11	160	60
-9.66	<0.50	1.00	3	4.50	8	150	70
-12.3	1.50	2.00	7	4.80	8	110	80
-14.9	0.50	1.10	5	3.80	8	140	60
-17.5	0.50	1.30	3	3.70	7	120	100
-28.3	<0.50	0.90	4	3.40	11	160	60
-34.1	2.00	1.90	3	4.80	12	160	50
-35.4	1.50	1.60	2	3.90	12	140	50

DEPTH /m	Ba /ppm	Y /ppm	Zr /ppm	Nb /ppm	Ge /ppm	Hg /ppb	Sn /ppm
-9.90	1160	10	170	20	10	<10	3
-12.9	1250	0	120	20	20	<10	3
-15.9	1130	0	130	10	20	10	3
-18.9	1150	0	170	10	20	<10	3
-24.9	1270	0	140	20	10	10	3
-33.9	1200	10	160	10	20	10	3
-39.3	1370	20	120	20	10	10	<3
-9.66	1240	20	140	20	<10	<10	3
-12.3	1550	0	140	30	10	<10	3
-14.9	1220	0	160	30	10	<10	3
-17.5	970	10	170	10	10	<10	<3
-28.3	1290	30	130	0	10	<10	3
-34.1	1440	0	130	30	20	<10	3
-35.4	1300	0	100	30	10	10	<3

	SiO_2 /Wt%	Al_2O_3 /Wt%	CaO /Wt%	MgO /Wt%	Na_2O /Wt%	K_2O /Wt%	Fe_2O_3 /Wt%	FeO /Wt%
VALID	50	50	50	50	50	50	50	50
MEAN	54.45	19.62	1.261	2.360	.7606	3.646	1.921	6.690
STDEV	4.433	2.141	1.202	.4873	.4634	.9584	1.207	1.921
MIN	44.50	15.70	0.29	1.70	0.01	1.20	0	4.30
MAX	61.50	25.70	5.06	3.73	1.82	5.18	6.84	11.30

	Fe_2O_3* /Wt%	MnO /Wt%	TiO_2 /Wt%	P_2O_5 /Wt%	LOI /Wt%	H_2O+ /Wt%	S /Wt%	Cl /ppm
VALID	50	50	50	50	50	50	50	11
MEAN	9.346	1.996	.9346	.1498	5.244	2.872	1.528	63.64
STDEV	2.333	3.379	.0974	.0643	1.349	.5322	.9169	32.33
MIN	6.27	0.19	0.58	0.09	2.85	1.80	0.18	50.00
MAX	15.60	11.10	1.24	0.33	8.77	4.00	3.73	150.0

	C /Wt%	CO_2 /Wt%	C* /Wt%	Au /ppb	As /ppm	Li /ppm	B /ppm	V /ppm
VALID	50	50	50	49	50	50	50	50
MEAN	.7520	.9340	1.007	16.06	59.44	87.08	83.40	139.0
STDEV	.6788	.8939	.7057	11.41	73.60	30.50	32.86	37.75
MIN	0	0.10	0.09	1	3	50	20	50
MAX	2.87	3.70	3.12	63	370	200	150	230

	Mo /ppm	Cr /ppm	Co /ppm	Ni /ppm	Cu /ppm	Zn /ppm	Pb /ppm	Cd /ppm
VALID	47	50	50	50	50	50	50	45
MEAN	10.26	139.0	33.30	69.52	66.68	3250	1360	11.51
STDEV	11.86	21.64	17.04	26.73	25.49	2924	1614	8.50
MIN	1	80	15	39	33	43	12	1
MAX	57	200	99	150	140	14000	8200	44

	Ag /ppm	Sb /ppm	W /ppm	U /ppm	Th /ppm	Rb /ppm	Sr /ppm	Ba /ppm
VALID	30	50	49	50	50	50	50	50
MEAN	1.050	2.172	4.86	4.718	9.84	134.4	198.6	1005
STDEV	.5144	1.318	2.16	2.144	1.57	41.85	166.7	223.0
MIN	0.50	0.40	1	2.20	7	30	10	550
MAX	2.50	6.10	12	12.40	12	200	530	1550

	Y /ppm	Zr /ppm	Nb /ppm	Ge /ppm	Hg /ppb	Sn /ppm
VALID	50	50	50	41	18	37
MEAN	12.80	162.2	19.60	15.12	11.11	3.22
STDEV	15.26	28.81	9.25	5.06	3.23	0.63
MIN	0	100	0	10	10	3
MAX	50	230	40	20	20	5

GENERAL STATISTICS FOR HALIFAX SLATE – UNIT 5

	SiO_2 /Wt%	Al_2O_3 /Wt%	CaO /Wt%	MgO /Wt%	Na_2O /Wt%	K_2O /Wt%	Fe_2O_3 /Wt%	FeO /Wt%
VALID	23	23	23	23	23	23	23	23
MEAN	55.51	21.15	.7487	2.001	1.060	3.788	1.508	6.057
STDEV	3.292	1.496	.8758	.1707	.2380	.4787	1.032	1.464
MIN	47.10	18.90	0.33	1.70	0.61	3.06	0	4.40
MAX	61.50	25.70	4.61	2.40	1.60	4.84	3.21	9.20

	Fe_2O_3* /Wt%	MnO /Wt%	TiO_2 /Wt%	P_2O_5 /Wt%	LOI /Wt%	H_2O+ /Wt%	S /Wt%	Cl /ppm
VALID	23	23	23	23	23	23	23	2
MEAN	8.217	.2996	.9835	.1078	5.990	2.817	1.797	100.0
STDEV	1.080	.0958	.0694	.0170	.7391	.5280	.5720	70.71
MIN	6.38	0.19	0.89	0.09	4.39	2.00	1.12	50.00
MAX	10.40	0.52	1.24	0.16	7.31	4.00	3.46	150.0

	C /Wt%	CO_2 /Wt%	C* /Wt%	Au /ppb	As /ppm	Li /ppm	B /ppm	V /ppm
VALID	23	23	23	22	23	23	23	23
MEAN	1.089	.6478	1.265	17.91	33.04	106.2	103.5	137.8
STDEV	.3418	.6687	.3904	14.74	35.74	20.52	22.88	25.22
MIN	0.56	0.30	0.64	1	3	61	80	100
MAX	1.89	3.60	2.15	63	150	140	150	190

	Mo /ppm	Cr /ppm	Co /ppm	Ni /ppm	Cu /ppm	Zn /ppm	Pb /ppm	Cd /ppm
VALID	23	23	23	23	23	23	23	18
MEAN	7.48	144.8	24.43	55.70	57.65	3682	1558	15.11
STDEV	4.48	15.11	4.30	8.55	14.55	3690	2077	10.06
MIN	2	125	15	41	33	50	26	4
MAX	19	185	32	70	97	14000	8200	44

	Ag /ppm	Sb /ppm	W /ppm	U /ppm	Th /ppm	Rb /ppm	Sr /ppm	Ba /ppm
VALID	13	23	22	23	23	23	23	23
MEAN	1.192	2.970	4.64	4.604	10.83	154.8	347.4	946.5
STDEV	.4804	1.165	2.26	1.563	0.83	23.91	110.6	109.7
MIN	0.50	1.60	1	2.90	10	110	180	730
MAX	2.50	6.10	10	8.60	12	200	530	1230

	Y /ppm	Zr /ppm	Nb /ppm	Ge /ppm	Hg /ppb	Sn /ppm
VALID	23	23	23	16	9	15
MEAN	13.91	180.9	21.74	15.00	12.22	3.27
STDEV	16.99	25.75	9.37	5.16	4.41	0.70
MIN	0	140	0	10	10	3
MAX	50	230	40	20	20	5

GENERAL STATISTICS FOR BLACK SLATE - UNIT 4

	SiO$_2$ /Wt%	Al$_2$O$_3$ /Wt%	CaO /Wt%	MgO /Wt%	Na$_2$O /Wt%	K$_2$O /Wt%	Fe$_2$O$_3$ /Wt%	FeO /Wt%
VALID	5	5	5	5	5	5	5	5
MEAN	50.78	18.92	2.154	2.162	.5620	3.868	3.696	6.700
STDEV	2.366	2.332	2.086	.1114	.3939	.7414	2.180	1.739
MIN	48.60	16.10	0.46	2.05	0.21	2.92	0.73	4.80
MAX	54.10	22.00	5.06	2.32	1.20	4.71	6.84	8.70

	Fe$_2$O$_3$* /Wt%	MnO /Wt%	TiO$_2$ /Wt%	P$_2$O$_5$ /Wt%	LOI /Wt%	H$_2$O+ /Wt%	S /Wt%	Cl /ppm
VALID	5	5	5	5	5	5	5	3
MEAN	11.14	1.816	.9520	.1800	7.280	2.980	2.996	50.00
STDEV	1.718	1.713	.0785	.0453	.9660	.2588	.7349	0
MIN	8.51	0.25	0.82	0.10	6.31	2.70	1.86	50.00
MAX	12.70	4.48	1.02	0.21	8.77	3.30	3.73	50.00

	C /Wt%	CO$_2$ /Wt%	C* /Wt%	Au /ppb	As /ppm	Li /ppm	B /ppm	V /ppm
VALID	5	5	5	5	5	5	5	5
MEAN	1.804	1.660	2.258	12.60	146.0	75.80	108.0	176.0
STDEV	.9572	1.579	.8762	6.43	167.0	19.41	34.93	39.12
MIN	0.80	0.30	1.06	7	5	63	70	140
MAX	2.87	3.70	3.12	20	370	110	150	230

	Mo /ppm	Cr /ppm	Co /ppm	Ni /ppm	Cu /ppm	Zn /ppm	Pb /ppm	Cd /ppm
VALID	5	5	5	5	5	5	5	5
MEAN	28.80	156.0	37.80	80.40	86.00	2290	995.2	7.20
STDEV	17.40	28.15	13.37	18.61	13.36	2235	1137	7.66
MIN	6	130	23	64	64	140	86	1
MAX	55	200	52	110	97	5800	2900	20

	Ag /ppm	Sb /ppm	W /ppm	U /ppm	Th /ppm	Rb /ppm	Sr /ppm	Ba /ppm
VALID	4	5	5	5	5	5	5	5
MEAN	1.125	3.220	6.00	8.620	9.60	148.0	174.0	1032
STDEV	.4787	1.059	1.41	3.590	1.52	32.71	135.0	242.6
MIN	0.50	1.80	4	4.00	8	110	90	760
MAX	1.50	4.20	7	12.40	11	180	410	1340

	Y /ppm	Zr /ppm	Nb /ppm	Ge /ppm	Hg /ppb	Sn /ppm
VALID	5	5	5	5	3	3
MEAN	18.00	160.0	22.00	14.00	10.00	3.00
STDEV	17.89	20.00	4.47	5.48	0	0
MIN	0	140	20	10	10	3
MAX	40	180	30	20	10	3

GENERAL STATISTICS FOR MANGANESE ZONE – UNIT 3

	SiO_2 /Wt%	Al_2O_3 /Wt%	CaO /Wt%	MgO /Wt%	Na_2O /Wt%	K_2O /Wt%	Fe_2O_3 /Wt%	FeO /Wt%
VALID	8	8	8	8	8	8	8	8
MEAN	47.64	16.69	2.521	3.065	.1100	1.934	2.468	9.825
STDEV	1.944	.6034	.9956	.5302	.1043	.7613	.6830	1.402
MIN	44.50	15.70	1.59	2.21	0.01	1.20	1.42	7.20
MAX	49.50	17.40	4.00	3.73	0.32	3.67	3.34	11.30

	Fe_2O_3* /Wt%	MnO /Wt%	TiO_2 /Wt%	P_2O_5 /Wt%	LOI /Wt%	H_2O+ /Wt%	S /Wt%	Cl /ppm
VALID	8	8	8	8	8	8	8	4
MEAN	13.39	9.274	.9513	.2588	3.896	2.738	1.189	62.50
STDEV	1.589	2.154	.0300	.0327	.8042	.5153	1.177	25.00
MIN	11.10	4.18	0.91	0.22	2.85	2.00	0.18	50.00
MAX	15.60	11.10	0.99	0.29	4.77	3.60	3.62	100.0

	C /Wt%	CO_2 /Wt%	C* /Wt%	Au /ppb	As /ppm	Li /ppm	B /ppm	V /ppm
VALID	8	8	8	8	8	8	8	8
MEAN	.2438	1.363	.6163	12.75	117.8	79.50	42.50	89.00
STDEV	.2346	1.154	.4106	6.61	50.89	49.48	22.52	34.36
MIN	0.07	0.10	0.25	8	74	50	20	50
MAX	0.78	3.40	1.41	27	220	200	90	160

	Mo /ppm	Cr /ppm	Co /ppm	Ni /ppm	Cu /ppm	Zn /ppm	Pb /ppm	Cd /ppm
VALID	6	8	8	8	8	8	8	8
MEAN	14.83	151.3	64.50	115.6	64.00	1699	483.2	6.37
STDEV	20.89	16.42	19.21	31.20	16.49	1847	470.8	4.57
MIN	1	120	41	72	39	43	12	2
MAX	57	170	99	150	87	5600	1300	16

	Ag /ppm	Sb /ppm	W /ppm	U /ppm	Th /ppm	Rb /ppm	Sr /ppm	Ba /ppm
VALID	2	8	8	8	8	8	8	8
MEAN	.5000	1.125	5.62	3.537	8.75	57.50	27.50	725.0
STDEV	0	.5946	2.88	1.532	1.04	32.40	22.52	123.8
MIN	0.50	0.50	3	2.30	7	30	10	550
MAX	0.50	2.30	12	6.90	10	130	80	930

	Y /ppm	Zr /ppm	Nb /ppm	Ge /ppm	Hg /ppb	Sn /ppm
VALID	8	8	8	7	1	8
MEAN	16.25	146.3	13.75	18.57	10.00	3.50
STDEV	15.98	17.68	9.16	3.78	--	0.93
MIN	0	120	0	10	10	3
MAX	40	180	30	20	10	5

GENERAL STATISTICS FOR INTERBEDDED ZONE – UNIT 2

	SiO_2 /Wt%	Al_2O_3 /Wt%	CaO /Wt%	MgO /Wt%	Na_2O /Wt%	K_2O /Wt%	Fe_2O_3 /Wt%	FeO /Wt%
VALID	14	14	14	14	14	14	14	14
MEAN	57.90	19.04	1.064	2.617	.7114	4.311	1.654	5.936
STDEV	1.848	1.276	.6983	.2662	.4724	.5078	.4473	.9645
MIN	54.20	17.10	0.29	2.03	0.18	3.60	0.87	4.30
MAX	60.20	20.80	2.14	3.01	1.82	5.18	2.44	8.00

	Fe_2O_3* /Wt%	MnO /Wt%	TiO_2 /Wt%	P_2O_5 /Wt%	LOI /Wt%	H_2O+ /Wt%	S /Wt%	Cl /ppm
VALID	14	14	14	14	14	14	14	2
MEAN	8.250	.6893	.8386	.1457	4.059	3.000	.7550	50.00
STDEV	1.197	.3048	.1040	.0556	.2934	.6276	.1818	0
MIN	6.27	0.32	0.58	0.10	3.47	1.80	0.37	50.00
MAX	10.40	1.35	0.96	0.33	4.54	4.00	1.01	50.00

	C /Wt%	CO_2 /Wt%	C* /Wt%	Au /ppb	As /ppm	Li /ppm	B /ppm	V /ppm
VALID	14	14	14	14	14	14	14	14
MEAN	.1136	.9000	.3586	16.29	38.57	64.00	65.00	156.4
STDEV	.0593	.5561	.1594	8.76	40.02	7.30	14.01	28.18
MIN	0	0.20	0.09	10	6	51	40	100
MAX	0.18	1.90	0.60	44	140	74	90	200

	Mo /ppm	Cr /ppm	Co /ppm	Ni /ppm	Cu /ppm	Zn /ppm	Pb /ppm	Cd /ppm
VALID	13	14	14	14	14	14	14	14
MEAN	5.92	116.4	28.43	62.00	76.14	3770	1664	11.36
STDEV	5.50	13.36	6.17	13.62	38.74	1829	1143	6.45
MIN	2	80	19	39	39	1400	410	3
MAX	23	130	43	87	140	6600	3500	22

	Ag /ppm	Sb /ppm	W /ppm	U /ppm	Th /ppm	Rb /ppm	Sr /ppm	Ba /ppm
VALID	11	14	14	14	14	14	14	14
MEAN	.9545	1.086	4.36	4.186	8.93	140.0	60.71	1253
STDEV	.5681	.4737	1.65	.9631	1.86	16.17	14.92	141.2
MIN	0.50	0.40	2	2.20	7	110	40	970
MAX	2.00	2.00	7	6.00	12	160	100	1550

	Y /ppm	Zr /ppm	Nb /ppm	Ge /ppm	Hg /ppb	Sn /ppm
VALID	14	14	14	13	5	11
MEAN	7.14	141.4	18.57	13.85	10.00	3.00
STDEV	9.94	21.79	9.49	5.06	0	0
MIN	0	100	0	10	10	3
MAX	30	170	30	20	10	3

APPENDIX 5 - Mineral Analyses

GARNET

SAMPLE	DESCRIPTION	SiO2	Al2O3	MnO
ZGB-0066	Gnt rim near po in slate	35.83	20.84	29.07
ZGB-0066	Gnt core in a blocky bed	38.11	20.24	33.87
ZGB-0066	Gnt core in a blocky bed	41.25	19.10	32.88
ZGB-0066	Gnt rim in slate	47.13	17.23	24.76
ZGB-0066	Gnt core in slate	38.11	19.55	30.65
ZGB-0066	Gnt rim in qtzite	36.72	20.82	30.82
ZGB-0066	Gnt core in qtzite	36.44	20.34	34.21
ZGB-0066	Gnt core in qtzite	44.25	18.00	29.27
ZGB-0145	Gnt core in black slate	36.55	20.67	29.63

Oxides in Weight Percent

SAMPLE	FeO	CaO	MgO	TiO2	K2O	Na2O	NiO	TOTAL
ZGB-0066	9.75	2.56	0.29	--	0.21	--	--	98.55
ZGB-0066	5.65	3.14	--	0.07	--	--	--	101.08
ZGB-0066	5.09	2.98	--	0.14	--	--	--	101.44
ZGB-0066	9.02	2.15	0.30	--	--	--	--	100.59
ZGB-0066	7.87	2.71	0.07	--	--	--	--	98.96
ZGB-0066	9.73	2.85	0.27	--	--	--	0.17	101.38
ZGB-0066	6.48	2.99	0.13	0.13	--	--	0.19	100.91
ZGB-0066	6.13	2.36	--	--	--	--	0.04	100.05
ZGB-0145	8.83	3.41	0.36	--	--	0.08	0.17	99.70

CARBONATES

SAMPLE	DESCRIPTION	CaO	MnO	FeO	MgO
ZGB-0132	Horiz profile on block	51.02	3.50	0.20	0.24
ZGB-0132	Horiz profile on block	49.79	5.30	0.39	0.44
ZGB-0132	Horiz profile on block	50.10	4.22	0.52	0.18
ZGB-0132	Horiz profile on block	52.44	3.39	0.18	--
ZGB-0132	Vertical profile on block	48.84	5.49	0.42	0.46
ZGB-0132	Vertical profile on block	50.99	3.47	0.22	--
ZGB-0132	Vertical profile on block	51.11	3.86	0.45	0.27
ZGB-0132	Vertical profile on block	47.40	5.82	0.44	0.93
ZGB-0131	Vein carbonate	55.29	0.04	0.05	--
ZGB-0131	Vein carbonate	54.86	0.08	--	--
ZGB-0131	Vein carbonate	55.11	0.21	0.28	--

Oxides and Elements in Weight Percent

SAMPLE	Al_2O_3	SiO_2	S	TOTAL
ZGB-0132	--	--	--	54.96
ZGB-0132	--	--	--	55.92
ZGB-0132	0.18	0.24	--	55.44
ZGB-0132	--	--	--	56.01
ZGB-0132	--	--	--	55.21
ZGB-0132	--	--	--	54.68
ZGB-0132	--	0.23	--	55.92
ZGB-0132	--	1.06	--	55.65
ZGB-0131	--	--	--	55.38
ZGB-0131	--	--	--	54.94
ZGB-0131	--	--	0.32	55.92

SULPHIDES

SAMPLE	DESCRIPTION	Zn	S	Fe	Mn
ZGB-0131	Vein sphalerite	62.29	34.21	4.96	--
ZGB-0131	Vein sphalerite	61.88	33.62	5.38	--
ZGB-0131	Vein sphalerite	60.34	34.40	6.08	--
ZGB-0131	Vein sphalerite	61.53	33.55	5.05	--
ZGB-0131	Vein sphalerite	65.28	33.20	1.62	--
ZGB-0131	Sphalerite in garnet core	58.66	33.60	5.52	1.22
ZGB-0131	Sphalerite in garnet core	58.78	33.64	6.12	1.10
ZGB-0131	Bedded sphalerite	60.47	33.04	5.16	0.04
ZGB-0131	Bedded sphalerite	61.81	33.91	4.31	0.07
ZGB-0131	Vein pyrite	0.62	53.46	43.47	--

Elements in Weight Percent

SAMPLE	TOTAL
ZGB-0131	101.46
ZGB-0131	100.88
ZGB-0131	100.82
ZGB-0131	100.13
ZGB-0131	100.10
ZGB-0131	99.00
ZGB-0131	99.64
ZGB-0131	98.71
ZGB-0131	100.10
ZGB-0131	97.55

OXIDES

SAMPLE	DESCRIPTION	TiO_2	FeO	MnO	SiO_2
ZGB-0023	Ilmenite in slate	51.28	36.73	9.13	0.57
ZGB-072a	Ilmenite in calc qtzite	48.65	24.22	21.28	0.69
ZGB-0133	Ilmenite in blocky bed	51.82	40.43	6.43	1.06
ZGB-0023	Rutile in slate	98.43	--	--	--
ZGB-0164	Rutile in and-gnt schist	91.96	2.20	--	0.91

Oxides and Elements in Weight Percent

SAMPLE	Al_2O_3	K_2O	Na_2O	V_2O_5	MgO	S	TOTAL
ZGB-0023	--	--	0.08	--	--	--	97.79
ZGB-072a	0.27	--	--	--	0.26	0.72	96.09
ZGB-0133	0.23	0.06	--	--	--	--	100.03
ZGB-0023	--	0.08	0.04	--	--	--	98.55
ZGB-0164	0.68	0.14	--	0.19	--	--	96.08

APPENDIX 6
Isotope Sample Descriptions and Procedure

SAMPLE	DESCRIPTION OF CARBONATE
23.5	clear yellow calcite with light yellow sphalerite mineralization in a 1cm wide vein (description and analysis from Ponsford, 1983)
51-1	pinkish quartz metawacke with carbonate cement, appears to be close to the granite contact
67-5	cement in quartz metawacke adjacent to a carbonate veinlet
68-2	cement in quartz metawacke adjacent to a carbonate veinlet
70-2	cement in contorted quartz metawacke adjacent to 70-4
70-4	very white, pure carbonate bleb adjacent to 70-2
73-1	veinlet cross-cutting 73-4
73-4	cement at the contact between a slatey and a metawacke layer cut by 73-1
75-1	veinlet
112-A	vein in quartz metawacke cross-cutting 112-B
112-B	carbonate blebs in quartz metawacke adjacent to 112-A
126-A	vein cross-cutting a dyke(?) in 126-B
126-B	cement in quartz metawacke cut by a dyke(?) and 126-A
131	vein with sphalerite mineralization cutting contorted calcareous quartz metawacke
132	cement in contorted "blocky" quartz metawacke
140	cement in fine laminated quartz metawacke and slate
151	carbonate blebs in quartz metawacke
166	vein in quartz metawacke
169	fracture-filling vein containing sphalerite cross-cutting metawacke

174	fracture-filling vein in contorted calcareous quartz metawacke
175.5	vein (may have some rhodochrosite) in a section of fine carbonate stringers in slate
176.5	cement in massive quartz metawacke
186-A	vein (or bed?) with galena mineralization cross-cutting 186-B
186-B	cement in quartz metawacke cut by 186-A
187	vein in metawacke and slate
189	slightly calcareous quartz metawacke
197	vein containing sphalerite and galena
208	cement in a black slatey bleb in calcareous quartz metawacke
210-A	filling fractures (ie. vein?) in a 1cm wide quartz vein which cuts 210-b
210-B	cement in metawacke cut by 210-A
215-A	coarse-grained carbonate vein containing pyrite cubes and cross-cutting 215-B
215-B	cement in quartz metawacke cut by 215-A
232	vein in quartz metawacke
235	vein with galena and pyrite (some rhodochrosite?)
238	cement in contorted quartz metawacke and slate
240	carbonate in abundant stringers (ie. veins) along fractures or foliation in slate
248	carbonate rim around a black, carbonaceous(?), slatey bleb
252	coarse-grained carbonate vein

Each carbonate sample was chipped from the hand samples. The sample size was generally less than one gram. Since the carbonate in the calcareous metawacke and slates was in the form of a fine grained cement, these samples contained large amounts of impurities. Each sample was crushed to a fine powder using a porcelain mortar and pestle, and placed in a small glass vial (~15 ml). Between samples, the mortar and pestle were washed first with dilute HCl if the sample contained abundant carbonate, then with tap water followed by distilled water and finally acetone to evaporate the water.

The isotopic analyses were carried out using a vacuum line and a ratio mass spectrometer by Dr. Peter Reynolds and Mr. Paul Durling at Dalhousie University. About 10 to 15 milligrams of sample were reacted with 100% phosphoric acid at a constant temperature of 25 ^{o}C with the evolution of H_2O, CO_2, and sometimes H_2S (due to reaction of sphalerite and galena with the acid) such that the gases entered the vacuum line system. The water and H_2S were removed from the vacuum line cryogenically at -93 ^{o}C. The CO_2 was then pumped into the mass

spectrometer where its isotopic composition was compared to that of the laboratory standard, the Carrara Marble (cm). The spectrometer detected the isotopic species of CO_2 having mass numbers 44, 45, 46 representing the combinations:

$$44 = ^{12}C^{16}O^{16}O$$
$$45 = ^{13}C^{16}O^{16}O$$
$$46 = ^{12}C^{16}O^{18}O$$
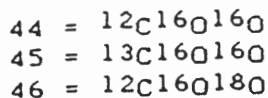
and the results were recorded as the mass ratios 45/44 (to get R_C) and 46/44 (for R_O). These values were converted to the PDB international standard using an Apple II computer program by means of the following equations:

$$\delta^{18}O_{cm} = 1.001(\delta^{46}) + 9.6 \times 10^{-3}(\delta^{45})$$

$$\delta^{18}O_{PDB} = \delta^{18}O_{cm} - 1.19$$

$$\delta^{13}C_{cm} = 1.067(\delta^{45}) + 0.03384(\delta^{46})$$

$$\delta^{13}C_{PDB} = \delta^{13}C_{cm} + 2.79$$

The $\delta^{18}O_{PDB}$ values were converted to SMOW by:

$$\delta^{18}O_{SMOW} = 1.03086(\delta^{18}O_{PDB}) + 30.86 \quad .$$